BRUNO HENRIQUE LOBO NETTO PEIXOTO

OPTIMIZATION AND LEARNING APPLIED TO CONTROL AND MODELING OF MECHATRONIC SYSTEMS

São Paulo
2023

BRUNO HENRIQUE LOBO NETTO PEIXOTO

OPTIMIZATION AND LEARNING APPLIED TO CONTROL AND MODELING OF MECHATRONIC SYSTEMS

Versão Corrigida

Dissertação apresentada à Escola Politécnica da Universidade de São Paulo para obtenção do Título de Mestre em Ciências.

São Paulo
2023

BRUNO HENRIQUE LOBO NETTO PEIXOTO

OPTIMIZATION AND LEARNING APPLIED TO CONTROL AND MODELING OF MECHATRONIC SYSTEMS

Versão Corrigida

Dissertação apresentada à Escola Politécnica da Universidade de São Paulo para obtenção do Título de Mestre em Ciências.

Área de Concentração:

Engenharia de sistemas

Orientador:

Prof. Dr. Felipe Miguel Pait

Co-orientador:

Prof. Dr. Bruno Augusto Angélico

São Paulo
2023

Este exemplar foi revisado e corrigido em relação à versão original, sob responsabilidade única do autor e com a anuência de seu orientador.

São Paulo, 6 de Janeiro de 2023

Assinatura do autor: 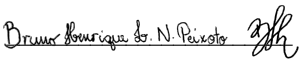

Assinatura do orientador: 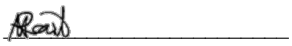

Catalogação-na-publicação

Peixoto, Bruno Henrique Lobo Netto
Optimization and learning applied to control and modeling of mechatronic systems / B. H. L. N. Peixoto -- versão corr. -- São Paulo, 2023.
110 p.

Dissertação (Mestrado) - Escola Politécnica da Universidade de São Paulo. Departamento de Engenharia de Telecomunicações e Controle.

1.Algoritmos 2.Otimização 3.Modelagem I.Universidade de São Paulo. Escola Politécnica. Departamento de Engenharia de Telecomunicações e Controle II.t.

To parents, Edimar Peixoto and Jaqueline Lobo Peixoto, and sibling Brenno Lobo.

ACKNOWLEDGMENTS

Acknowledgments aim to attribute gratitude to someone or something when the number of causal corroborating facts to significant events may not be countable or comprehensible. To write this thesis feels like plucking fruits from a vast garden along with comrades' support and discovering its treasures. Names and work contributions are below.

To academic advisors, Professors Felipe Miguel Pait and Bruno Augusto Angélico: for insightful conversations and lectures during the stay at Polytechnic School and provisions in Applied Control Laboratory. Their support is fundamental to self-improvement, subject comprehension, and inspiration about work vocation. In particular, Professor Felipe's patience in teaching geometry perks, soft skills in both digital and interpersonal communication, endurance, and resilience throughout daily anxiety and demotivation during activities.

To Polytechnic School Professors: their trust in students and concern about learning difficulties are notorious. For the fundamentals of applied control theory, physical systems modeling and simulation, and Genuity on experiment results evaluation.

To graduation mates and friends: Jorge Augusto Vasconcelos Alves and our discussions about the nature of physical systems, ideas about possible control projects, and coffee breaks; Lucas Koleff for lunch breaks, motivational support on the daily academic routine, and control projects; my laboratory colleagues Matheus Mussi, Fábio Yukio, Gabriel Pereira, Rafael Bachega, and Reviane Lopes for discussions about education and self-organization aspects.

To family Lima and Lichtenstein: Flávio and Regina Lichtenstein, Gabriela Lima Lichtenstein's parents, and their lovely dogs Brownie, Black, and Teddy, for mental support, shelter provision, and host during a partial period of the master program. Their help was mentally and physically fundamental in finding a calm-paced environment to concentrate on this work.

To Gabriela Lichtenstein: for comprehension, affection, and confidence during moments of reclusion.

To relatives: due support, comprehension, and motivation. My education would not be possible without their both emotional and structural assistance. We will embark briefly on a comforting digression by following Carl Sagan's quotation [1]:

> My parents were not scientists. They knew almost nothing about science. But in introducing me simultaneously to skepticism and to wonder, they taught me the two uneasily cohabiting modes of thought that are central to the scientific method.

Finally, to the sun's heat, the plant's oxygen, and the great masters' burning curiosity and inspiration through world comprehension. To whom it may concern, thank you sincerely for life.

"Namu Myōhō Renge Kyō."

- Nichiren Daishonin

ABSTRACT

The source seeking is a relevant topic on autonomous robotics. In a few words, it consists of seeking a scalar signal source position with only local information on base $\mathcal{X}$-space. In such, the seek agent, for instance, a mobile tracking $\mathcal{A}$-robot, samples by hypothesis $\mathcal{C}^{\infty}$-class source signal ϕ-map constrained by $\text{hull}\,(\mathcal{A}) \subseteq \mathcal{X}$. Among available seeking methods, this work utilizes the *barycenter method*, first presented on work [2], as a direct optimization method due to derivatives' absence. The applied algorithm estimates the source $\hat{y}_n$-position and designs a suitable reference $\hat{\gamma}(t)$-curve, hopefully towards a sufficiently close vicinity of the actual source $y_s^{\star}$-position. In case there are multiple critical points, the $\{d(y_s^{\star},\, \hat{y}_n)\}$-sequence may not converge asymptotically to a sufficiently close neighborhood of zero due to its local behavior, a challenge for these garden-like optimization algorithms. This work succeeds to obtain results in direction of the source signal position. Therefore, the proposed methodology provides an alternative for source-seeking applications by defined-to-be exploration strategy by different agent seekers, source signal maps, and obstacle modeling.

Keywords – source seeking, optimization, barycenter.

RESUMO

A busca da fonte de um sinal tem relevância em robótica autônoma. Seu enunciado consiste na busca estimada da $y_s^\star$-posição de uma fonte de sinal escalar apenas com informação local sobre sua disponibilidade no $\mathcal{X}$-espaço base. Em tal situação, o agente de busca, por exemplo, um $\mathcal{A}$-robô rastreador móvel, tem acesso à magnitude do ϕ-mapa sinal de $\mathcal{C}^\infty$-classe (por hipótese) restrito ao (hull $(\mathcal{A}) \subset \mathcal{X}$)-feixo do agente de busca. Esta dissertação de mestrado utiliza o *método do baricentro*, disponível em artigo [2], como método de otimização direta, por satisfazer critério de ausência de derivadas. O algoritmo proposto estima $\hat{y}_n$-pontos para a posição da fonte e sintetiza uma $\hat{\gamma}(t)$-curva de referência em direção à estimativa calculada, a fim de atingir a vizinhança de um $y_s^\star$-ponto extremal. Caso múltiplos pontos críticos existam, a $\{d_{Y_s}(y_s^\star, \hat{y}_n)\}$-sequência pode não convergir assintoticamente a uma vizinhança suficientemente próxima de zero devido à característica local do método de otimização aplicado, um desafio a algoritmos desta classe. Os resultados em direção à fonte do sinal escalar são satisfatórios. Portanto, a metodologia oferece uma alternativa à aplicações da busca de fonte para diferentes combinações de estratégias de exploração, por meio de agentes de busca, mapas de sinal de fonte e modelagem de obstáculos a definir.

Palavras-Chave – busca de fonte, otimização, baricentro.

LIST OF FIGURES

ALPHABET

Number theory

$\mathbb{N}$, $\mathbb{R}$, $\mathbb{C}$	Natural, real and complex fields
$\mathbb{K}_{\neq 0}$, $\mathbb{K}_{<0}$, $\mathbb{K}_{>0}$	$\mathbb{K}$-Field respectively without, with lower, or greater than null 0-element, according to comparison ($\neq$, $\geq$, $\leq$)-operators
$\mathbb{D}$, $\mathbb{I}\mathrm{m}$	Morphism domain and image sets
$\mathfrak{R}$, $\mathfrak{I}$	Complex real and imaginary parts

Set theory

card, #, $\lvert\cdot\rvert$	Set cardinality
$\{x_k\}_n$, $\{x_n\}$	Ordered sequence or set with n elements given by enumeration k-index
$a \in A$	a-Element belongs to A-set
$\bar{A}$	Complement set or complex conjugate of A-element
$\mathbb{I}_n$	Family of index sets with cardinality equal to natural n-constant

Real analysis

ε	Real scalar arbitrarily greater than real 0-element
α	Real simplex α within $[0, 1]$-interval
λ	Forgetting factor, eigenvalue or Lagrange multiplier
O	Big-O complexity
C^k	Class of k-differentiable maps

Abstract algebra

f^{-1}	Inverse map
$SO(n)$	Special orthogonal group of n-dimension
$\mathbb{M}_{m\times n}(\mathbb{K})$	Matrix linear space of (m, n)-dimension with $\mathbb{K}$-field scalar entries
${}^k a^i_j$	(j^{th}) i^{th} element (co-)element of a-(co-)vector on k-basis
$A^\intercal$	Transpose operation i.e. $(A^\intercal)^i_j \coloneqq A^{\intercal i}_{\ \ j} = A^j_i$
A^{-1}	Inverse operation i.e. $(A^{-1})^i_j \coloneqq A^{ij}$

A^+	Moore-Penrose pseudoinverse i.e. $(A^+)^i_j \coloneqq A^{ij}$
A^*	Conjugate transpose operation i.e. $(A^*)^i_j \coloneqq \bar{A}\mathsf{T}^i_j = \bar{A}^j_i$
$\det(A)$	Determinant map of A-matrix
Id_A	Identity map on A-space i.e. $\mathrm{Id}_A\ a \coloneqq a$
$\beta_{m,n}$	Matrix of $(m,\ n)$-dimension with β-only scalar entries
$\oplus$	Direct sum operator i.e. $A \oplus B \coloneqq \mathrm{blkdiag}(A, B)$
$\otimes$	Tensor or Kronecker product operator
$\circ$	Hadamard product operator i.e. $(A \circ B)^i_j \coloneqq A^i_j B^i_j$
$:$	Double inner product operator i.e. $A : B \coloneqq \sum_{ij} (A \circ B)^i_j$

Euclidean geometry

$\overline{AZ}$	Line segment between $(A,\ Z)$-points
$\widehat{AB}$	Normalized vector i.e. versor $\frac{AB}{\|AB\|}$
$A\hat{B}C$	Argument between line $(\overline{AB},\ \overline{CB})$-segments on B-point
$\arg(v)$	Polar arguments of v-vector

Stochastic calculus

$\mathbb{E}$	Expected value
Var	Variance
$\mathcal{N}(\mu, \Sigma)$	Gaussian distribution with mean μ-vector and variance Σ-tensor

Differential geometry

d	One-form i.e. map differential
$\dot{a},\ D\,a$	First-order derivative of real-valued $(a \in \mathbb{F}(\mathbb{R}))$-map
$D_a,\ \partial_a$	Differential vector field operator respective to either index or a-vector
$f_{;\,a}$	f-Map partial derivative respective to either indexed coordinate or a-vector
$D^{(n)}_i$	n^{th} derivative operator
$\mathcal{E}(B)$	Maps section on vector B-bundle
$\mathbb{F}(M)$	Family of maps on topological M-space
$\mathbb{V}(M)$	Family of vector fields on topological M-space
L_X	Lie derivative operator respective to vector X-field
$[X,\ \cdot\ ],\ \mathrm{ad}_X$	Lie bracket operator respective to vector X-field

CONTENTS

1 INTRODUCTION: THE SOURCE SEEKING STATEMENT

"Without continual growth and progress, such words as improvement, achievement, and success have no meaning."

-- Benjamin Franklin

The source-seeking statement consists of agent navigation around the environment. It searches for an unknown source locus with its local available scalar signal magnitude. There are physical source examples with signal magnitude proportional to their position. Among others, we cite chemical or biological concentration and acoustic or thermal intensities.

Verbosely, the statement corresponds to seeking a source position $y_s^\star$-point by signal reading samples of distributed sensors on an $\mathcal{A}$-agent, e.g., a mobile robot, while it traverses the environment, also known as *configuration $\mathcal{X}$-space*. Given $\mathcal{X}$-space and dynamical Σ-system descriptions necessary for the statement under investigation, the current work proposes a solution based on the estimation of source signal map gradient grad ϕ-field to provide a reference for the dynamical source seeker representation.

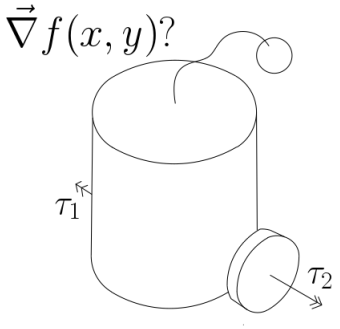

Figure 1: Source seeking ilustration.

Originally this work stems from authors Aström and Wittenmark's concerns in [3]-textbook about the extremum-seeking algorithm in control applications. Its nature relies on sinusoidal disturbance and numerical differentiation, prone to noise amplification. The most prolific research team among topic-concerned researchers corresponds to Prof. Dr. Miroslav Krstic's laboratory at UCSD San Diego. They apply the *extremum seeking algorithm* for the source position search and hence gradient vector field estimation of a scalar signal map. [4]-Textbook describes the estimation procedure for source localization.

Among others, the researchers Angélico *et al.* on article [5] explore in his recent work a simulation application of the above-mentioned method. The proposed systematic overcome the challenging requirements combination of unknown source signal topology and obstacle avoidance. As a requirements configuration alternative, the current work explores statement topological features to provide insights for further methodologies on a similar scenario. This work investigation succeeds in its research results and presents its main results in published [6]-article on the XV Brazilian Simposium of Smart Automation

- SBAI 2021 (English translation for original "XV Simpósio Brasileiro de Automação Inteligente - SBAI 2021").

In addition to the above application, we cite the following works: the authors in [7]-article consider a unicycle as the source seeker and linear speed tune as a control strategy; similarly, researchers in [8]-work tune the angular velocity instead. The same author, in work [9], modulates the estimated linear velocity by the extremum seeking algorithm through *sensor reading feedback*, with further improvement on [10]-work. [11]-Application exploits the *stochastic extremum seeking*. Other application examples are available in ([12], [13])-articles.

The source-seeking statement allows requirement relaxation by the introduction of distributed sample points available by embedded sensors and/or multiple seeker agents: in [14]-article, mobile agents utilize the Particle Swarm algorithm to locate an electromagnetic source. In [15]-essay, multiple UAVs tracks the source gradient vector by reference input tracking map. Azuma *et al.* on [16]-article apply a stochastic simultaneous perturbation for source estimation by nearby waypoints. [17]-Reference utilizes a mobile sensor network based on the finite difference mesh grid-specific points in a distributed stochastic source-seeking fashion for signal gradient field estimation.

The current Master thesis explores the *Barycenter method* properties, first suggested by the physicist Richard Feynman in its [18]-work and further developed by Prof. Dr. Felipe Pait on vector X-space on [2]-work. Intuitively, the method computes the weighted sum of reading positions by the respective exponential negative of evaluated reading samples. The discrete acquisition of reading samples derives from the agent's environment exploration.

The current author organizes methodologically this work, aside from this introduction, into seven chapters and the appendix: *chapter two* explains the building blocks necessary to compose the here-proposed source seeking heuristics, given by applied optimization method for source position estimation, dynamic modeling aspects as well as source-seeking agent control; *chapter three* proposes trajectory curves planning synthesis between two points, either with or without initial and final orientations; the *fourth chapter* introduces the obstruction topology and allows to treat obstacles from a geometric perspective; based on previous chapters topics, *chapter five* depicts the proposed source seeking solution rationale in a flow diagram format and presents briefly some possible exploration possibilities; *chapter six* deals with application examples for each building block presented on previous chapters: we choose a flat surface as navigation environment, a curvature-free curve as reference trajectory i.e. a line, an omnidirectional robot as seeker agent, simulation instances for multiple scenarios with environmental curious exploration and multiple simulation instances averaging for behaviour investigation; we discuss on *chapter seven* the main project development decisions, method properties and computational implementation caveats; we conclude this work on *chapter eight* with a summary of this work main results both from development construction, results investigation and future research opportunities. Finally, in the appendix chapter, we compile geometric control topics necessary for reading comprehension, reproduction instructions on a computational environment, and the algorithmic rationale for control map synthesis and source-seeking.

2 SOURCE SEEKING BUILDING BLOCKS

"When a new building block is discovered, the result is usually a range of innovations."

-- John Henry Holland

Barycenter method: The source seeking optimizer

This chapter summarizes the original [2]-work. Optimization is a recurrent topic in Robotics. From the source-seeking perspective, we aim to obtain a well-suited scalar source signal configuration, e.g., for communication. Among thematic works, the possible algorithms and scenarios provide multiple application opportunities.

In this work, the applied source-seeking algorithm corresponds to the *Barycenter Method*. It resembles stochastic optimization algorithms and emulates the map gradient vector field based on the weighted average of available local information. The local data availability requirement is suitable for the source-seeking statement. In words, the barycenter method consists of an optimization algorithm of non-degenerate critical $x^\star$-points on the linear position X-space of so-called *oracle f-map*. In addition, it requires only signal evaluations available on given points $\{x_n\}$-sequence.

In a nostalgic recall, the arithmetic average corresponds to the sum of each element divided by its set n-cardinality. In turn, the weighted average of the same set represents the sum of each element x_i-point weighted by a scalar w^i-map divided by these weights sum. This description induces the following property: the greater the w^i-weight, the greater its contribution to the resulting barycenter $\hat{x}_n$-point. The barycenter method exploits this property to obtain either local or global critical points.

This method presents batch and recursive procedures. For narrative, we present the former. On this work, we utilize often Einstein's summation convention: the lower-index notation x_i accompanied by upper-index $w^i \coloneqq e^{-\nu f^i}$ refers to the sum over repeated indexes i.

$$\frac{x_i \; w^i}{1_i \; w^i} \tag{2.1}$$

The recursive form

In recursive form, the method exhibits the (2.2).-formula In the case of coincidental evaluation points, the resulting point for both batch and recursive points coincide.

$$\boxed{\begin{cases} m_n = m_{n-1} + e^{-\nu f_n} \\ \hat{x}_n = \frac{m_{n-1}}{m_n}\,\hat{x}_{n-1} + \frac{e^{-\nu f_n}}{m_n} x_n \end{cases}} \tag{2.2}$$

This method belongs to the class of direct optimization algorithms whose gradient vector and Hesse 2-form are unknown, present in [19]-textbook. However, for a judicious choice of curiosity term as Gaussian stochastic noise, the recursive version estimation $\Delta\hat{x}_n$-steps converges proportionally to the gradient $\mathrm{grad}^X f$-vector on $(\hat{x}_{n-1} + z_n)$-point, for Gaussian support $p(z)$-map of stochastic z_n-vector as the 2.3-expression.

$$\frac{1}{\sqrt{(2\pi)^{n_z}\,|\Sigma|}} \exp\left(-\frac{1}{2}(z-\bar{z})^{\intercal}\Sigma^{-1}(z-\bar{z}) \right) \tag{2.3}$$

We achieve the right-hand term of point $(\hat{x}_n - \hat{x}_{n-1})$-difference on equation (2.2) equal to stochastic linear expression $F_n\, z_n$, for map F_n equal to $\left(\frac{e^{-\nu f(\hat{x}_{n-1}+z_n)}}{m_{n-1}+e^{-\nu f(\hat{x}_{n-1}+z_n)}}\right)$-expression. (2.4)-Expression presents the most relevant method result: it determines the barycenter step expected $\mathbb{E}[\Delta\hat{x}_n]$-value along with the algorithm recursion.

$$\boxed{\mathbb{E}[\mathrm{F}_n]\,\bar{z}_n - \nu\,\Sigma\;\mathbb{E}[\bar{\mathrm{F}}_n\,\mathrm{grad}^X_{\hat{x}_n}\,f]} \tag{2.4}$$

We call (ν, Σ)-hyperparameters as real speed enhancer scalar and covariance tensor: The former intensifies the map magnitude; the latter provides the points dispersion broadness around space. This property allows utilizing the method both as a minimizer for $(\nu > 0)$-condition or a maximizer for $(\nu < 0)$-condition as [20]-work explains. The corner case equality $(\nu = 0)$-condition degenerates to the usual arithmetic average with weights equal to 1. Moreover, the exponential curve slope suggests a careful parameter choice.

Remark 1. The exponential map is positive for every point of the real line. Its steep slope for exponents lower than 0 suggests the addition of linear coefficient η i.e. $\eta - \nu\, f$, to mitigate numerical undesirable truncation. Intuitively, we do not wish to stop the barycentric optimal search in the extremum direction. Therefore, for the batch version, it is reasonable to apply the difference $f - f_-$ for minimization $(\nu > 0)$ i.e. $f - f_+$ for maximization $(\nu < 0)$. The $(f_-,\, f_+)$-symbols stand for lowest i.e. greatest batch values. The recursive version adopts the same strategy for values acquired so far.

Remark 2. A further numerically motivated remark regards the floor/ceiling numerical evaluation $\pm E$-limits. The barycentric operations require algebraic sums and exponential maps. A due statement lack of magnitude information suggests the application of minimum/maximum $(\min(E, \cdot), \max(-E, \cdot))$-operators to involving entries respective to maximization/minimization statement goals.

Improvement on convergence performance

Pait suggests a method's convergence improvement by choice of mean $\bar{z}_n$-vector as proportional $\xi\Delta\hat{x}_{n-1}$-step. The approach considers the Gaussian support mean vector proportional to the previous algorithm step, in turn, proportional to the gradient esti-

mation at the previous $\hat{x}_{n-1}$-point. We choose it as the null vector if it is not given beforehand. Additionally, we may choose the mean $\bar{z}_n$-vector as the barycentric weighted average of the previous steps. The proposed approach is proportional to the last step and recovers the gradient information of earlier estimations. The improvement may not account for all previous estimation $\hat{x}_i$-points of the evaluation set, but rather a subset: In the recursive application, we call it *historical barycentric horizon.*

Let us consider for mean $\bar{z}_n$-vector the barycentric average of the previous steps. Therefore, its batch and recursive formulas follow below.

$$\boxed{\bar{z}_n = \frac{\Delta\, \hat{x}_i\, e^{-\nu\, f^i}}{1_i\, e^{-\nu\, f^i}} \iff \bar{z}_n = \frac{e^{-\nu f_{n-1}}}{m_{n-1}}\, \Delta\, \hat{x}_{n-1} + \frac{m_{n-2}}{m_{n-1}}\, \bar{z}_{n-1}} \tag{2.5}$$

An inquiry arises about mean vector convergence on stochastic support $p(z)$-map given convexity assumptions almost everywhere for the map under optimization. Then, the following lemma contributes to the barycenter method respective to the parameter choice.

Lemma 2.1. *The $\eta_n\, \Delta\hat{x}_{n-1}$-map, proportional to the barycentric step, majorates the mean vector deviation $\Delta\bar{z}_n$-step.*

Proof. Its proof begins by $\big(\frac{m_{n-2}}{m_{n-1}} < 1\big)$-condition respective to denominator m_n-term. In words, the m_n-term is monotonically crescent. Since this ratio never holds null values for finite natural n-constant, also the η_n-term, equal to $\Big(1 - \frac{m_{n-2}}{m_{n-1}}\Big)$-expression.

$$\begin{aligned} m_{n-1} = m_{n-2} + e^{-\nu\, f(x_{n-1})} &\overset{\frac{(\cdot)}{m_{n-1}}}{\Longrightarrow} 1 = \frac{m_{n-2}}{m_{n-1}} + \frac{e^{-\nu\, f(x_{n-1})}}{m_{n-1}} \\ &\overset{\frac{(\cdot)}{m_{n-1}}}{\Longrightarrow} \frac{e^{-\nu\, f(x_{n-1})}}{m_{n-1}} = 1 - \frac{m_{n-2}}{m_{n-1}} = \eta_n < 1 \end{aligned}$$

Since the mean vector $\Delta\bar{z}_n$-step corresponds to $(\bar{z}_n - \bar{z}_{n-1})$-difference , we obtain the decay formation $\big(-\eta_n\, \bar{z}_{n-1} + \eta_n\; F_{n-1}\, z\big)$-rule. ■

Remark 3. We remark $(\eta_n < 1)$-condition, for scalar $\big(\eta_n \in \mathbb{R}\big)$-constant, as a decreasing behavior to mean vector sequence, similar to a discrete linear system for an eigenvalue within unit $\big(\|\bar{z}_n\| < 1\big)$-locus.

Exploration with forgetting factor

The method aims to explore the oracle map's $\mathbb{D}_f$-domain to seek critical points with map evaluation lower than on the current point. A judicious choice of forgetting λ-factor, such that $\big(\lambda < 1\big)$-condition holds, broadens the exploration domain to both batch and recursive versions. For a constant forgetting factor λ, both batch and recursive forms are below. For the current work, the forgetting factor application justifies time-variant oracle maps.

$$\boxed{\hat{x}_n = \frac{\lambda^{n-i} x_i e^{-\nu f^i}}{\lambda_i^{n-i} e^{-\nu f^i}}}$$

$$\boxed{\begin{cases} m_n = \lambda_n m_{n-1} + e^{-\nu f_n} \\ \hat{x}_n = \frac{1}{m_n}\left(\lambda_n\, m_{n-1}\hat{x}_{n-1} + e^{-\nu f_n} x_n\right) \end{cases}}$$

The mean vector enhancement from subsection 2 might carry on gradient history. Thus, the application of a forgetting λ_z-factor mitigates the effect of afar gradient vectors. The relation with the additional factor follows below. We notice an upper bound on decreasing behavior of $\bar{z}_n$-vector, since it multiplies a natural power of forgetting factor λ_z.

$$\boxed{\bar{z}_n = \frac{\lambda_z^{n-i} \Delta\, \hat{x}_i\, e^{-\nu\, f^i}}{\lambda_z^{n-i}\, e^{-\nu\, f^i}} \iff \bar{z}_n = \frac{e^{-\nu f_{n-1}}}{m_{n-1}}\, \lambda_z\, \Delta\, \hat{x}_{n-1} + \frac{m_{n-2}}{m_{n-1}}\, \bar{z}_{n-1}} \tag{2.6}$$

Discrete application on a continuous curve

The barycenter method statement requires an evaluation points set. The current application suggests the choice of the points on a $\gamma(t)$-curve. Henceforth, we state the following result based on its batch form.

Corollary 2.1. *Given $\gamma(t)$-curve, for instant $t \in [t_0,\, t_1]$, and instant partition $\{t_n\}$ such that $(t_{i-1} < t_i)$-condition holds, for $(t_i \in [t_0, t_1])$-instants. Then, the barycenter $\hat{\gamma}_n$-point for $\{t_n\}$-partition corresponds to batch evaluation* (2.1) *on curve $(\gamma_n \coloneqq \gamma(t_n))$-points.*

Corollary 2.1 allows the barycenter point definition within interval $[t_0,\, t_1]$. Its recursive version also emerges from the statement below.

Corollary 2.2. *Given $\gamma(t)$-curve, for $(t \in [t_0,\, t_1])$-instant and instant partition $\{t_n\}$-sequence such that $\left(t_i \in [t_0,\, t_1],\, t_{i-1} < t_i\right)$-conditions hold. Then, the barycenter $\hat{\gamma}$-point for $\{t_n\}$-partition follows by recursive evaluation of formula* (2.2) *as curve $\left(\gamma_n \coloneqq \gamma(t_n)\right)$-points.*

Although numerically equivalent to the batch version, the above result presents a computational advantage of online data sampling for a given evaluation set. The recursive version is preferable for online applications due to its compact design and is suitable for data sampling.

Convergence analysis

This subsection discusses the convergence criterium for the barycenter method probabilistic version. Due to its discrete stochastic behavior, *expected value* and discrete Lyapunov's stability criterium are helpful interpretations. Moreover, Jensen's inequality is also proof-relevant.

Lemma 2.2 (Jensen's inequality [21]). $\mathbb{E}\left[f(x)\right] < f(\mathbb{E}\left[x\right])$.

Theorem 2.1 ([2]). *Given barycenter* $\{\hat{x}_n\}$*-sequence and respective evaluation* $\{\hat{f}_n\}$*-sequence,* (2.7)*-condition is necessary for barycenter method convergence.*

$$\mathbb{E}[\hat{f}_n - \hat{f}_{n-1})] < 0 \tag{2.7}$$

Proof. The following steps explore the Lyapunov stability criterium for discrete dynamical systems, on [22]-work. Consider for instance the series formation rule for the recursive barycenter method, given by $\big(\hat{x}_{n-1} + F_n\, z_n\big)$-expression. By first-order approximation, we obtain (2.8)-equality. The $R(\cdot)$-map corresponds to the Taylor series residuum.

$$\begin{aligned}
\hat{f}_n - \hat{f}_{n-1} &= f(\hat{x}_{n-1} + F_n\, z_n) - f(\hat{x}_{n-1}) \\
&= d\hat{f}_{n-1}\, \Delta\, \hat{x}_n + R(F_n^2) \\
&= \underbrace{F_n}_{\coloneqq \frac{e^{-\nu f_n}}{m_{n-1} + e^{-\nu f_n}}} d\hat{f}_{n-1}\, z_n + R(F_n^2) \\
&= \frac{1}{m_{n-1}\, e^{\nu \hat{f}_{n-1}}\, e^{\nu\, df_{n-1}\, z_n} + 1}\, d\hat{f}_{n-1}\, z_n + R(F_n^2)
\end{aligned} \tag{2.8}$$

We rename above equality by equalities $\big(d\hat{f}_{n-1} = a^{\intercal}, m_{n-1}\, e^{\nu f(\hat{x}_{n-1})} = \bar{m}_n\big)$-notation, the above difference expression exhibits the formula below.

$$\Delta \hat{f}_n = \frac{a^i\, z_i^n}{\bar{m}_n\, e^{\nu\, a^i\, z_i^n} + 1} + R(F_n^2) \tag{2.9}$$

We develop its expected $\mathbb{E}[\Delta \hat{f}_n]$-value from Jensen's 2.2-condition for stochastic processes, available on [23]-textbook, resulting on (2.10)-condition.

$$\boxed{\mathbb{E}\left[\frac{a^i\, z_i^n}{e^{\nu\, a^i\, z_i^n}\, \bar{m}_n + 1} + R(F_n^2)\right] \leq \frac{a^i\, \bar{z}_i^n}{e^{\nu\, a^i\, \bar{z}_i^n}\, \bar{m}_n + 1} + R(\mathbb{E}[F_n^2])} \tag{2.10}$$

The mean $\bar{z}_n$-vector is a degree of freedom: for the null vector choice, the right-hand-side is lesser than 0; for other reasonable mean vector choices e.g. to cite $\xi\, \Delta \hat{x}_{n-1}$, its expected value, analogous to (2.4)-expression, is proportional to oracle differential $-df(\hat{x}_{n-1})$-map. The squared F_n^2-term decreases congruently to the F_n-term, strictly lesser than 1. Since the m_n-term increases monotonically and the F_n-expression is greater than 0, it converges asymptotically to zero as m_n-term increases. Hence, stability according to (2.10)-condition is necessary for algorithm convergence.

■

Mechatronic robotic systems as source seekers

Source seeking relies on dynamic agents to explore the environment and sample source signals. In this work, we apply mobile robots as source seekers. In special, terrestrial mobile robots utilize wheels to provide their steering movement. From an engineering perspective, a mobile robot is a mechatronic system with sensors and actuators in the physical world.

In topological terms, we call state $\mathcal{Q}$-space and observation $\mathcal{Y}$-space, which we relate $(q \in \mathbb{D}_h)$-points to output $\big(y \in \mathcal{Y}\big)$-points by a $\mathcal{C}^\infty$-class observation h-map on $\big(\mathcal{Q} \to \mathcal{Y}\big)$-relation. Their dynamical description exhibits linear equality constraints respective to velocity $(\dot{q} \in T_q\mathcal{Q})$-vector, we call *Pfaffian constraint equalities*.

The following subsections describe both kinematic and dynamic modeling descriptions: we describe affine-constrained mechatronic systems in the Lagrangian framework.

Lagrangian maps under Pfaffian constraints: a brief overview

Physical systems description emerges from the Euler-Lagrange variational statement (2.11): Mathematicians call this integral the curve length minimization problem and physicists as action minimization. The Lagrangian ℓ-map on $\big(\mathcal{Q} \times T\,\mathcal{Q} \to \mathbb{R}\big)$-relation corresponds to the difference $\big(m_{ij}\,\dot{q}^i\,\dot{q}^j - \varrho\big)$-map, for $\big(m_{ij},\, \varrho\big)(q)$-maps as geometrical and potential contributions respectively: the former relates to kinetic density throughout geometry respective to velocity $\big(\dot{q} \in T_q\,\mathcal{Q}\big)$-vector; ϱ-map represents a potential map on given state $\big(q \in \mathcal{Q}\big)$-point. The formal statement and its solution, if exists, emerges from developments on subjects like *Variational Calculus*, *Differential Geometry*, among others. It also receives further treatment on theories like *Measure* and *Stochastic processes* theories.

$$\int_\sigma^\tau \ell(q(s), \dot{q}(s))\, ds \text{ under } n_a < n \text{ Pfaffian constraints } \big(A_k\,\dot{q}^k = 0\big)\text{-equalities} \tag{2.11}$$

The common resolution approach for the above statement utilizes Lagrange linear λ-multipliers to span the dual space of constraint $A^\intercal$-codistribution. For completeness, authors Udwadia and Kalaba propose in their [24]-textbook an extension approach for non-conservative contributions e.g. Coulomb friction forces on Lagrangian maps. Additionally, they obtain the Lagrange λ-multipliers for given linear constraints.

The Euler-Lagrange equality takes (2.12)-format for a Lagrangian system subject to Pfaffian constraints $\big(A_j\,\dot{q}^j = 0\big)$-equalities, on every state $\big(q \in \mathbb{D}_m \cap \mathbb{D}_\varrho\big)$-point and velocity $\big(\dot{q} \in \text{span}\,(\text{Ann}\,(A)) \subset T_q\mathcal{Q}\big)$-vector. The statement extension by Pfaffian equalities appears on Frobenius' [25]-work. American researchers Bloch *et al.* figure among subject-concerned researchers. His formal description on this particular class of dynamical systems refers to $\big([27],\, [26]\big)$-works. This class's first appearance in literature reports to Gauss' [28]-work.

$$D\,(\partial_{\dot{q}}\ell) - \partial_q\ell = A_k^\intercal\,\lambda^k + f_q \tag{2.12}$$

The right-hand f_q-term on (2.12)-equality refers to the generalized state forces respective to state $\big(q \in \mathcal{Q}\big)$-points: it represents each external effort's contribution to or from the system. However, usual applications describe f_x-efforts in configuration tangent $T_x\,\mathcal{X}$-space on configuration $\mathcal{X}$-space.

The necessary toolset to obtain state f_q-efforts calls *Virtual Displacement Method* (VDM) or *D'Alembert principle*, available on classical [29]-textbook. Given an effort $\big(f_q \in T_q\,\mathcal{Q}\big)$-vector, equivalence equality between a f_x-vector in configuration tangent $T_{x(q)}\,\mathcal{X}$-space emerges naturally from lemma below.

Lemma 2.3 (Virtual Displacement Method on Manifolds [29])**.** *The equivalence equality between respective f_q-vectors on tangent state $T_q\mathcal{Q}$-space and f_x-vectors on tangent configuration $T_{x(q)}\mathcal{X}$-space for given locally isomorphic[1] x-map on $\big(\mathcal{Q} \to \mathcal{X}\big)$-relation corresponds to equivalence (2.13)-relation, for q-map on $\big(\mathcal{X} \to \mathcal{Q}\big)$-relation such that $\big(x \circ q = \mathrm{Id}_{\mathcal{X}}, q \circ x = \mathrm{Id}_{\mathcal{Q}}\big)$-equalities hold on open $\big(\tilde{\mathcal{X}} \subseteq \mathcal{X}, \tilde{\mathcal{Q}} \subseteq \mathcal{Q}\big)$-sets.*

$$f_x = x_*\, f_q \iff f_q = q_*\, f_x \tag{2.13}$$

We require a further toolset to clear away Lagrange's λ^k-multipliers dependency. The forthcoming statement originates from the dual vector spaces relation from linear algebra, available in $\big([30], [31]\big)$-textbooks. We represent these distributions and co-distributions as well as their dual spaces respectively by $\big(B, A, B^\intercal, A^\intercal\big)$-letters.

Given codistribution spanned by $\{a^i\}_{n_a}$-covectors, its annihilator B-distribution spans from $\mathcal{C}^\infty$-class column $\{b_{n-n_a}\}$-vectors, defined on [32]-textbook, such that variant as well as covariant $\big(a^i_k\, b^k_j,\, b^j_k\, a^k_i\big)$-products are equal 0 for the open $\mathbb{D}_{a^i} \cap \mathbb{D}_{b_j}$-set. It means the velocity $\dot{q}$-vector corresponds to the linear $B_j\, p^j$-span of distribution column b_j-vectors. Researchers Baruh and Tsai calls p-vector as *quasi-velocities*.

The $A^\intercal_k \lambda^k$-contribution constrains the velocity $\dot{q}$-vector to directions spanned by its co-annihilators $\{b^{n_b}\}$ on cotangent $T^*\,\mathcal{Q}$-space. As a further interpretation step, we left-multiply (2.12)-equality by annihilator $B^\intercal$-codistribution: It annihilates $A^\intercal$-codistribution, resulting in a constrained covariant derivative equality as follows.

$$B^\intercal\, D\,(\partial_{\dot{q}} \ell) - B^\intercal \partial_q \ell = B^\intercal\, q_*\, f_x \tag{2.14}$$

We expand the $D\,\big(\partial_{\dot{q}^i} \ell\big)$-derivative by chain $\big(D\varphi(x) = \varphi_*(\dot{x}) = (d_k \varphi)\, \dot{x}^k \coloneqq \mathrm{L}_{\dot{x}}\, \varphi\big)$-rule. In our case, the desired result corresponds to the expression below. In this work, we consider Clairaut's theorem[2]-compatible maps. The required map derivative exhibits (2.14)-equality for differential d-operator.

$$D\,(\partial_{\dot{q}} \ell) \coloneqq d_{\dot{q}^c}\,(\partial_{\dot{q}} \ell)\; \ddot{q}^c + d_{q^k}\,(\partial_{\dot{q}} \ell)\; \dot{q}^k$$

---

[1] An isomorphic x-map corresponds to a morphism with right and left inverse $\big(x \circ x^{-1} = \mathrm{Id}_X,\, x^{-1} \circ x = \mathrm{Id}_Y\big)$-equalities.

[2] Clairaut's Theorem states the 2-order derivative symmetry $\big(\partial_i \partial_j = \partial_j \partial_i\big)$-equality, available on [35]-textbook.

[3] The Levi-Civita connection corresponds to a well-defined unique affine symmetric operator on $\mathcal{Q}$-manifold endowed with parallel transport linear L-relation on tangential vector $T\,\mathcal{Q}$-bundle that preserves $\langle \cdot, \cdot \rangle^{\mathcal{Q}}$-metric

Time derivatives on 2.14-expression represent map dependency on q-states and its velocity $\dot{q}$-vector. Velocity vector derivative $D\dot{q}$-operation is the usual acceleration $\ddot{q}$-vector and corresponds to linear combination $\big((DB_c)\; p^c + B_c\, \dot{p}^c \big)$-span. We express the distribution derivative DB_c-operation by the Lie derivative linear $\big(d(B_c)\, B_b\, p^b \;\coloneqq\; (L_{B_b}\, B_c)\; p^b \big)$-span, here-denoted by Λ_{cb}.

$$B^{\intercal}\, d_{\dot{q}^c}\, (\partial_{\dot{q}} \ell)\; \ddot{q}^c + B^{\intercal}\, d_{q^k}\, (\partial_{\dot{q}} \ell)\; \dot{q}^k - B^{\intercal}\, \partial_q \ell = B^{\intercal}\, f_q \tag{2.15}$$

We also require the differential $\big(d_{q^k}\, (\partial_{\dot{q}^a} \ell)\,,\; d_{\dot{q}^c}\, (\partial_{\dot{q}^a} \ell)\, \big)$-terms with row and column $\big(a, c, k\big)$-indexes, below.

$$\begin{cases} \partial_{q^a} \ell = m_{ij;a}\, \dot{q}^i\, \dot{q}^j - \varrho_{;\, a} \\ \partial_{\dot{q}^a} \ell = m_{ij}\; \big(\delta_{ia}\, \dot{q}^j + \dot{q}^i\, \delta_{ja} \big) = m_{aj}\, \dot{q}^j + m_{ai}\, \dot{q}^i \\ d_{q^k}\, (\partial_{\dot{q}^a} \ell) = m_{aj;k}\, \dot{q}^j + m_{ia;k}\, \dot{q}^i \\ d_{\dot{q}^c}\, (\partial_{\dot{q}^a} \ell) = m_{ac} + m_{ca} = 2\, m_{ac} \end{cases} \tag{2.16}$$

The above differential results substitution on (2.16)-equalities and velocity vector derivative $D\, \dot{q}$-operation leads to expanded (2.17)-format of equality left-hand-side (2.15)-term.

$$\underbrace{B_a^{\intercal}\, m_{ac}\, B_c}_{\theta_{ac}}\; \dot{p}^c + \underbrace{\frac{1}{2}\, B_a^{\intercal}\; \big(m_{aj;k}\, B_b^j\, B_c^k + m_{ia;k}\, B_b^i\, B_c^k - m_{ij;a}\, B_b^i\, B_c^j + 2\, m_{ac} \Lambda_{cb} \big)}_{I_{abc}}\; p^b\, p^c \tag{2.17}$$

Due document spacing, we omit the potential $\big(\frac{1}{2}\, B_a^{\intercal}\, \varrho_{;\, a} \big)$-contribution. Likewise, the right-hand-side term on (2.17)-equality turns into constrained force $\frac{1}{2}\, B^{\intercal}\, q_*\, f_x$-vector. Finally, the above equality left-multiplication by tensor inverse θ^{da} and equality $\big(\theta^{da}\, \theta_{ac} = \delta_c^d \big)$-property application leads to (2.18)-equality, the constrained geodesic curve differential equality.

$$\dot{p}^d + I_{bc}^d(q)\, p^b\, p^c + (\mathrm{grad}^{\vartheta}\, \varrho)^d(q) = f_p^d \tag{2.18}$$

It represents the geodesic $\gamma(t)$-curve on foliation i.e. $\big(\vartheta \subseteq \mathfrak{Q} \big)$-submanifold endowed with Θ-metric: it emerges from covariant derivative $\nabla_{\dot{p}}\, \dot{p}$-vector, by means of the constrained Levi-Civita connection[3], under potential map gradient vector $\mathrm{grad}^{\vartheta}\, \varrho$-field and external force f_p-vectors at $\big(q \in \mathfrak{Q} \big)$-point constrained by ϑ-foliation[4]. We utilize the Hadamard's equality $\big(\sum_{ij} (A \circ B)_{ij} \coloneqq \mathrm{tr}\, (A\, B^{\intercal}) \big)$-identity to define each row $\big(I^d(q,\, p) \coloneqq \mathrm{tr}\, (I^d\, p\, p^{\intercal}) \big)$-element of constrained Christoffelian $\big(I(q,\, p) \in T_q\, \vartheta \big)$-vector.

$$\dot{p} + I(q, p) + \mathrm{grad}^{\vartheta}\, \varrho = f_p \tag{2.19}$$

Remark 4. The differentiable structure of constrained ϑ-manifold relies on metric inverse Θ^{-1}-tensor. Therefore, the domain open set corresponds to the collection of state points

[4]We remark on the composition of foliation ϑ by holonomic and non-holonomic coordinate frame since its original Pfaffian distribution does not exhibit a particular holonomicity.

q such that the equality $\det(\Theta) \neq 0$ holds.

$\mathcal{B}_\beta$-Objects' total potential ϱ_β-map corresponds to the integral (2.20)-calculation over each $(\mathcal{B}_\beta \subset \mathcal{X})$-body. Given the object's geometrical and inertial representation in configuration $\mathcal{X}$-manifold, by notation abuse, x-map brings state $\big(q \in \mathcal{Q}\big)$-points to $\big(x(q) \in \mathcal{X}\big)$-points and vice-versa. We adopt dense continuous measures for both local mass and potential density $\big(\rho_\beta, \mu_\beta\big)$-maps as well as metric g-tensor for configuration $\mathcal{X}$-manifold.

$$\begin{aligned} \int_{\mathcal{B}_\beta} \mu_\beta(x)\, dm &= \int_{\mathcal{B}_\beta} \rho_\beta\, \mu_\beta(x)\, d\upsilon_\beta = \int_{\mathcal{B}_\beta} \rho_\beta\, \mu_\beta\, \sqrt{|g|}\, d^{n_x} x \\ &= \int_{x^{-1}\left(\mathcal{B}_\beta\right)} \Big[\Big(\rho_\beta\, \mu_\beta\, \sqrt{|g|}\, |dx|\Big) \circ x^{-1}\Big]\, d^{n_q} q \end{aligned} \tag{2.20}$$

The resulting dynamical Σ-system consists of the velocity $\dot{\mathrm{p}}$-vector on product $\big(\mathcal{Q} \times T_q\, \vartheta\big)$-space defined by the affine vector field below:

$$\begin{bmatrix} B\, p \\ -I(q,\, p) - \mathrm{grad}^\vartheta\, \varrho \end{bmatrix} + \begin{bmatrix} 0 \\ \mathrm{Id}_{T_q \vartheta} \end{bmatrix} f_p \tag{2.21}$$

Objects' kinetic measure in classical mechanics corresponds to the sum of each β-object kinetic continuous $m_{ij}^\beta\, \dot{q}^i\, \dot{q}^j$-map. Each such map composes of translational and rotational additional kinetic differentiable measures. Commercial computer-aided analysis software embeds numerical algorithms to compute the inertial tensor given mass density ρ_β-map distributed over each $\mathcal{B}_\beta$-body.

For the current application, configuration $\mathcal{X}$-manifold is our familiar 3-dimensional Euclidean $\mathbb{R}^3$-manifold. The geometrical $m_{ij}^\beta\, \dot{q}^i\, \dot{q}^j$-contribution follows below.

$$\frac{1}{2}\, \bar{m}\, {}^\beta v_g^\intercal\, {}^\beta v_g + \frac{1}{2}\, {}^\beta \omega^\intercal\, I\, {}^\beta \omega \tag{2.22}$$

Thus, the 2-form g-metric regarding the center of the mass point of each body, familiar to geometers, follows on (2.23)-expression below.

$$\frac{1}{2} \sum_\beta \begin{bmatrix} \bar{m}\, v_*^\intercal\, v_* & 0 \\ 0 & \omega_*^\intercal\, I\, \omega_* \end{bmatrix}_\beta \tag{2.23}$$

In the next section, we describe the input-output partial linearization control synthesis for regular affine dynamical systems; its sufficient conditions under the given hypothesis set, i.e. morphism construction and zero inner dynamics, in close. Finally, we expose briefly the dynamic partial compensator for non-regular affine dynamic systems. [36]-Textbook provides in 5-chapter an elucidative topic introduction. Further thematic research is available in $\big([37],\, [38]\big)$-works.

The input-output partial linearization on affine dynamical system

This section presents the partial linearization of smooth affine system structure as described in A.22-appendix on smooth manifolds. Its description is to find standard geometric control theory $\big($[39], [40], [41], [36]$\big)$-textbooks. It aims to provide the main concepts and educate the reader regarding the elements involved. [42]-Textbook provides theme-related applications on this section, as well as Ph.D. [43]-thesis and [44]-reference.

Formerly, the desired procedure evaluates on output-point y given by smooth $\mathcal{C}^{\infty}$-class h-map on $\big(\mathcal{X} \to \mathcal{Y}\big)$-relation to obtain a diffeomorphic φ-map from affine dynamical Σ-system to a feedback equivalent linear system, even if partially. A prior necessary property for the existence of such output h-map is called *flatness*, presented by authors Fliess *et al.* on [45]-work. In usual control terms, *flatness* is a synonym to *controllability*. Since there is such a map h, the next verification step is to test its observability.

Although the topic development accounts for the broad class of smooth dynamical systems, we aim our attention on affine smooth dynamical systems. For simplicity, we consider square input-output systems i.e. given n_u-input and n_y-output dimensions respectively, we consider the family of the affine dynamical system such that the equality $\big(n_y = n_u\big)$-condition holds. The current author remarks on research for the over- and underactuated case, i.e., $\big(n_y \lesseqgtr n_u\big)$-condition if there is insufficient work on the subject.

The control map

In this section, we present procedural statements for the construction of control u-map with the goal to track the desired trajectory $\gamma^{\star}(t)$-curve by means of y-output given by h-map on $\big(\mathcal{X} \to \mathcal{Y}\big)$-relation. For brevity, the current author omits the local dependency under subject for vector $\big(f, g_k\big)$-fields as well as h-map if it is not confusion-prone from context.

Lemma 2.4 ([40])**.** *An affine dynamical Σ-system, defined in A.22-appendix, is exactly linearizable if there is a (local) diffeomorphic φ-map from linear Z-space to $\mathcal{X}$-manifold and control $u(x, v)$-map such that the Σ-system is (partially) feedback equivalent to the controllable linear affine dynamical system below:*

$$\tilde{\Sigma} : \begin{cases} \dot{z} & = A\, z + B\, v \\ y & = C\, z \end{cases} \tag{2.24}$$

The result above is strong enough to allow the following question: we pursue a φ-diffeomorphism to bring an affine non-linear smooth system to a feedback equivalent affine linear system on a coordinate (Z, φ)-chart.

Theorem 2.2. *The control u-map on $\big(\mathcal{X} \times \mathcal{V} \to \mathcal{U}\big)$-relation at* (2.25)*-expression converts, partial or exact, an affine dynamical system Σ to the feedback equivalent linear 2.24-form. The structure for $\big(A^{\kappa},\, B^{\kappa},\, A^{i},\, B^{i},\, A,\, B\big)$-matrices follows on* (2.26)*-equalities.*

$$\Delta^{-1}\left(y^{\kappa} + B^{\kappa}_{k} v^{k} - A^{\kappa}_{l}\, \tilde{z}^{l}_{\kappa} - L^{\kappa}_{f} h\right) \tag{2.25}$$

$$\begin{cases} A^i = \begin{bmatrix} 0_{\delta_i-1,1} & \mathrm{Id}_{\mathbb{R}^{\delta_i-1}} \\ -a^i & \end{bmatrix} & \textit{and } B^i = \begin{bmatrix} 0_{\delta_i-1,m} \\ b^i \end{bmatrix} \\ A = \mathrm{blkdiag}\left(\{A^i\}_{n_y}\right) & \textit{and } B = \begin{bmatrix} B^1 \\ \vdots \\ B^{n_y} \end{bmatrix} \\ A^\kappa = \mathrm{blkdiag}\left(\{a^i\}_{n_y}\right) & \textit{and } B^\kappa = \begin{bmatrix} b^1 \\ \vdots \\ b^{n_y} \end{bmatrix} \\ C = \mathrm{blkdiag}(\{e_i^1\}_{n_y}), & \textit{for co-versor } e_i^1 \in \mathbb{R}^{1\times\delta_i} \end{cases} \tag{2.26}$$

Proof. Let us consider indexed output h^i-map of the system under subject, then indexed derivative $D^{(j)}y^i$-map is equal to Lie $L_f^j h^i$-derivative, for $\left(j \in \mathbb{N}^*_{\leq \delta_i - 1}\right)$-index. The system exhibits the following form for j-index equal to relative δ_i-degree .

$$(y^i)^{(\delta_i)} = L_f^{\delta_i} h^i + \underbrace{\left(L_{g_k} L_f^{\delta_i - 1} h^i\right)}_{\Delta_j^i} u^j \tag{2.27}$$

The control u-map converts the non-linear affine dynamical system on A.22-appendix to a, partial or exact, feedback equivalent linear dynamical $\tilde{\Sigma}$-system. For such, we consider the error decay for $\left(i \in \mathbb{N}^*_{\leq n}\right)$-index below.

$$(\tilde{y}^i)^{(\delta_i)} + a^i_{\delta_i - 1}(\tilde{y}^i)^{(\delta_i - 1)} + \cdots + a^i_0 \tilde{y}^i = b^i_j v^j \tag{2.28}$$

Real $\left(a_k^i \in \mathbb{R}\right)$-coefficients, for k-index within 0 and $\delta_i - 1$, correspond to monomials of the characteristic polynomial whose roots are given by $\{\lambda_{i,j}\}$-set of δ_i $\left(\lambda_j^i \in \mathbb{C}^-\right)$-eigenvalues. We define a new state δ coordinate $(X_\delta, \varphi_\delta)$-chart employing δ $L_f^{(j)} h^i$-maps. Hence, the equivalent dynamical system on the constructed coordinate chart is linear and the deviation velocity $\dot{\tilde{z}}^i$-vector is below.

$$A^i_k (\tilde{z}^i)^k + B^i_k v^k \tag{2.29}$$

In the above description, $\tilde{z}^i$-vector, for $\left(i \in \{\zeta_i, \cdots, \zeta_{i+1} - 1\}\right)$-index[5] corresponds to output states and its $\delta_i - 1$ derivatives, given by map $\begin{bmatrix} \tilde{z}^{\zeta_i} & \cdots & \tilde{z}^{\zeta_{i+1}} \end{bmatrix}^\intercal$-vector. A necessary condition consists of controllable linear (A^i, B^i)-tuples. We assemble equality (2.27) to obtain control equality below:

$$\Delta_j u^j + L_f^\kappa h = y^\kappa - A^\kappa_l \tilde{z}^l_\kappa + B^\kappa_k v^k \tag{2.30}$$

The rearrangement and left-multiplication by resulting coupling (co-)distribution Δ_q^{-1}-inverse on regular $\left(q \in \mathcal{Q}\right)$-points brings the control u-map on (2.25)-expression to light. ■

[5]Definition of accumulated relative degree ζ_i is on appendix.

The poles for the deviation polynomial are relevant for system tracking precision and dynamic behavior. 2.5-Lemma provides physical time constants intuition for the one-variable case. The systematic is similar to the multivariable case, such that λ-factor corresponds to the eigenvalue with the greatest real part negative magnitude.

Lemma 2.5. *Given an ordinary differential linear* $\big(\dot{x} = -\lambda\, x\big)$*-equality ,* $\lambda \in \mathbb{C}^{-}$*, than the states come close to 0 by a p-factor on time* T_p*-scalar if the real* $\mathfrak{R}\{\lambda\}$*-part corresponds to real* $\big(-\frac{1}{T_p}\ln p\big)$*-constant.*

Proof. The $x(t)$-solution for the proposed equation is $e^{\lambda t}\, x_0$. For decay time T_p-constant and x-point at this instant as $\big(x(T_p) = p\, x_0\big)$-equality, then the steps to obtain λ-factor follow.

$$\exp\left(\lambda\, T\right) x_0 = p\, x_0 \iff \lambda = \frac{1}{T_p}\,\ln\left(p\right) \tag{2.31}$$

■

We complete the φ_δ-map composed by δ maps relative to y-outputs and its δ_i Lie-derivatives with a ψ-map of $\big(n - \delta\big)$-dimension.

The diffeomorphic state-coordinate map

Given output h-map, the interpretation of diffeomorphic φ-map as a coordinate map of coordinate $(Z,\, \varphi_\delta)$-chart to $\mathcal{X}$-manifold is natural by the collection of δ_i output Lie derivatives as a new coordinate map.

For system dimensionality and geometry constraints, it is impossible to exist a diffeomorphism of n_x-dimension only by choice of δ maps, lesser than state manifold dimension. Hence, we must choose a map ψ to obtain the required morphism.

In a broad sense, it is not simple to acquire the necessary ψ-map. Additionally, for given ψ-map, the inverse $\varphi^{-1}(\varphi_\delta,\, \psi)$-map may require cumbersome implicit maps. A possible choice procedure for ψ-map is e.g. to annotate missing variables of acquired Lie-derivative z^i-maps and aggregate them as map-elements ψ-vector. In this way, we bring ease to the inverse procedure. The unavoidable drawback of the inverse φ^{-1}-computation corresponds to its $\mathbb{D}_{\varphi^{-1}}$-domain.

$$z^i = \begin{bmatrix} L_f^0 h^i \\ L_f^1 h^i \\ \vdots \\ L_f^{\delta_i - 1} h^i \end{bmatrix},\quad \varphi_\delta = \begin{bmatrix} z^1 \\ \vdots \\ z^p \end{bmatrix}, \varphi = \begin{bmatrix} \varphi_\delta \\ \psi \end{bmatrix} \tag{2.32}$$

Remark 5. The resting $\big(x_e \in \mathcal{X}_e\big)$-points of the original affine dynamical Σ-system remain unchanged by this map since the $\big(\left(L_f^k\, \varphi\right)\left(x_e\right) = \left(\varphi_* \circ f\right) \circ x_e \coloneqq 0\big)$-equalities hold.

The zero dynamics

The zero dynamics refers to the geometrical locus of initial x^0-points such that flow trajectory $\phi(\tau, x^0)$-curve is indistinguishable from observation output $(h \circ \phi)(\tau_0, x^0, t)$-map and equal to 0. Author Isidori provides an instructive bibliographic review of its historical evolution and influence on controller synthesis strategies in [46]-textbook: It relates to the observability concept of dynamical systems, available on [47]-work. Related to system observability, the zero dynamics of nonlinear dynamical systems are equivalent to transmission zeros on multivariable linear systems. For this concept, an interested reader may refer to ([48], [49])-textbooks.

Lemma 2.6 ([36]). *An affine dynamical Σ-system exhibits zero dynamics if its total relative δ-degree is lesser than the $(n_q + n_p)$-dimension of product $(\mathcal{Q} \times T\vartheta)$-manifold.*

Map ψ on diffeomorphic map (2.32) represents a such complementary map. The first-order $D\psi$-derivative on the (2.33)-expression represents the system zero-dynamics respective to ψ-map. Since it does not exhibit any particular structure, its stability analysis depends on the system under study.

$$\psi_* \, \dot{x} = L_f \, \psi + (L_{g_i} \, \psi) \, u^i \tag{2.33}$$

Observation and tracking maps as outputs

We consider a further extension for affine dynamical Σ-system by an observation h_o-map. The additional requirement is to design a tracking control $\hat{u}$-map, with hat notation long description explained shortly, of trajectory curve y defined by h-map through its h_o-observations along time. The above-obtained control map requires available states to evaluate the control map. Hence, it is sufficient for the observation h_o-map to be observable on interest regions according to A.5-criterium in appendix such that it allows control $\hat{u} \coloneqq u(\hat{x}, v(\hat{x}))$-map to converge to desired input $u(x, v)$-map.

Since the under-study system requires observability according to map h_o, an observer development solves the state reconstruction issue. In the linear case, we dispose of the linear Luenberg observer based placement and Kalman filter based on noise mitigation for the observable case. Several nonlinear observers' propositions are on [50]-work. For the current work, our interest is the state estimation for affine systems. The current author may cite constructive research ([51], [52], [53])-sources.

The dynamic extension for non-regular systems

The dynamic extension algorithm stems from the partial linearization procedure in the rank-deficient decoupling Δ-distribution case. In such a case, its rank is 0 for every $(x \in \mathcal{X})$-state. We find the solution for the issue in textbook [41]. It consists of an extension by r integrators, input u-vector redefinition for some new w-input, followed by the usual well-known output derivation procedure until the input w appears again. It iterates until the decoupling matrix exhibits full rank for some non-empty open set.

The current author summarizes the algorithm from [41]-textbook to the computational 1-algorithm in C-appendix.

A natural question about the abovementioned procedure concerns its stop criterium. From intuition, the extended total relative degree *must* be lesser than $(n_x + n_u)$-cardinal. Sastry on his [41]-textbook provides a stop criterium by *regularity assumption*: at each iteration step, if the decoupling Δ_k-matrix exhibits constant rank on some non-empty neighborhood $\big(\mathcal{W}_k \subseteq \mathcal{X}\big)$-set, then the algorithm will terminate in at most n_x iterations. Hence, the extended system has a well-defined vector relative κ-degree, and the compensator exhibits an affine dynamic system structure as on (2.34)-equalities. A detailed version about regularity i.e. system invertibility is in $\big([54], [37]\big)$-references.

$$\begin{aligned} \dot{z} &= a + b_i\, w^i \\ u &= \alpha + \beta_j\, w^j \end{aligned} \tag{2.34}$$

The linearization control strategy of affine dynamical systems extends to approximate control maps for a particular family of affine systems: in such case, we consider topological obstructions on the Σ-structure e.g. regions of non-regular coupling distribution or disjoint submanifolds. We remain on extended non-regular systems, but an interested reader may refer to illustrations in the respective linearization chapters in the [41]-textbook.

3 SOURCE SEEKING EXPLORATORY REFERENCE CURVES

"There are no wrong turnings. Only paths we had not known we were meant to walk."

-- Guy Gavriel Kay, Tigana

Source seeking requires a dynamic agent to acquire signal data and estimate the source position locus. Hence, we require a reference tracking curve to reach its estimation point. The current chapter brings design ideas regarding continuous curve synthesis. Necessary conditions for trajectory synthesis correspond to boundary conditions on start and end points[6]. Since reference $\gamma^{\star}(t)$-curve is free to choose, it disposes of creative design opportunities.

Physical systems may exhibit particular topological behavior respective to their kinematics. Among others, our interest constrains the movement. Slippage might appear and is critical but not relevant to the current work. Nevertheless, the driftlessness hypothesis requires constrained reference trajectories on $\mathcal{X}$-manifold. The following sections develop some possible strategies for trajectory design. Manfredo Perdigão's [55]-textbook is a proper textbook for here-presented concepts.

As smooth continuous

Reference trajectory planning consists of curve synthesis which may not violate kinematic constraints and obeys established configuration points. Among possible algebraic linear basis for trajectory time-series, we choose canonical basis as (3.1)-sets, for some natural $\big(n,\, k \in \mathbb{N}_{>1}\big)$-constants, as observed on [56]-work. The current author provides several numerical and graphical examples in 6-chapter.

$$\begin{cases} \{1,\, t,\, \cdots,\, t^{n}\} \\ \{1,\, e^{t},\, \cdots,\, e^{n\,t}\} \\ \{1,\, t^{k}\,\cos(2\,\pi\,m\,t),\, t^{k}\,\sin(2\,\pi\,m\,t)\} \end{cases} \tag{3.1}$$

A common-used interpolation curve constitutes on the *Bézier's curve*. It coincides with given end-points on its extrema and control points in-between "pull" the curve towards them. It is a natural choice for mobile robots' path planning since it fulfills the coincidental extrema and orientation conditions and is suitable for the constrained case as shown in [57]-work. $B^{i}(\alpha)$-Monomial on (3.2)-expression aids $P(t)$-curve definition within time $[t_0,\, t_1]$-interval, given by $(B^{i}\,P_{i})$-summation in Einstein's sum convention. Bézier

[6]We call "start" and "end" points in computer science as *head* and *tail* points.

monomial B^i depends on simplex linear $\alpha(t)$-map, given by $\frac{t-t_0}{t_1-t_0}$-ratio, both available on 3.2-expression below.

$$\binom{n}{i}\,\alpha^{n-i}\,(1-\alpha)^i \tag{3.2}$$

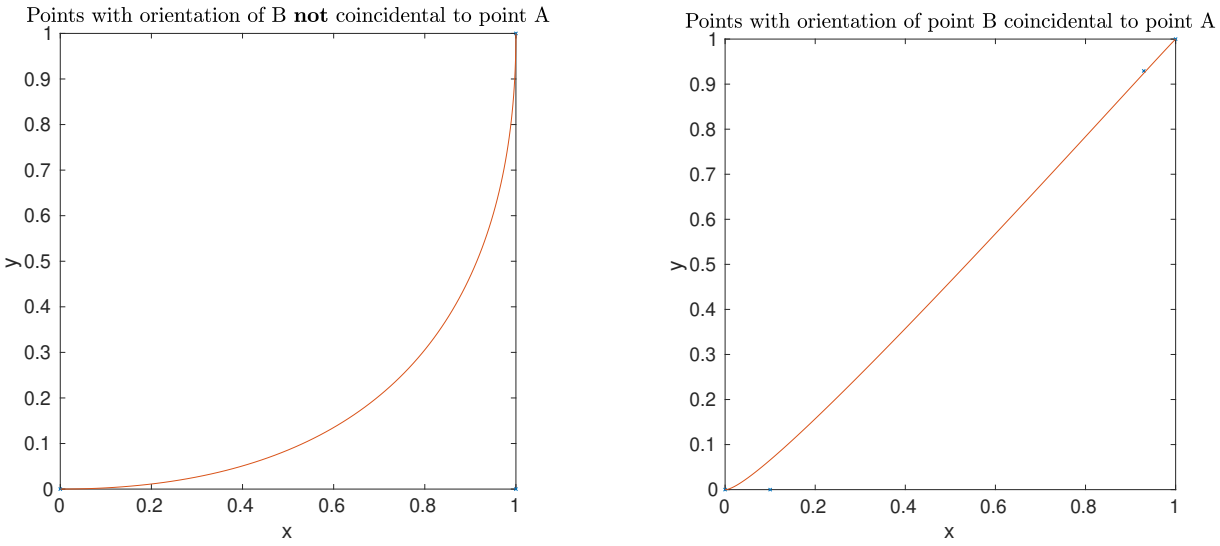

Figure 2: Bézier's curve examples for (non-)concurrency regarding orientation on B-point to A-point. The blue crosses correspond to points added after and before the extremal points.

For plausibility, it may not be possible to either design or perform trajectories from initial to final poses. For instance, we consider the following examples: formerly, the extended line over each point orientation does not contain one another, and in the latter, it does contain.

We solve the above issue under Bézier's curve design. A useful Bézier's curve property follows on 3.1-definition. It suggests further addition of after and before points to start and end $\left(P_0, P_n\right)$-points on ε-weighted orientation directions.

Definition 3.1 (Bézier's curve interpolation property)**.** Given boundary points $\{P_k\}_{k\in\mathbb{N}_{[1,n_p]}}$-set, Bézier's curve velocity $\dot{P}(t)$-vector is tangent to the connecting lines between points $\left[\left(P_0, P_1\right), \left(P_{n-1}, P_n\right)\right]$-tuples.

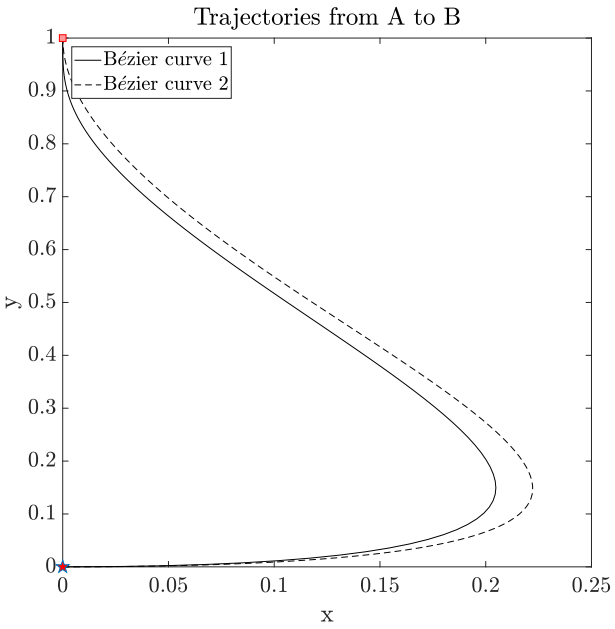

Figure 3: Bézier's curve and its first derivative. The ($\star$, $\blacksquare$)-markers designate respectively the curve start and endpoints.

Bézier's $P(t)$-curve contains a recursive version, the *Casteljeau's Algorithm*, on (3.3)-expression, to consult on [58]-work. Since trajectory tracking requires a finite set of

curve derivatives, its computation in summation form is computationally intensive. The recursive $P_j^i(t)$-form brings ease to both curve and derivative computations. $\big(i, j\big)$-Indexes belongs respectively to ordered index $\big(\mathbb{I}_n, \mathbb{I}_{n-i}\big)$-families.

$$(1-t)\, P_{j-1}^i + t\, P_{j-1}^{i+1} \tag{3.3}$$

The equation above allows us to compute arbitrary explicit derivatives for Bézier's curve. Hence, its k-derivative emerges from the following claim.

Claim 3.1. *The recursive k-derivative $(P_j^i)^{(k)}(t)$-curve of recursively defined Bézier's* (3.3)*-curve corresponds to formation* (3.4)*-rule.*

$$\begin{cases} (1-t)\,(P_{j-1}^i)^{(k)} + t\,(P_{j-1}^{i+1})^{(k)} + k\,\Big((P_{j+1}^{i+1})^{(k-1)} - P_{j-1}^{i,(k-1)}\Big) & ,\ on\ \big(k < j\big)\text{-}condition, \\ k\,(P_{j-1}^{i+1,(k-1)} - P_{j-1}^{i,(k-1)}) & ,\ on\ \big(k = j\big)\text{-}condition \end{cases} \tag{3.4}$$

Proof. We utilize the finite induction concept for proof construction. The first and second derivatives are below. We here-denote i-row and j-column. The term related to condition $\big(j = k\big)$-equality also comes by finite induction: since $\big[(P_1^i)^{(1)} = P_0^{i+1} - P_0^i\big]$-identity as well as $\big[(P_2^i)^{(2)} = 2\,(P_1^{i+1})^{(1)} - (P_1^i)^{(1)}\big]$-identity, than we conclude the k-derivative is $k\,(P_{j-1}^{i+1})^{(k-1)} - (P_{j-1}^i)^{(k-1)}$

$$\begin{array}{rcl} (P_j^i)^{(1)} & = & (1-t)\,(P_{j-1}^i)^{(1)} + t\,(P_{j-1}^{i+1})^{(1)} + P_{j-1}^{i+1} - P_{j-1}^i \\ (P_j^i)^{(2)} & = & (1-t)\,(P_{j-1}^i)^{(2)} + t\,(P_{j-1}^{i+1})^{(2)} + 2\,\big((P_{j-1}^{i+1})^{(1)} - (P_{j-1}^i)^{(1)}\big) \\ \vdots & = & \vdots \\ (P_j^i)^{(k)} & = & (1-t)\,(P_{j-1}^i)^{(k)} + t\,(P_{j-1}^{i+1})^{(k)} + k\,\big((P_{j-1}^{i+1})^{(k-1)} - (P_{j-1}^i)^{(k-1)}\big) \end{array} \tag{3.5}$$

■

We present in 3-Fig both batch and recursive curve derivatives. Although naively given by the close-related formulas, they are not coincidental. The current author encourages future readers to comprehend this algebraic difference.

As piecewise continuous

There are cumbersome choices of discontinued trajectories i.e., reference discrete commands to physical systems to achieve specific points. Despite the familiar concept of continuous control maps, piecewise continuous trajectory curves are less recurrent in literature. We begin with a velocity-driven system and extend it to acceleration.

For simplicity, consider a constrained system by the following approach: Given initial and final pose configurations of a differential robot, also known as *Dubin's car*, we look for a curve synthesis procedure in finite time on points $(A \to B)$-relation. Sastry on his [41]-textbook suggests two possible trajectory families: *piecewise constant* and *optimal*

trajectories. For practical issues under the jurisdiction, an optimal curve is not necessary, although possible. Hence, a naïve choice of a piecewise constant path satisfies given boundary constraints.

Proposition 3.1. *Let us compose a $\gamma(t)$-curve by two time intervals: a former rotation with constant angular ω_0-speed and a latter translation with linear v_0-speed. From previous kinematic parameters, we set the steering $(\Delta t_1,\, \Delta t_2)$-intervals according to $\left(\frac{\theta_1-\theta_0}{\omega_0},\, \frac{d}{v_0}\right)$-tuple*[7].

A time-variant choice for angular and linear speed $\big(\omega, v\big)(t)$-curves smooth transitions out. The smoothed transitions between lower and upper step values avoid abrupt, also known as *non-Lipschitz*, control map measures. Among the possible smoothstep time series, we consider a normalized $\mathrm{S}_n(\alpha)$-polynomial, for an arbitrary natural n-degree on its definition (3.6)-expression.

$$\begin{cases} 0 & \text{if } \alpha \leq 0 \\ \displaystyle\sum_{k=0}^{n} \binom{n+k}{k} \binom{2n+1}{n-k} (-\alpha)^{k+n+1} & \text{if } 0 \leq \alpha \leq 1 \\ 1 & \text{if } 1 \leq \alpha \end{cases} \tag{3.6}$$

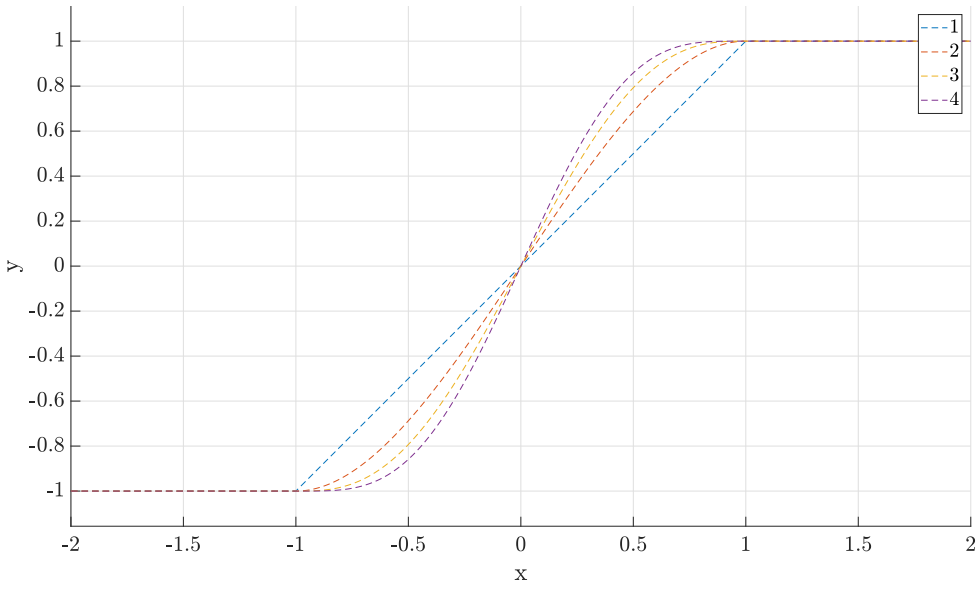

Figure 4: Smoothstep polynomial map for maximal $\big[1 \quad 2 \quad 3 \quad 4\big]$-degrees.

As mentioned above, trajectory derivatives are necessary curves for the control map computation. For the n_s-derivative $D^{(n_s)}\,\mathrm{S}_n(x)$-curve, we follow (3.7)-formula. Since the polynomial ring family belongs to C^∞-class, we may differentiate (3.7)-map respective to α-variable a $\big(n+1\big)$-cardinal times and beyond.

$$\begin{cases} 0 & \text{if } \alpha \leq 0 \vee \alpha \geq 1 \\ \displaystyle\sum_{k=0}^{n-n_s} (-1)^k \binom{n+k}{k} \binom{2n+1}{n-k} \binom{n+k+1}{n_s} \alpha^{n+k-n_s+1} & \text{if } 0 \leq \alpha \leq 1 \end{cases} \tag{3.7}$$

[7]For the Euclidean $\mathbb{R}^n$-space, θ_1-angle is equal to $\arg\left(P_1 - P_0\right)$-formula and d-distance is equal to $\|P_1 - P_0\|$-norm.

A question remains about curve scale: since the above map presents unitary amplitude, the scale σ-map on $\big([-1,1]\times\mathbb{R}^2 \to \frac{a+b}{2}+\frac{b-a}{2}\,x\big)$-relation translates and scales, for $\big(a,b\big)$-parameters as lower and upper step bounds. Also, we require inverse σ_x^{-1}-map respective to x-entry i.e. $\sigma_x^{-1}(a,b,y)$-map on $\big([a,b]\to[-1,\,1]\big)$-relation, given by $\big(-\frac{a+b}{b-a}+\frac{2}{b-a}\,y\big)$-formula. Therefore, for instant $[t_0,t_1]$-interval and given lower and upper $\big(m_-,m_+\big)$-bounds, we obtain the scaled smoothstep $S(t)$-map by cascade composition $\sigma(m_-,\,m_+,\,x)\big|_{x=\left(S_n\,\circ\,\sigma_x^{-1}\right)(t_0,\,t_1,\,t)}$-map.

Alternatively, we compose a piecewise smooth continuous curve of straight lines and circular arcs. The circular arc loci are not coincidental but appear for finite constant angular and linear speeds. Among theme-concerned researchers, authors Dubins, Reeds & Shepp develop extensively minimal curves in Euclidean $\mathbb{R}^2$-space in $\big([59],\,[60]\big)$-articles.

The pairwise point-to-point trajectory planning (P2P for short) consists of developing a piecewise line-circle-based curve. Among possible configurations, we describe the trajectory synthesis below.

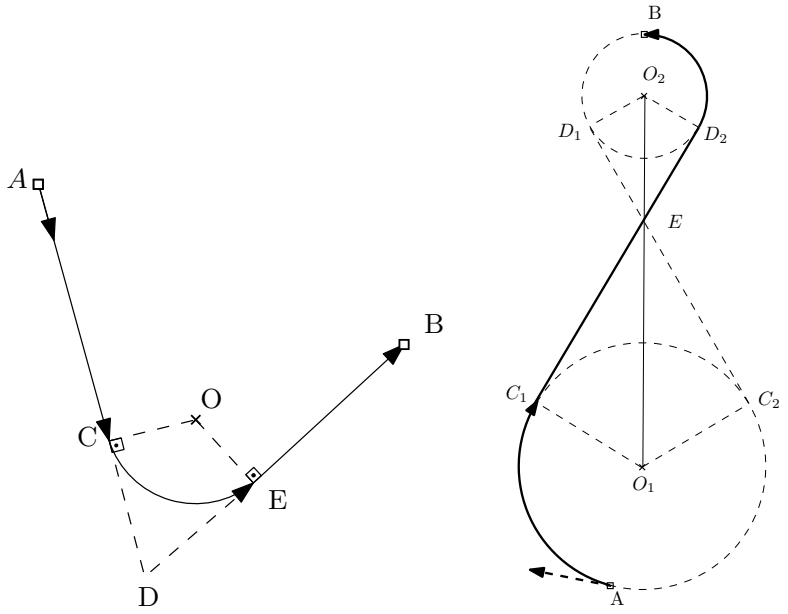

a. Line-arc-line trajectory b. Arc-line-arc trajectory

Figure 5: Piecewise circle-line-based continuous curve

Proposition 3.2 (5a.-Figure)**.** *Given $\big(A,B\big)$-points and respective $\big(\hat{r}_0,\hat{r}_1\big)$-orientations, we depict on 5a.-Figure a piecewise smooth $\gamma(t)$-curve between these two points by below formulation.*

$$\begin{cases} A+v_0\,t\,\hat{r}_0 & t\in[0,t_0] \\ \rho\begin{bmatrix} c(\omega\,(t-t_1)+\phi) \\ s(\omega\,(t-t_1)+\phi)\end{bmatrix}-O & t\in(t_0,t_1] \\ E+v_2\,(t-t_2)\,r_1 & t\in(t_1,t_2]\end{cases}\text{, for }\begin{cases} t_0=\alpha\,\frac{d(A,\,D)}{v_0} \\ t_1=t_0+\frac{C\hat{O}E}{\omega} \\ t_2=t_1+\frac{d(E,\,B)}{v_2}\end{cases}\text{ -instants.} \tag{3.8}$$

Proof. $\gamma(t)$-Curve exhibits notable $\big(C,D,E,O\big)$-points on 5b.-figure. Given orientation

column $\big(\hat{r}_0, \hat{r}_1\big)$-vectors respective to $\big(A, B\big)$-points, then C-point comes from the conjugate point $\big(D \coloneqq A + \mu\,\hat{r}_0 = B + \lambda\,\hat{r}_1\big)$-equality, for real-valued $\big(\mu,\, \lambda \in \mathbb{R}\big)$-constants. We build a solution up on (3.9)-equality.

$$\begin{bmatrix} \mu \\ \lambda \end{bmatrix} = A_{\mu\lambda}^{-1}\, b_{\mu\lambda}, \text{ for parameters } \begin{cases} A_{\mu\lambda} = \begin{bmatrix} \hat{r}_0 & -\hat{r}_1 \end{bmatrix}, \\ b_{\mu\lambda} = B - A \end{cases} \tag{3.9}$$

$$\begin{cases} D = A + \mu\,\hat{r}_0,\ \mu \in \mathbb{R} \\ C = A + d(A, C)\ \ \hat{r}_0, \quad \text{such that } d(A, C) = \alpha\, d(A, D) \\ E = D + d(C, D)\ \ \hat{r}_1, \quad \text{such that } d(C, D) = (1 - \alpha)\, d(A, D) \end{cases} \tag{3.10}$$

Since we require existing solution(s) for (3.9)-equality, determinant $\det\left(A_{\mu\lambda}\right)$-map must not be null: it is necessary and sufficient for orientation $\hat{r}_i$-vectors to be non-parallel. Furthermore, conjugate D-point must exist. In the same manner, as for conjugate D-point, O-point corresponds to a conjugate point of straight lines (i.e. geodesic curves) given by the point-vector $\big[(D,\, s_0), (E,\, s_1)\big]$-tuples, for every s_i-vector such that $\big(\langle \hat{r}_i, s_i \rangle = 0\big)$-equality holds. Hence, it corresponds to a solution on $\big(O \coloneqq D + \upsilon\, s_0 = E + \tau\, s_1\big)$-equality, for real-valued $\big(\upsilon,\, \tau\big)$-constants.

$$\begin{bmatrix} \upsilon \\ \tau \end{bmatrix} = A_{\upsilon\tau}^{-1}\, b_{\upsilon\tau}, \text{ for parameters } \begin{cases} A_{\upsilon\tau} = \begin{bmatrix} s_0 & -s_1 \end{bmatrix} \\ b_{\upsilon\tau} = E - D \end{cases} \tag{3.11}$$

$$\begin{cases} \rho = d(O,\, D) = \|O - D\|_2 \\ \omega = \frac{v_1}{\rho} \\ \phi = \tan^{-1}(\arg\left(C + O\right)) \end{cases} \tag{3.12}$$

Additionally, the argument between $\big(\overline{CD}, \overline{CE}\big)$-segments i.e. $C\hat{D}E$-argument, supplemental in flat space to argument $C\hat{O}E$ given by computation $\arg\left(-r_0, r_1\right)$. Therefore, $C\hat{D}E$-argument is equal to $\pi - \arg\left(-r_0, r_1\right)$. The corner case is once more the parallel orientation, which leads to null $C\hat{O}E$-argument. Finally, we describe the $\gamma(t)$-curve with initial and end $\big(A, B\big)$-points by $\gamma_3(t)$-parametrization equal to $E + (v_2\,\hat{r}_1)\,t$, for $t \in \left[0, \frac{d(E,B)}{v_2}\right]$-instant. The local parametrization by t-instant starts from the absolute instant on A-point, here as null 0-constant.

$$\begin{cases} A + v_0\, r_0\, t & t \in [0, t_0] \\ \rho \begin{bmatrix} c(\omega\,(t - t_1) + \phi) \\ s(\omega\,(t - t_1) + \phi) \end{bmatrix} - O, & t \in (t_0, t_1] \\ E + v_2\, r_1\,(t - t_2) & t \in (t_1, t_2] \end{cases}, \text{ for } \begin{cases} t_0 = \alpha\, \frac{d(A,D)}{v_0} \\ t_1 = t_0 + \frac{C\hat{O}E}{\omega} \\ t_2 = t_1 + \frac{d(E,B)}{v_2} \end{cases} \tag{3.13}$$

■

The above proposition provides a systematic procedure to obtain the trajectory curve

from $\big(A, B\big)$-points with given $\big(\hat{r}_0, \hat{r}_1\big)$-orientations. However, in a counter-example pursuit, the 3.2-proposition algorithm fails to design a trajectory if given orientations are (quasi-)parallel: the arc sector decreases monotonically to zero, infeasible for the case of finite angular speed.

We present a trajectory curve candidate without the drawback mentioned above in 5b.-figure. Differently from the former, it constitutes an arc-line-arc partition. Its main kinematic properties to obtain r_i-radii, ϕ_i-argument and O_i-point, for $\big(i \in \{0, 1\}\big)$-index, follows below. Their main properties were firstly given by Dubins on [59]-work.

Lemma 3.1 ([59])**.** *Given non-tangent $\big(O_0, O_1\big)$-circles, we obtain the inner tangent lines through finite logical steps of geometric and analytic relations on manifolds.*

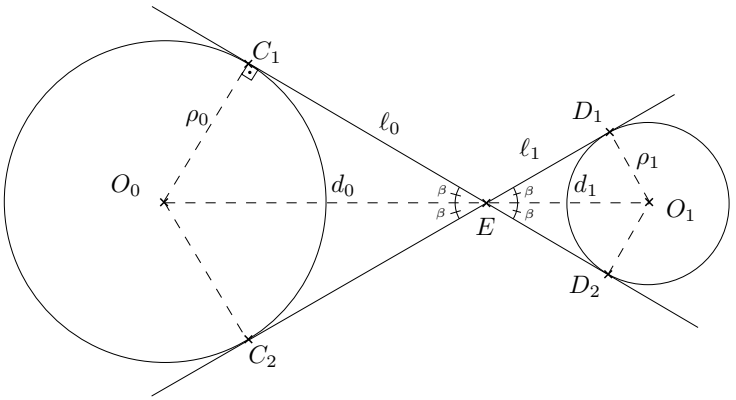

Figure 6: Inner tangent lines to non-tangent circles 0 and 1

Proof. We start this proof statement with $d(O_0, O_1)$-distance between circle center $\big(O_0, O_1\big)$-points equal to d_{01}, given by $\big(d_0 + d_1\big)$-sum. The conjugate E-point of $\big(\overline{C_1D_1}, \overline{C_2D_2}\big)$-segments divides $\overline{O_0O_1}$-segment into two $\big(\overline{O_0E}, \overline{O_1E}\big)$-segments with respective $\big(\ell_0, \ell_1\big)$-lengths. From triangle likeness in a flat space[8], we conclude that d_0-distance corresponds to $\frac{r_0}{r_1}\, d_1$-expression. Thus, it leads to equivalence $\Big(d_{01} = \Big(1 + \frac{r_0}{r_1}\Big)\, d_1 \iff d_1 = \Big(\frac{r_1}{r_0 + r_1}\Big)\, d_{01}\Big)$-relation, which we recognize the simplex $\frac{r_1}{r_0+r_1}$-term. The resulting distances d_0 and d_1 turns into $\big((1-\alpha)\, d_{01}, \alpha d_{01}\big)$-computations.

From Pythagorean relation in flat space, the (ℓ_0, ℓ_1)-lengths between tangency and interception points corresponds to $(\sqrt{d_0^2 - r_0^2}, \sqrt{d_1^2 - r_1^2})$-tuple. Finally, we calculate interception E-point equal to weighted $\big((1-\alpha)\, O_0 + \alpha\, O_1\big)$-sum. $O_0\hat{E}C_1$-Argument, equal to $O_1\hat{E}D_1$ in flat space and here-denoted by greek β-symbol, is useful to obtain tangency points, on (3.14)-equalities.

$$\begin{cases} C_1 &= E + R(\beta)\, \widehat{O_0\, E}\, \ell_0 \\ C_2 &= E + R(-\beta)\, \widehat{O_0\, E}\, \ell_0 \\ D_1 &= E + R(\beta)\, \widehat{O_1\, E}\, \ell_1 \\ D_2 &= E + R(-\beta)\, \widehat{O_1\, E}\, \ell_1 \end{cases}, \text{ with } \beta \text{ equal to } \arctan 2\Big(\frac{\rho_0}{d_0}, \frac{\ell_0}{d_0}\Big) \tag{3.14}$$

[8]For triangulation in a curved space, we require the famous Gauss-Bonnet theorem. It relates to a two-dimensional manifold with its K-curvature, geodesic k_g-curvature, and its Euler $\chi(\mathcal{M})$-characteristics on polyedric enclosed geodesics.

■

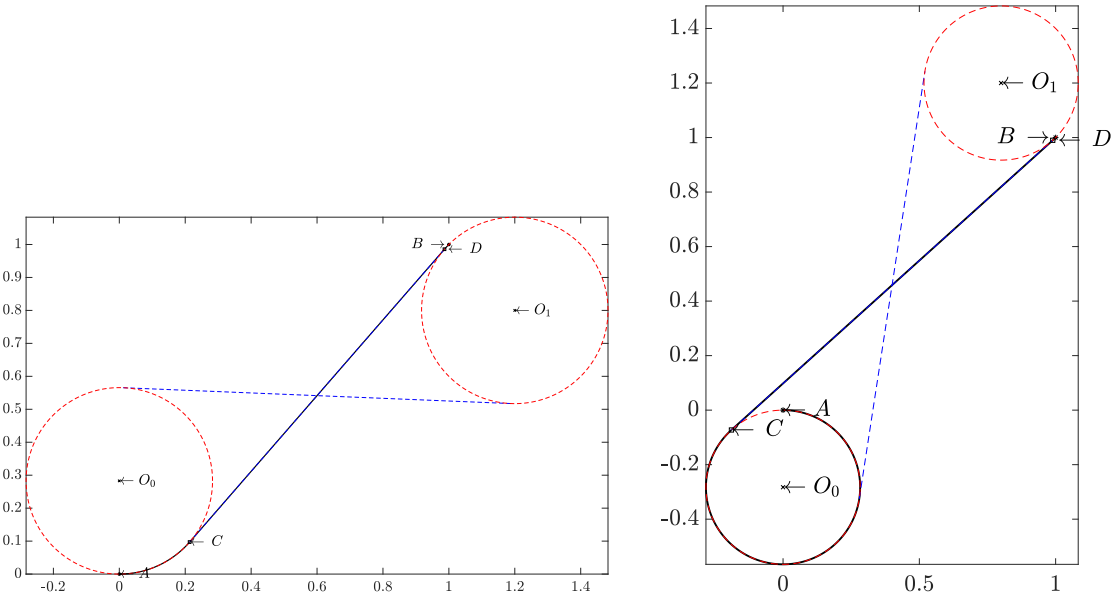

a. Clockwise-anticlockwise trajectory b. Anticlockwise-clockwise trajectory

Figure 7: Feasible curves from origin point oriented on 0 rad to $[1,\, 1]^{\intercal}$-point on $\frac{\pi}{4}$ rad.

Proposition 3.3 (7-Figure)**.** *Given continuous $\gamma(t)$-curve on 3.1-lemma and circles on 6-figure, the piecewise $\big(\gamma_1(t), \gamma_2(t), \gamma_3(t)\big)$-curves on curly-braced* (3.15)*-map connects both given $\big(A, B\big)$-points by boundary $\big(r_0, r_1\big)$-orientations.*

$$\begin{cases} r_0 \begin{bmatrix} c(\omega_0\, t + \phi_0) \\ s(\omega_0\, t + \phi_0) \end{bmatrix} + O_0 & t \in [0,\, t_1] \\ C + v_{01}\,(t - t_1)\,\widehat{CD} & t \in (t_1, t_2] \\ r_1 \begin{bmatrix} c(\omega_1\,(t - t_2) + \phi_1) \\ s(\omega_1\,(t - t_2) + \phi_1) \end{bmatrix} + O_1 & t \in (t_2,\, t_3] \end{cases} \tag{3.15}$$

for instant $(t_1,\, t_2,\, t_3)$-tuple given by relations below:

$$\left(\frac{A\hat{O}_1 C}{\omega_0},\, t_1 + \frac{d(C, D)}{v_{01}},\, t_2 + \frac{B\hat{O}_2 D}{\omega_1} \right)$$

Proof. The available data on the issue corresponds to the start and end $\big(A, B\big)$-points, and their respective $\big(r_0, r_1\big)$-orientations. Thus, it is free and reasonable to choose each circle radius by the distance ratio between $\big(A, B\big)$-points, such that the sum of both does not extrapolate the actual $d(A,\, B)$-distance. Formally, we obtain necessary $\big(\rho_0 + \rho_1 \overset{!}{\leq} d(A, B)\big)$-condition, or also given by simplex-proportional $\big(\alpha_0\, d(A, B), \alpha_1\, d(A, B)\big)$-scalars such that $\big(\alpha_0 + \alpha_1 \leq 1\big)$-condition holds. Similarly, center $\big(O_0, O_1\big)$-points belong to lines extended by perpendicular $\big(0, 1\big)$-orientations, respectively. Therefore, from the perpendicularity condition, we obtain r_i-orientation and perpendicular s_i-vector, for $\big(i \in \{0,\, 1\}\big)$-index, there are four possible center points, here-denoted by superscript $\pm$-notation.

$$\begin{aligned} O_0^{\pm} &= A \pm \rho_0\, s_0 \\ O_1^{\pm} &= B \pm \rho_1\, s_1 \end{aligned} \tag{3.16}$$

We look for the sufficiency of point $\big(C, D\big)$-tuple: it emerges from curve smoothness and continuity criteria. For curve $\gamma_i(t)$-parametrization on (3.17)-expression and at t_i-instant, curve $\gamma_i(t_i)$-point coincides respectively to $\big(C, D\big)$-pointsin. As such, the orientation compatibility $\big(\dot{\gamma}_i(t_i) = \dot{\gamma}_{i+1}(t_{i+1})\big)$-equalities must hold.

$$\rho_i \begin{bmatrix} \cos\left(\omega_i\, t + \phi_i\right) \\ \sin\left(\omega_i\, t + \phi_i\right) \end{bmatrix} + O_i, \text{ for } \big(i \in \{0,\, 1\}\big)\text{-index} \tag{3.17}$$

Since we obtain two argument ϕ_i-solutions, we require a disambiguation condition: at both $\big(t_1, t_2\big)$-instant, the orientation of normalized velocity $\widehat{\dot{\gamma}}$-vector must coincide due $\left(\left\langle \widehat{CD},\, \widehat{\dot{\gamma}}(t_j) \right\rangle = 1\right)$, for $\big(j \in \{1,\, 2\}\big)$-index. Hence, we may choose the shortest length $\gamma(t)$-curve.

Finally, we compute the time interval tuples and respective $(t_1,\, t_2,\, t_3)$-timestamps. Firstly, we assign Q_i-notation to element on ordered point $\{C, D\}$-set and $\bar{Q}$-point to its complement, as well as $\big(P, \bar{P}\big)$-points belongs to ordered point $\{A,\, B\}$-set. It means, $\widehat{\bar{Q}Q}$-argument corresponds to either $\widehat{DC}$-argument or $\widehat{CD}$. Therefore, the time intervals for each curve piece correspond to $\left(\frac{\varphi_i}{\omega_i}, \frac{d(C,\,D)}{v_{01}}, \frac{\varphi_i}{\omega_i}\right)$-tuple, for φ_i-argument equal to $\arg\left(Q - O_i,\, P - O_i\right)$ and $\big(i \in \{0,\, 1\}\big)$-index. ■

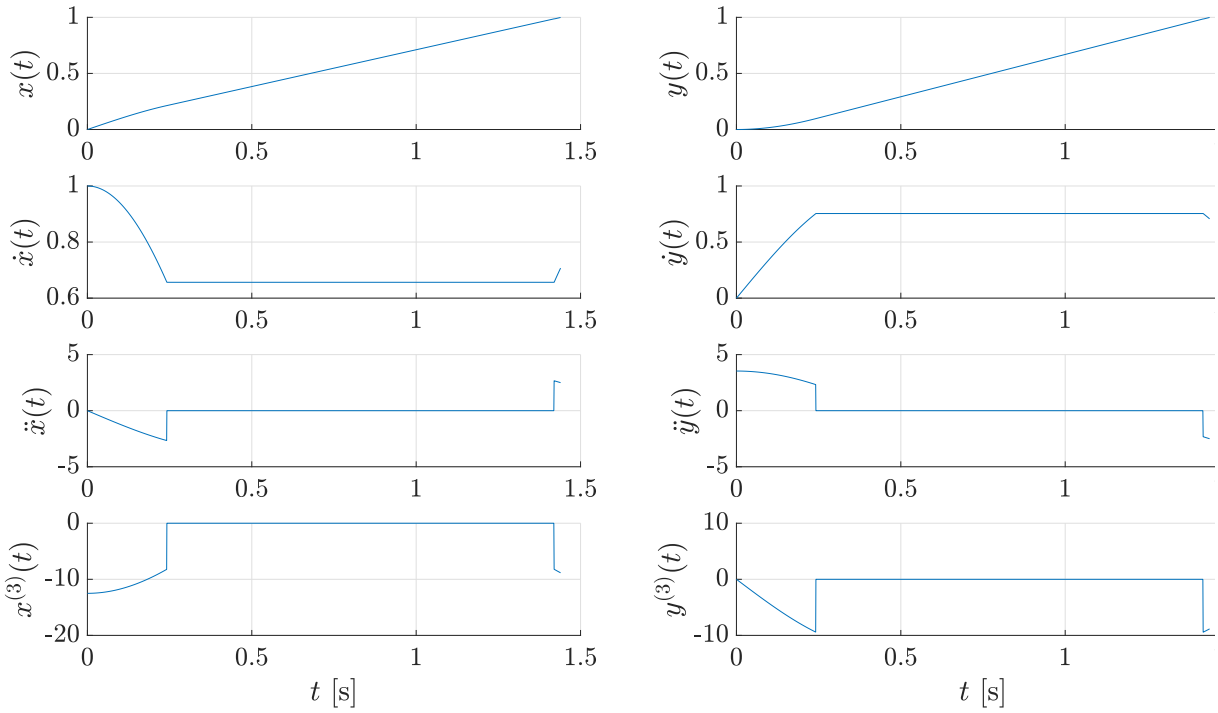

a. Clockwise-anticlockwise orientation

Figure 8: Trajectory $s(t)$-curves from 7-figure and its derivative $\big(\dot{s}, \ddot{s},\, \dddot{s}\big)(t)$-curves

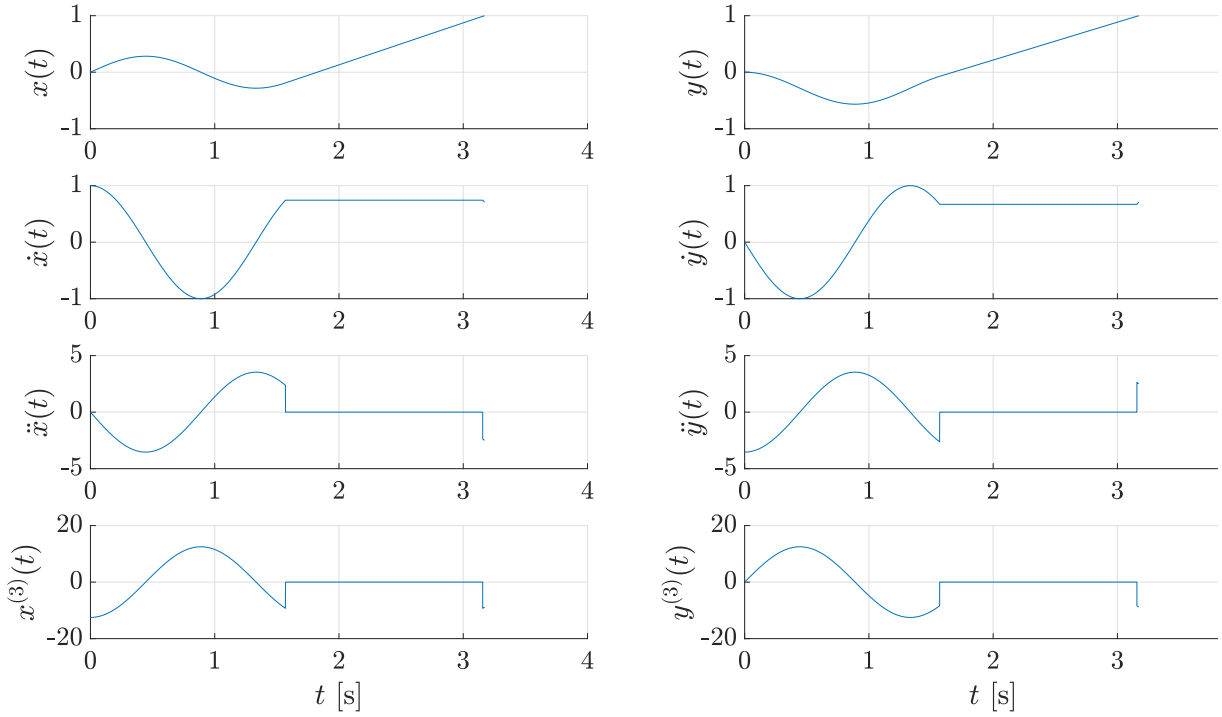

b. Anticlockwise-anticlockwise orientation

In mobile robotic applications, it is common for agents to navigate on flat obstacle-free surfaces. However, these are unrealistic conditions since, in most compelling commercial and industrial applications, robots navigate among obstacles and humans on a topologically curved surface. This requirement suggests developing obstacle avoidance strategies for free-collision steering around navigation space.

4 OBSTACLE AVOIDANCE IN SOURCE SEEKING

"You measure the size of the accomplishment by the obstacles you must overcome to reach your goals."

-- Booker T. Washington

From a navigation perspective, a common obstacle representation relies on a surface definition with low curvature near target points and high curvature nearby obstacles. Although this approach is possible, it creates moral-equivalent local minima by a combination of positive and negative curvatures: the competing attraction and repulsion forces. Paternain *et al.* on [61]-work deal with this duality by exponents and map root evaluations. Such arguments are unreasonable for practical matters: they smooth zero–gradient points out and flatten space enough to turn applications numerically ineffective.

Common strategies in control theory set velocity equal to map gradient. Likewise, Newton sets accelerations similar to forces, and Koditschek sets robot torques equal to gradients. Geometry innovates on the issue with pertinent concepts: by space endowment with a Riemannian metric, such that each point has a continuous *obstruction measure*, which relates to its curvature.

The above procedure embeds a 2D surface in 3D space: the two plane coordinates plus obstruction degree. The Riemannian metric components for the defined surface is a routine calculation procedure, dependent on closed-form derivative computation — explicit formulas are to consult in ([55], [62])-textbook. Curves nearby inaccessible points are long and the shortest curve between two points avoids obstacles.

The equivalent concept to straight lines in Riemannian geometry is geodesics. Unless accelerated, robots move on geodesics: it reinforces the argument of second-order movement by an acceleration set instead of velocity as the input signal. In flat geometry, the velocity derivative along straight lines is zero. Additionally, following geodesics with constant speed means zero covariant derivatives of velocity $\dot{\gamma}$-vector respective to itself. The curvature related to space metric g-tensor corresponds intuitively to a virtual force: it pushes trajectories away from inaccessible points. Navigation now consists in moving towards the goal over short distances.

In summary, the approaches under consideration in this introduction are:

1. Paternain *et al.* approach sets torque proportional to map gradient vector field: descent direction may climb walls up and geometry-related "fictitious forces" slow movement down. It leads the robot to resort to moral-equivalent local minima;

   Workaround: add exploration terms in varying directions. As avoiding-obstacles movement are easier than otherwise, the exploration efforts move the robot away from the configuration stuck points.

2. Geodesic curve frequent computation from the current point to the desired destination: it is hard to compute and may not be unique.

   Workaround: perform offline at–the–large computations, leaving fine-tuning local calculations for explicit formula. A close approach investigation requires further differential geometry research.

3. Recursive optimization of error plus distance: it also requires further research development;

Obstruction geometry

As mentioned in this chapter introduction, the *obstruction surface* requires high curvature values near obstacles respective to its base surface. A manner to represent obstacles on manifolds is by compact submanifolds, with or without borders. Geometrically, a possible construction procedure for obstacles constitutes "glued" submanifolds by application of the lemma for smooth manifold construction from [63]-textbook.

From an engineering perspective, we require algebraic explicit expressions for surface construction and further computation of local and global geometrical properties on the state $\mathcal{Q}$-manifold. Dombrowski develops in [64]-work the required geometrical equalities for geodesic calculation on implicit-defined submanifolds. The main constructive results follow below.

Definition 4.1 (Submanifolds defined by implicit equalities)**.** Let us define a n-dimensional $\mathcal{C}^{\infty}$-class Riemannian $\mathcal{X}$-manifold endowed with inner $\langle \cdot, \cdot \rangle^{\mathcal{X}}$-product i.e. metric g-tensor. Additionally, let us define implicit real-valued maps $\{\varphi_m\}$-set on a base $\mathcal{X}$-manifold, such that vector $\operatorname{grad}_p^{\mathcal{X}} \varphi_i$-fields are linearly independent. Thus, we define the $\mathcal{F}$-submanifold given by set-defined (4.1)-region.

$$\{p \in \mathcal{X} \,|\, \varphi_\mu(p) = 0, \text{ for index } \mu \text{ from 1 to } m\} \tag{4.1}$$

Theorem 4.1 ([64])**.** *Let c-curve on $\big([\alpha, \beta] \to \mathcal{X}\big)$-relation represent $\mathcal{C}^{\infty}$-class curve in manifold $\mathcal{X}$ such that velocity vector $\big(\dot{c}_\alpha \in T_{c(\alpha)}\mathcal{F}\big)$-field. The below statements are equivalent:*

1. *c is a geodesic curve on Riemmanian $\mathcal{F}$-submanifold*[9]
2. *c satisfies the differential (4.2)-equality below:*

$$\overset{\mathcal{X}}{\nabla}_D \dot{c} = -\sum_{\lambda\,\mu=1}^{m} (\Phi_{\lambda\,\mu} \circ c)\, hess^{\mathcal{X}} \varphi_\lambda(\dot{c},\, \dot{c})\, c^*\, grad^{\mathcal{X}}\, \varphi_\mu \tag{4.2}$$

Remark 6. In Einstein's sum convention, the geodesic curve differential (4.2)-equality exhibits format as on (4.3)-equality. Gramian $\Phi_{\lambda\,\mu}$-matrix is a symmetric-defined regular matrix.

[9] A geodesic c-curve in $\mathcal{X}$-manifold exhibits null covariant derivative $\Big(\overset{\mathcal{F}}{\nabla}_D \dot{c} = 0\Big)$-equality.

$$\overset{\mathcal{X}}{\nabla}_D \dot{c}^{\nu} = -\Upsilon^{\nu}_{\mu}\, \Phi^{\mu}_{\lambda}\, \eta^{\lambda} \tag{4.3}$$

The required column/row-defined $\big(\Upsilon_{\mu}, \eta^{\lambda}\big)$-matrices follow below.

$$\begin{aligned} \Upsilon_{\mu} &= c^{*}\, \mathrm{grad}^{\mathcal{X}}\, \varphi_{\mu} \\ \eta^{\lambda} &= \mathrm{hess}^{\mathcal{X}}\, \varphi_{\lambda}(\dot{x},\, \dot{x}) \end{aligned} \tag{4.4}$$

Example 4.1 ([64])**.** The canonical Euclidean $\mathbb{R}^n$-manifold with canonical Euclidean $\left(\langle a,\, b\rangle \coloneqq \sum\limits_i a_i\, b_i\right)$-metric, for $(a,\, b \in T\,\mathbb{R}^n)$-vector given on positive-oriented canonical vector e_i-basis[10] of a $\mathcal{C}^{\infty}$-class oriented Riemannian $\mathbb{R}^n$-manifold.

Let $\big(D_i \coloneqq \frac{\partial}{\partial x^i} \in \mathcal{E}(T\mathbb{R}^n)\big)$-operator represent the right-invariant vector field derivative operator of n-Euclidean $\mathbb{R}^n$-manifold. For every $(\varphi \in \mathcal{C}^{\infty}(\mathbb{R}^n))$-map, the i-column entry of pushforward φ_*-covector, corresponds to the i-partial derivative $(D_i\varphi)$-operation on its $\mathbb{D}_{\varphi}$-domain.

For every $(p \in \mathbb{R}^n)$-point and $(v \in T_p\mathbb{R}^n)$-vector, we define the $\big(v^i\, D_{i|p}\big)$-operator. In case of f-map is a $\mathcal{C}^{\infty}$-class map from $\mathcal{N}$-manifold in $\mathbb{R}^n$ and a vector operator $(Z \in \mathcal{E}(f^*\, T\,\mathcal{N}))$-field, thus the Z-map on $(\mathbb{D}_f \to \mathbb{R}^n)$-relation is a real-valued $\mathcal{C}^n$-class n-tuple vector field on $(Z_1, \cdots, Z_n)$-basis with Z-domain $\mathbb{D}_Z$ given by equalities below.

$$Z = \sum_i Z_i(f^*D_i), \;\text{ i.e. }\; Z_p = \sum_i Z_i(p)\, D_{i|f(p)} \text{ for every } (p \in \mathbb{D}_Z)\text{-point} \tag{4.5}$$

For the covariant derivative operator on $\mathbb{R}^n$-space, it follows from (4.5)-equality:

$$(\nabla_X Z)_i = X\, Z_i, \text{ for every vector } (X \in \mathcal{E}(T\mathcal{N}))\text{-field} \tag{4.6}$$

Also, in case of $(\mathcal{N} \equiv \mathbb{R}^m)$-condition holds:

$$(\nabla_X Z)_i = (Z_{i\mu})\, X^{\mu} \text{ for every vector } X \in \mathcal{E}(T\mathbb{R}^m)\text{-field} \tag{4.7}$$

Therefore, let $\mathcal{C}^{\infty}$-class c-curve on $([\alpha, \beta] \to \mathbb{R}^n)$-relation curve and first-derivative D-operator, thus the velocity $\dot{c}$-vector field identities below holds:

$$(\dot{c})^i = D\, c^i \text{ and } (\nabla_D\, \dot{c})^i = DDc^i \tag{4.8}$$

Finally, we describe in A-appendix the gradient vector field and 2-form Hesse tensor of each $(\varphi \in C^{\infty}(\mathbb{R}^n))$-map respective to the canonical Riemannian metric on canonical n-Euclidean $\mathbb{R}^n$-manifold.

Theorem 4.2 ([64])**.** *Given $\mathcal{X}$ an $\mathcal{C}^{\infty}$-class open submanifold of Euclidean $\mathbb{R}^n$-space, thus according to 4.2-equality, the geodesic* (4.9)*-equality holds:*

[10]The column $(e_i \in \mathbb{R}^n)$-vector exhibits real 1 at i-index and 0 otherwise. We also represent it by j-row δ^j_i-element.

$$\ddot{c}_h = -\sum_{i,\,j=1}^{n} \underbrace{\left(\sum_{\lambda,\,\mu=1}^{m} \left(\Phi_{\lambda\mu}\,(D_i D_j \varphi^{\lambda}) D_h \varphi^{\mu}\right) \circ c \right)}_{\Gamma_{ij}^{h}} \dot{c}_i\,\dot{c}_j \tag{4.9}$$

From terms verification, the second-kind Christoffel Γ_{ij}^{h}-map corresponds to the inner sum on (4.9)-equality. The term benefits from Hadamard product due its identity $(x^{*}\,(A \circ B)\,y = \mathrm{tr}(\mathrm{diag}\,(x)^{*}\,A\,\mathrm{diag}\,(y)\,B^{\intercal}))$-property. For entries of column vectors x and y equal to 1's, the respective property becomes $\mathrm{tr}\,(A\,B^{\intercal})$-expression. Hence, the Christoffel Γ_{ij}^{h}-map corresponds to concise $\mathrm{tr}\,(\Phi\,\varphi_{;\,h}\,\varphi_{;\,ij}^{\intercal})$-term.

Likewise, the (4.9)-equality benefits as well from this property. Finally, the Christoffelian column $(\Gamma(c,\,\dot{c}) \in T_q \mathfrak{Q})$-vector results from local geometrical description and exhibits h-row $\mathrm{tr}(\Gamma^{h}\,\dot{c}\,\dot{c}^{\intercal})$-element. Finally, the geodesic curve differential equality for every $(t \in \mathbb{R}_{\geq 0})$-instant follows:

$$\ddot{c} + \Gamma(c,\,\dot{c}) = 0 \tag{4.10}$$

Lemma 4.1 ([63])**.** *There is a countable covering coordinate (U_α, η_α)-chart of Riemmanian $\mathcal{X}$-manifold around a vicinity $\tilde{\mathcal{X}}$-region to $((p \coloneqq \eta_\alpha(u)) \in \mathcal{X})$-point, in such geodesic curve 4.10-equality and composition $\varphi \circ \eta_\alpha$-map hold.*

Lemma 4.2. *There is a countable covering coordinate (U_α, η_α)-chart of Riemmanian $\mathcal{X}$-manifold around vicinity $\eta_\alpha(U)$-region of $(p \in \mathcal{X})$-point such that geodesic $(c(t) \in \eta_\alpha(U_\alpha))$-curve on $(t \in [0, 1])$-interval, maps to $(\omega(t) \in U_\alpha)$-curve given by $\eta_\alpha^{-1}(c(t))$-map and pullback vector $\eta_\alpha^{*}\dot{c}$-field equal to $((\eta_\alpha^{-1})_{*} \circ \eta_\alpha^{-1} \circ c)\,\dot{c}$-expression.*

Remark 7. The evaluation of geodesic $(c(t) \in \mathcal{X})$-curve by inverse η^{-1}-map, for given coordinate $(U,\,\eta)$-chart, confirms the common-sense of curved lines on the respective chart.

Algebraic-based surfaces are convenient from an engineering perspective due to numerical computation. On Dombrowski's [64]-work, there are real and complex-valued surface examples. The forthcoming examples illustrate well-known algebraic-defined surfaces: quadrics offer standard surfaces set in 3-Euclidean $\mathbb{R}^3$-manifold. Among its benefits, its tensorial compact expression has explicit derivatives and geodesic curve formulas. Thus, it models common real surfaces like planes, paraboloids, and spheres.

Example 4.2. Let us define a quadric surface as a submersion of Euclidean $\mathbb{R}^3$-space given by $(x^{\intercal} A\,x + p^{\intercal}\,x + r = 0)$-equality, for $(A \in \mathbb{M}_3(\mathbb{R}))$-matrix and column $(p \in \mathbb{R}^3)$-vector. This topological locus exhibits both expanded $\left(\sum_{kl} a_{kl}\,x^{k}\,x^{l} + \sum_{q} p_q\,x^{q} + r\right)$-expression and alternative parametrization $((x - x_0)^{\intercal}\,A\,(x - x_0) - 1)$-versions[11].

The required gradient vector and Hesse bilinear form for geodesic computation are below to consult:

$$\begin{cases} \quad D_x \varphi = (A + A^{\intercal})\,x + p \\ D_x\,D_x^{\intercal} \varphi = A + A^{\intercal} \end{cases} \tag{4.11}$$

[11]In alternative parametrization, the origin point depends on (p, r)-variables, respectively given by $\left(H\,x_0, x^0\,A\,x_0 - 1\right)$-expressions.

$(H \coloneqq A + A^{\intercal})$-Matrix[12] emerges naturally from the quadric map first-derivative operator. The Christoffel second-kind Γ_{ij}^{h}-map requires $(D_h\varphi \coloneqq \varphi_{;\,h}, D_iD_j\varphi \coloneqq \varphi_{;\,ij})$-maps as well as Gramian Φ-matrix, in this case, respectively given by $\left(H_h^{\intercal}x + p_h, H_{ij}\frac{1}{\|Px+p\|_2^2}\right)$-expressions. Therefore, we obtain its expression (4.12) below.

$$\frac{H_h^{\intercal}x + p_h}{\|H\,x + p\|_2^2}\,H_{ij} \tag{4.12}$$

The above calculation holds for every $(x \in \mathbb{R}^3)$-point not equal to $\left(H^{+}\,p + H^{\perp}\,w\right)$-point, for every $(w \in T_x\mathbb{R}^3)$-vector. By algebraic manipulation, the following Christoffelian $\Gamma(x,\,\dot{x})$-contribution emerges:

$$\frac{H\,x + p}{\|H\,x + p\|_2^2}\;\mathrm{tr}\,(H\,\dot{c}\,\dot{c}^{\intercal}) \tag{4.13}$$

Remark 8. Euclidean tangential vector $T\mathbb{R}^3$-bundle of submerged $(\mathcal{S} \subset \mathbb{R}^3)$-surface defined by $(\varphi(x) = 0)$-equality spans from perpendicularity $\left(\langle \mathrm{grad}_x^{\mathbb{R}^n}\,\varphi, v\rangle^{\mathbb{R}^3} \coloneqq \varphi_{;\,x}^{\intercal}\,v = 0\right)$-condition of its gradient vector $\left(\mathrm{grad}_x^{\mathbb{R}^n}\,\varphi \coloneqq \varphi_{;\,x}\right)$-field, for every $(x \in \mathbb{D}_{\varphi})$-point. By its turn, the row vector kernel $\ker(u^{\intercal})$-space[13] corresponds to linearly independent columns of $(W \coloneqq \mathrm{Id}_{\mathbb{R}^n} - \hat{u}\,\hat{u}^{\intercal})$-matrix, for $\hat{u}$-versor corresponding to normalized $\frac{u}{\|u\|_2}$-vector. We left-multiply kernel space basis matrix by row echelon unitary W-matrix and obtain the following implication chain that leads to W-matrices and tangent space basis T-matrix.

$$\begin{aligned} W(\mathrm{Id}_{\mathbb{R}^n} - \hat{u}\,\hat{u}^{\intercal}) &= \begin{bmatrix} T_{n\times n-1} & 0 \end{bmatrix} \\ W(\mathrm{Id}_{\mathbb{R}^n} - \hat{u}\,\hat{u}^{\intercal}) \begin{bmatrix} \mathrm{Id}_{\mathbb{R}^{n-1}} & 0 \\ 0 & \mathrm{Id}_{\mathbb{R}} \end{bmatrix} &= \star \end{aligned}$$

$$\Downarrow$$

$$\begin{cases} W(\mathrm{Id}_{\mathbb{R}^n} - \hat{u}\,\hat{u}^{\intercal}) \overbrace{\begin{bmatrix} \mathrm{Id}_{\mathbb{R}^{n-1}} \\ 0 \end{bmatrix}}^{F} = T \\ W \underbrace{(\mathrm{Id}_{\mathbb{R}^n} - \hat{u}\,\hat{u}^{\intercal}) \overbrace{\begin{bmatrix} 0 \\ \mathrm{Id}_{\mathbb{R}} \end{bmatrix}}^{e_n}}_{v} = 0 \end{cases}$$

$$\Downarrow$$

$$\begin{cases} v &= e_n - \hat{u}\,\hat{u}^n \\ W &= \mathrm{Id}_{\mathbb{R}^n} - \hat{v}\,\hat{v}^{\intercal} \\ U &= \mathrm{Id}_{\mathbb{R}^n} - \hat{u}\,\hat{u}^{\intercal} \\ T &= W\,U\,F \end{cases}$$

[12] Square $(A + A^{\intercal})$-matrix appears and receives H-notation due correspondence to Hessian matrix for the Euclidean case.

Example 4.3. We represent an ellipsoid with center x_0-point on o-origin and A-matrix equal to $(\Lambda \coloneqq \operatorname{diag}(\lambda^1,\, \lambda^2,\, \lambda^3))$-matrix, for positive real-valued λ^k-scalar. The k-row represents each 3D canonical Euclidean axis and its total length is equal to $\frac{2}{\sqrt{\lambda^k}}$-computation.

$$\Gamma^h(x,\, \dot{x}) = \frac{1}{2} \frac{\sum\limits_k \lambda^k (\dot{x}^k)^2}{\sum\limits_l (\lambda^l\, x^l)^2}\, \lambda^h\, x^h \tag{4.14}$$

Example 4.4. Given *eigen* time $\frac{1}{\sqrt{\lambda^k}}$-constant repective to each *eigen* axis as mentioned on 4.3-example, the ellipsoid parametrization emerges naturally from ellipsoidal coordinate $(1 \times [0,\, 2\pi] \times [-\pi,\, \pi],\, \eta)$-chart given by map on 4.15-equality on its vectorial (4.15)-version.

$$u_3\, \Lambda^{-\frac{1}{2}}\, \underbrace{\begin{pmatrix} \cos(u_1)\, \sin(u_2) \\ \sin(u_1)\, \sin(u_2) \\ \cos(u_2) \end{pmatrix}}_{\sigma(u)} \tag{4.15}$$

Ellipsoidal chart transformation (4.15)-map turns into an Euclidean $\mathbb{R}^2$-space given by $(u_3 - 1 = 0)$-equality. Since the η-map brings every u-point of linear $(\mathbb{D}_\eta \subseteq U)$-space into $(x \in \mathcal{X})$-points, it also induces a smooth section $\mathcal{E}(\eta^* T\, U)$. Furthermore, it induces a pullback $\tilde{g}_{ab}$-metric, available in A.1-appendix, from the Euclidean δ-metric in $\mathbb{R}^3$-space.

$$\operatorname{tr}(\eta_{;a}\, \eta_{;b}^{\intercal}\, \delta) = \eta^1_{;a}\, \eta^1_{;b} + \eta^2_{;a}\, \eta^2_{;b} + \eta^3_{;a}\, \eta^3_{;b} \tag{4.16}$$

Finally, we calculate the submersion first-kind Christoffel Γ^k_{ij}-maps with aid of metric $\tilde{g}$-tensor and formula on appendix A.10-definition.

Elementwise, we may represent an $\mathcal{B}$-object in coordinate P-chart given by polar coordinates $((d,\, v) \in \mathbb{R}_{>0} \times T_o \mathcal{X})$-parametrization respective to origin $(o \in \mathcal{X})$-point: it depends only on origin $(o \in \mathcal{X})$-point and hyperparameter $(p \in \mathcal{P})$-set with finite cardinality. Below, the example exhibits a familiar representation.

Example 4.5. In canonical Euclidean $\mathbb{R}^2$-manifold, there are familiar object locus radially defined by $\rho(\theta)$-map, for $(\theta \in \mathbb{S}^1)$-argument: a circumference has constant R-radius; and a cardioid exhibits radius $R\,(1 - \cos(\theta))$-parametrization. Both loci have center $(o \in \mathbb{R}^2)$-point and rotation φ-argument respective to perpendicular z-axis.

$$\rho(\theta)\, \begin{bmatrix} \cos(\theta + \varphi) \\ \sin(\theta + \varphi) \end{bmatrix} + o \tag{4.17}$$

The above polar objects' description inspires further development. Its Cartesian representation comes from (4.18)-relation, first published by Lamé in 1818.

[13] In case of a row $(A \in \mathbb{C}^{m \times n})$-matrix such that $(n \geq m)$-condition holds, its kernel spams from linearly independent columns of $(I - A^+ A)$-matrix, originally available on famous [65]-work, and equal to $A^*(A\, A^*)^{-1}$-matrix.

$$\left|\frac{x}{a}\right|^r + \left|\frac{y}{b}\right|^r = 1 \iff \begin{cases} x(s) = a\ |\cos(s)|^{\frac{2}{n}} \\ y(s) = b\ |\sin(s)|^{\frac{2}{n}} \end{cases}, \quad \text{for } s \in \mathbb{S}^1 \tag{4.18}$$

The above curve locus does not exhibit a polar-dependent $\rho(\theta)$-radius as on (4.17)-expression, although it exhibits a parametric version. Gielis suggests a closed-form in extension to the expressive curve. In his [66]-work, he considers the $(n_1, n_2, n_3 \in \mathbb{R}_{>0})$-exponents as well as additional term $\frac{m}{4}$, for coefficient $m \in \mathbb{N}_{>0}$, we call *superformula* (4.19) and denote by script letter $\wp$.

For completeness, we define parameter $\mathscr{P}$-space by product $(\mathbb{N}^3_{>0} \times \mathbb{R}^3_{>0})$-space. Additionally, we redefine radius $\wp(\theta)$-map for $\wp(v)$-map, given tangent $(v \in T_o\mathcal{M})$-vector, oftentimes referred in literature as *exponential map*, to consult on [55]-textbook. We call *position vector*, since its inner product square-root $\sqrt{\langle v, v \rangle^{\mathcal{X}}}$-computation induces the distance map d from point o to respective nearby point $\gamma(1)$ along the geodesic $\gamma(t)$-curve that satisfies position and velocity equality $(\gamma(t) = o, \dot{\gamma}(t) = v)$-conditions.

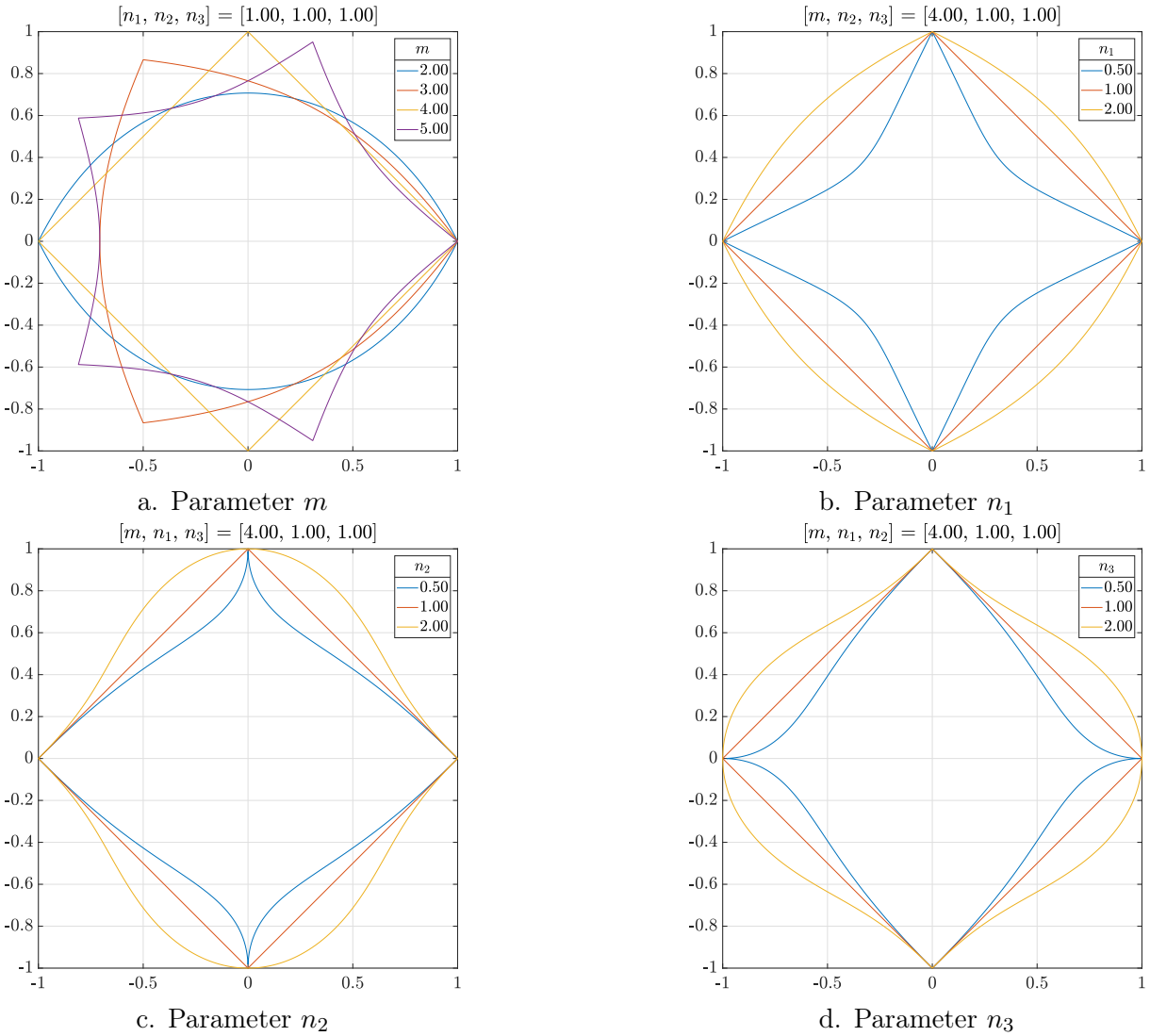

a. Parameter m

b. Parameter n_1

c. Parameter n_2

d. Parameter n_3

Figure 9: Hyperparameters investigation on superformula parametrization

Figure 9-cluster explores these hyperparameters: the m-parameter denotes the lobes

cardinality on the resulting curve; the (n_2, n_3)-exponents represent moral-equivalent to a symmetrical curve curvature, respective to (x, y)-axes; the n_1-exponent either reduces or expands the inner curve area towards a rectangular-shaped curve.

Our main interest in (4.19)-superformula is its polar description, which suits obstacle synthesis. In original (4.19)-work, vectorial v-entry refers to polar (i.e. spherical) chart with $\frac{1}{4}\, m\, \theta$-argument. It suggests, on a Riemannian $\mathcal{M}$-manifold, the parametrization by $(v \in T_p\mathcal{M})$-vector on $(p \in \mathcal{M})$-point in a spherical coordinate $\mathbb{S}^n$-patch.

The useful (4.19)-superformula describes obstacles for two arguments: it exhibits interior and exterior spaces and flexible tuning by parameter space low-cardinality. However, the obstruction $\mathcal{H}_k$-surface still requires a ß-measure for each $(p \in \operatorname{ext}_{\mathcal{X}} \mathcal{O}_k)$-point, respective to $\mathcal{O}_k$-object's exterior space contribution. A convenient manner for this statement follows:

$$\left(\left| \frac{v_1}{a} \right|^{n_2} + \left| \frac{v_2}{b} \right|^{n_3} \right)^{-\frac{1}{n_1}} \tag{4.19}$$

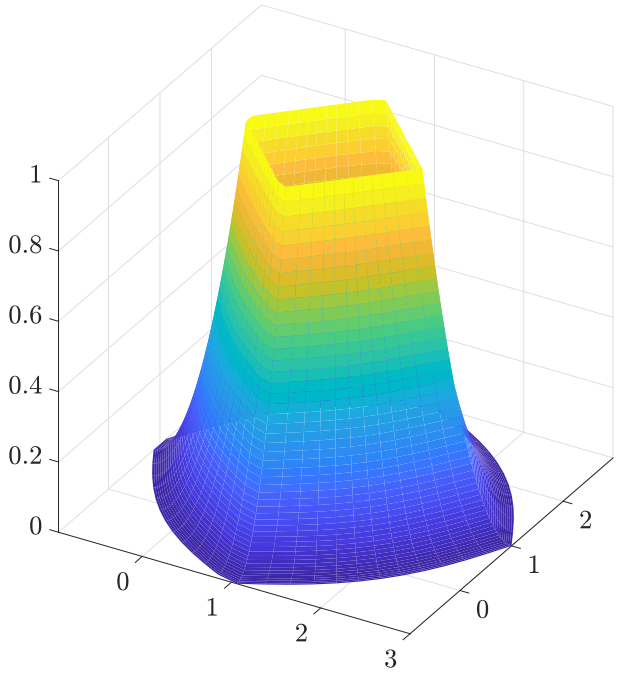

Figure 10: Quadrilateral surface with center $1_{2\times1}$-point and parameter $\begin{bmatrix} 1_{2\times1} & 4 & 1_{3\times1} \end{bmatrix}^{\intercal}$-vector

Proposition 4.1. *Let an $\mathcal{O}$-object given by superformula and its parameter $\tilde{p}$-set on parameter $\left(\tilde{\mathcal{P}} \equiv \mathbb{R}^2_{\geq 0} \times \mathcal{P}\right)$-space, equal to $(c_0,\, d_0,\, p)$-tuple and center o-point. The obstruction map at radial $(\rho(v) + d)$-distance respective to center $(o \in \mathcal{X})$-point, for parameters $\tilde{p}$-set with scaled*[14] *$\{a, b\}$-parameters given by $(r\, a,\, r\, b)$-tuple, corresponds to $(ß(v)\, v)$-map respective to center o-point.*

Among possible definitions for radial ß(v)-map, we provide the following description: at obstacle $\partial\mathcal{O}_k$-boundary, its ß $(\partial\mathcal{O}_k)$-measure exhibits some finite high c_0-value; at certain d_0-distance on $\partial\mathcal{O}_k$-boundary, its value is equal to 0, i.e., tuning $(c_0,\, d_0 \in \mathbb{R}_{>0})$-parameters. Two obstruction map examples corresponds to the polynomial $\left(c_0 \left(1 - \frac{d}{d_0}\right)^m\right)$-map and Gaussian-kernel $\frac{c_0}{e-1}\left(e^{\frac{\rho(v)+d_0-d}{d_0}} - 1\right)$-map, within the distance $(0 \leq d \leq d_0)$-interval to $\mathcal{O}_k$-object. The resulting obstruction $\mathcal{H}$-surface corresponds to the $\sum_k \mathcal{H}_k$-sum respective to each $\mathcal{O}_k$-object.

So far, we define modeling procedures for optimization applied methods, physical dynamical systems, and trajectory curve synthesis. The next chapter presents a manner to connect these three elementary tools. The utilized representation is a flow diagram, a common way to represent block-defined processes with intermediary flow conditions.

[14] The scale $r(d, \theta)$-map on $(\mathbb{R}_{>0} \times \mathbb{S}^n \to \mathbb{R}_{\geq 1})$-relation corresponds to the $\left(1 + \frac{d}{\rho(v)}\right)$-map.

5 SOURCE SEEKING ALGORITHM

"A goal is not always meant to be reached; it often serves simply as something to aim at."

-- Bruce Lee

The barycenter-based flow diagram

Autonomous behavior and exploration description are great challenges in the robotics context. The previous chapters propose optimization and control synthesis strategies. However, they are standalone and appropriate for their purpose. Hence, we require a heuristic to amend both together.

In the current work, the robot must find a maximum point for the signal source and steer the agent to its location. We organize the search procedure into two complementary phases, an *exploration* and *pursue*: The former acquires the source signal on sample points to comprehend the signal topology; the latter develops a curve toward the source estimation configuration.

We start at some non-negative τ_0-instant, commonly adopted as 0. The initial source estimation $\hat{y}^0$-point may be the initial $y_s(\tau_0)$-point added by a stochastic noise z-variable, in the absence of a better guess. We update the interval source estimation $\bar{y}_{i,j}$-point along discrete curiosity $[\tau_i,\, \tau_{i+1}]$-intervals: we adopt likewise the equivalent initial point in source y^0-point. Both curiosity and sample iteration (τ_i, τ_s)-instants are initially τ_0. Thus, a (possible) initialization $\big(p_0 \coloneqq \big(\hat{y}^0 \quad \bar{y}^{0\,0} \quad \tau_i \quad \tau_s\big)\big)$-tuple corresponds to parameter $\big(\big(y_s(x_0) + z \quad y_s(x_0) \quad \tau_0 \quad \tau_0\big)\big)$-vector.

The above-mentioned stochastic innovative term z provides the exploration property to the barycenter method: its addition to commands allows vicinity exploration. Other possible curious contributions correspond to control as $(u + z_u)$-vector, along the trajectory as $(\hat{\gamma} + z_\gamma)$ and/or to destiny point as $(\bar{y}^{i\,j} + z_{\hat{y}})$-vector. We also may add intermediate points randomly in the vicinity to the nominal trajectory τ_z-instants, for τ_z-instant within $[\tau_i,\, \tau_{i+1}]$-interval.

In the flow diagram in 11-figure, each block describes an application-suitable algorithm. The orange block initializes variable $(i,\, j,\, \tau_s,\, \hat{y}^i,\, \bar{y}^{i\,j})$-tuple as described on previous paragraphs. The red blocks embed decision-making commands regarding instant control verifications. The cyan block computes the trajectory $\hat{\gamma}(\tau)$-curve between current and extremum point estimations given $\Delta\tau_e$-interval. The green block represents the computation and application of the control u-measure based on the current $x(\tau)$-state and reference trajectory $\hat{\gamma}(\tau)$-curve. Finally, the yellow blocks update its extremum estimation $\bar{y}^{ij}$-point by scalar signal sample on $x(\tau)$-poin, the sample and update (τ_s, τ_i)-points, and (i, j)-indexes.

Each block of 11-diagram may embed an application-suitable algorithm. The current

issue constraints follow the systematic below.

1. ***Initialize***: the (i, j)-indices to 0 as well as time-related (τ_0, τ_s, τ_i)-variables and source estimation $(\bar{y}^{0,\,0}(\tau_0))$-points to source initial state $(y_s^0 + z)$-point;
2. ***Compute* trajectory $\hat{\gamma}(\tau,\, \hat{y}^{ij}(\tau))$-curve and control $u(x,\, \hat{\gamma})$-value**: given source estimation $\hat{y}^{ij}$-point at τ_i-instant, with possible a posteriori addition of a bounded disturbance on both signal maps;
3. ***Apply control u-rule***: as input map of dynamical Σ-system;
4. ***Verify***: if current τ-instant lays within the $[\tau_i, \tau_{i+1}]$-interval. In positive case, it verifies the $(\tau \in [\tau_s, \tau_s + \Delta\tau_s])$-condition. In both positive cases, repeat from step 3; in negative former, follow step 5; or, in positive former and negative latter, it goes to step 6;
5. ***Update***: the estimation $\hat{y}_{i,\,0}$-point to its previous estimation $\hat{y}_{i-1,\,j}$-point and i-increment by 1. Repeat step 2;

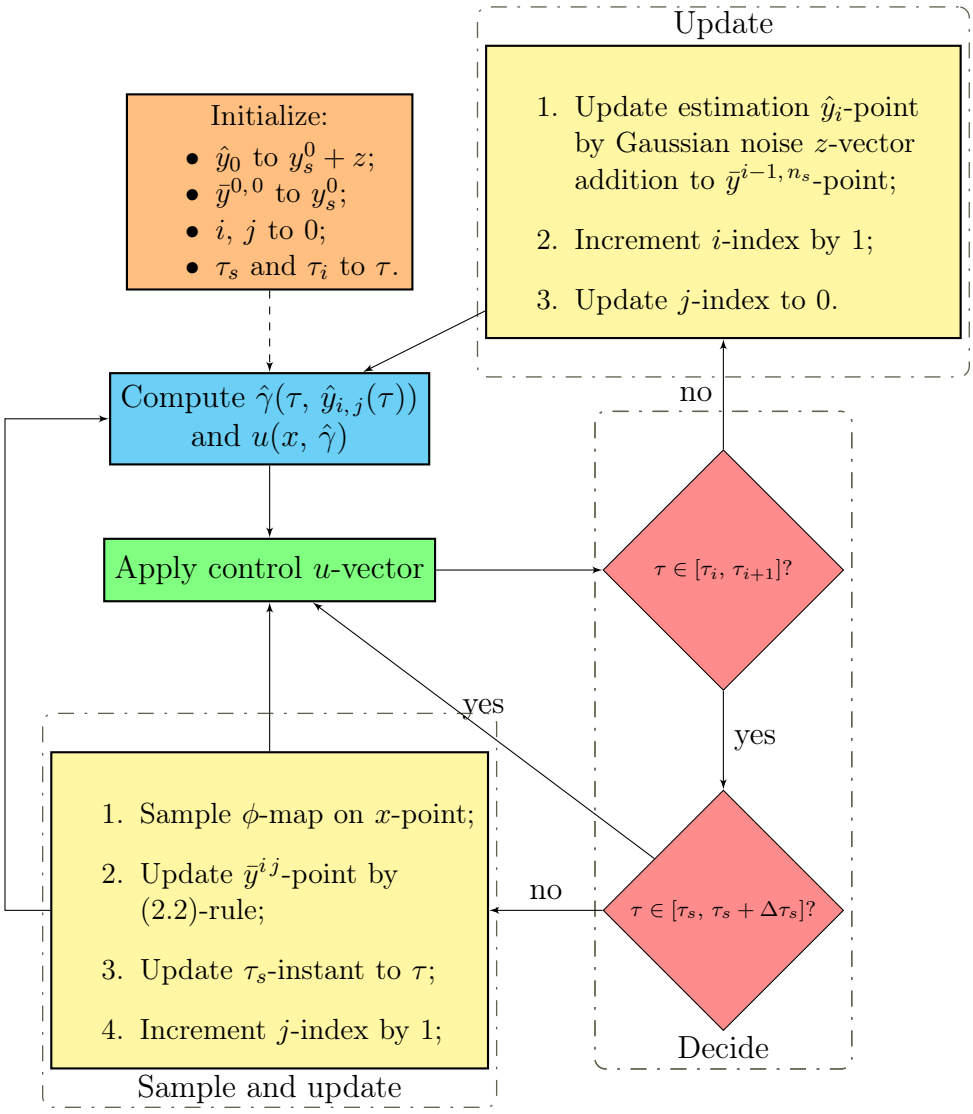

Figure 11: Barycenter-based source seeking flow diagram.

6. ***Sample and Update***: the signal ϕ-map on $x(\tau_s)$-points, update the source estimation $\hat{y}^{i,j}$-point by (2.2)-equality, the τ_s-instant to the τ-variable, increment j-index by 1 and go to step 2.

Theorem 5.1. *Let $\Delta\tau_n$ be the simulation time interval, $\Delta\tau_s$ the source signal sampling interval, $\Delta\tau_e$ the curious exploration time interval and finally $\Delta\tau_t$ the trajectory planning time interval, such that the condition $(\Delta\tau_n \leq \Delta\tau_s \leq \Delta\tau_e \leq \Delta\tau_t)$-chain hold.*

Proof. By construction, the right-hand $\Delta\tau_t$-term is a natural choice since we look for a greater interval than the simulation's and exploration's intervals. Subsequently, there must lay the curious exploration $\Delta\tau_c$-interval. The source signal sampling $\Delta\tau_s$-interval must be lower than $\Delta\tau_e$-interval since we must acquire at least a signal instance within the time $[\tau_i, \tau_{i+1}]$-interval. Finally, the lower left term corresponds to $\Delta\tau_n$-interval, which provides the precision to the simulation scheme and majorates computational simulation complexity. ■

We must not violate the intervals magnitude ordering to allow simulation feasibility and the flow 11-diagram implementation. It brings a reasonable rationale to light.

Remark 9. For simulation reasons, the convenient choice for time-constant scale factors exploits the case of numerical simulation. We require a time $\Delta\tau_n$-interval for numerical integration algorithms e.g. Runge-Kutta methods, scaled steps for $(n_s\,\Delta\tau_n, n_e\,\Delta\tau_n)$-instants given by $\left(\frac{\Delta\tau_s}{\Delta\tau_n}, \frac{\Delta\tau_e}{\Delta\tau_n}\right)$-ratios, such that $(1 \leq n_s \leq n_e)$-condition holds, for natural $(n_s,\, n_e \in \mathbb{R}_{>1})$-constant.

5.1-Remark provides a hierarchy-like condition for the choice of heuristic time constants. However, its definition depends on the study case. Available prior information about the source signal characteristics may help. It is plausible, for example, to choose the trajectory planning $\Delta\tau_t$-interval significantly longer than the curiosity $\Delta\tau_c$-interval, i.e., which satisfies the $(\Delta\tau_t \gg \Delta\tau_c)$-condition, to allow the agent to explore its neighborhood in the early search stages.

Finally, the current approach relies on a time $\Delta\tau_t$-interval to generate an exploration trajectory and recursive barycenter version. Hence, it is straightforward to retrieve periodically a barycenter point candidate and recalculate the exploration trajectory in the hand of the barycenter $\{\bar{y}^{ij}\}_{n_s}$-set within $[\tau_i,\, \tau_{i+1}]$-interval.

Exploration strategies

The flow diagram depicted on 11-diagram provides intuition about source seeking. A pure deterministic and asymptotic control map towards the source estimation is prone to get stuck on the calculated estimation point. To avoid particularities, we resort to curiosity addition on either the actuation map or during the curiosity time interval to explore the environment. In the former case, it is reasonable to consider a zero-mean support distribution map as a Gaussian stochastic variable. Compact distribution support maps like triangular or bell-shaped ones may also apply due to the stochastic central limit theorem. A candidate to support mean vector $\bar{z}_n$ corresponds to the weighted barycentric mean vector given on (2.6, 2.5)-equalities.

A stochastic z-innovation provides the exploration property for the barycenter method and hence vicinity exploration by its addition to dynamical system commands. As cited in the previous section, other possible noise additions correspond to: on the control map as $(u + z_u)$-vector; along the trajectory curve as $(\hat{\gamma} + z_\gamma)$-vector; and/or on estimation point as $(\hat{y}^{i\,j} + z_{\hat{y}})$-vector. Also, an exploration choice is the addition of the intermediate points in the vicinity to the nominal trajectory at τ_z-instants within $[\tau_i,\, \tau_{i+1}]$-interval.

6 MODEL DEVELOPMENT AND RESULTS

"Experience without theory is blind, but theory without experience is mere intellectual play."

-- Immanuel Kant

Barycenter method simulations

Hyperparameters under investigation

A prior investigation concerns the hyperparameters' influence on source seeking given a smooth unknown-to-source-seeker-agent source signal ϕ-map. The simulation results in 18-figure illustrates optimization instances of a two-dimensional parable map for forgetting $(0, 0.5)$-factors. A preliminary qualitative analysis comprehends a crescent broadness, i.e., the moral-equivalent standard deviation, by decrescent forgetting λ-factors.

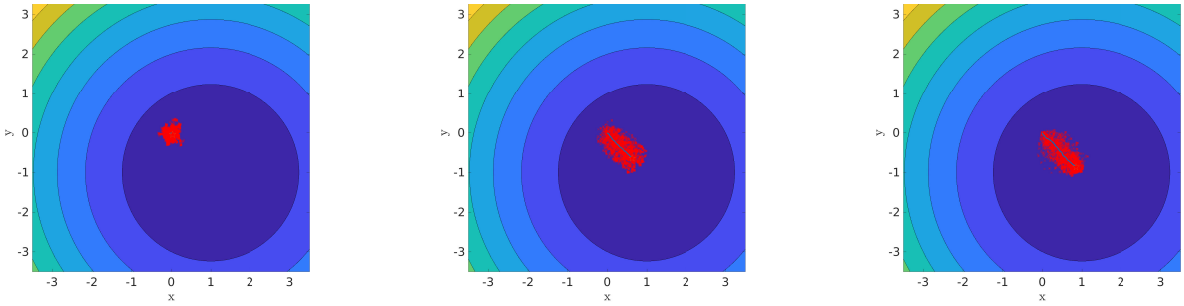

a. (0.1, 1.0, 1.0) b. (0.1, 10.0, 1.0) c. (0.1, 20.0, 1.0)

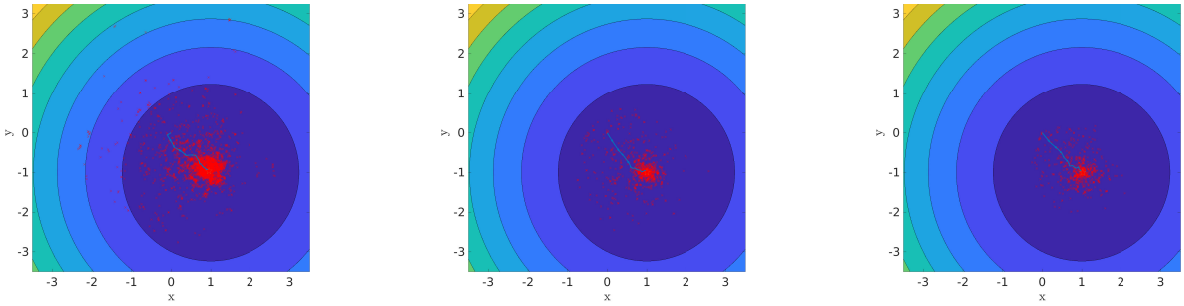

d. (1.0, 1.0, 1.0) e. (1.0, 10.0, 1.0) f. (1.0, 20.0, 1.0)

Figure 12: Discrete barycenter method on ϕ-map as the paraboloid $(x^2 + y^2)$-map for forgetting λ-factor equal to 1 and distinct values for hyperparameter (σ, ν, λ)-tuple.

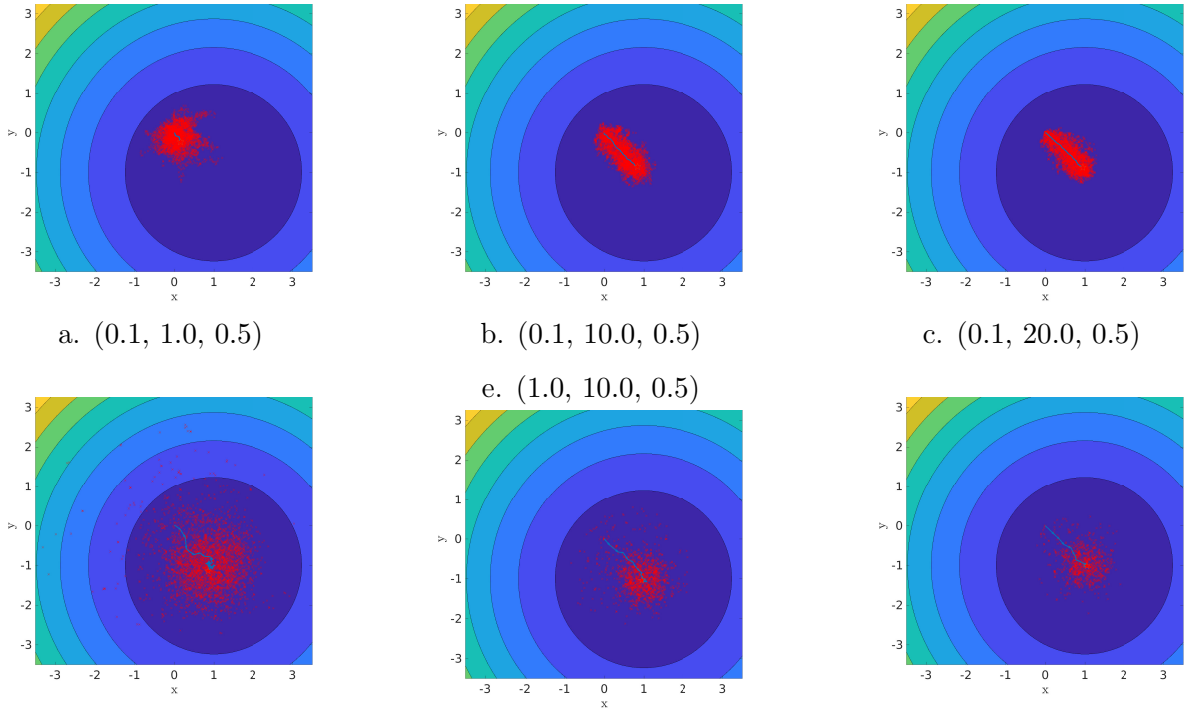

a. (0.1, 1.0, 0.5)

b. (0.1, 10.0, 0.5)

c. (0.1, 20.0, 0.5)

e. (1.0, 10.0, 0.5)

d. (1.0, 1.0, 0.5)

f. (1.0, 20.0, 0.5)

Figure 13: Discrete barycenter method on ϕ-map as the paraboloid $(x^2 + y^2)$-map for forgetting λ-factor equal to 0.5 and distinct values for hyperparameter (σ, ν)-tuple.

Convergence enhancement under investigation

This brief section contains the simulation results for the decrescent forgetting λ_z-factor. The corner case corresponds to null ξ-hyperparameter and represents a curiosity mean vector equal to null element. 15-Figure denotes the average result of 1000 simulation instances with 25 iterations each. According to qualitative analysis for results on 15-figure, there is no significant remarkable improvement for given $\mathcal{C}^2$-class oracle ϕ-map given by parable $(x^2 + y^2)$-map.

14c.-Figure corresponds respectively to the barycenter method iterations on Euclidean $\mathbb{R}^2$-plane and their position as well as map evaluation along the algorithm steps. The green curve constitutes the sample average of 1000 experiment instances, each given by 100 iterations. The initial condition for both accumulative m_0-term and $\hat{y}^0$-point depends on statement elements, but typically m_0-accumulator value is equal to 0.

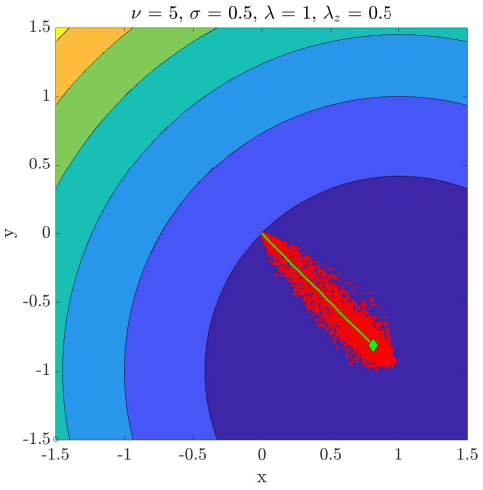

a. Barycenter $\{\hat{x}_n\}$-point behavior

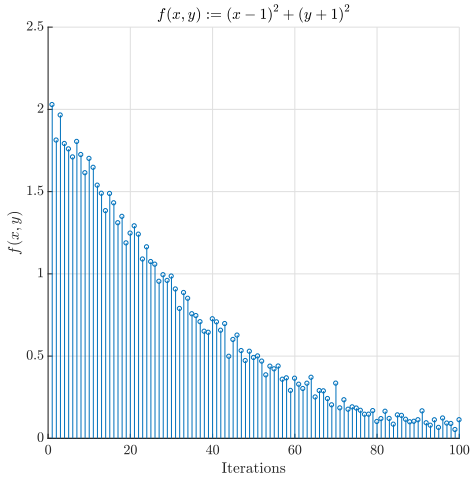

b. Oracle map $\{f(\hat{x}_n)\}$-evaluations

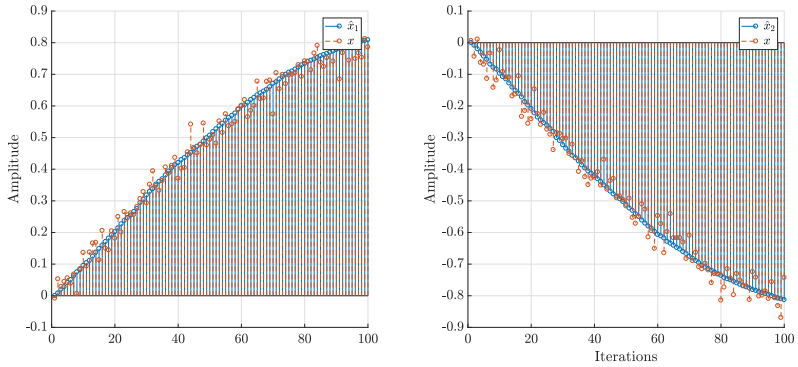

c. Discrete barycenter method average sequence for parable as oracle map. The forgetting λ-factor is equal to 1.

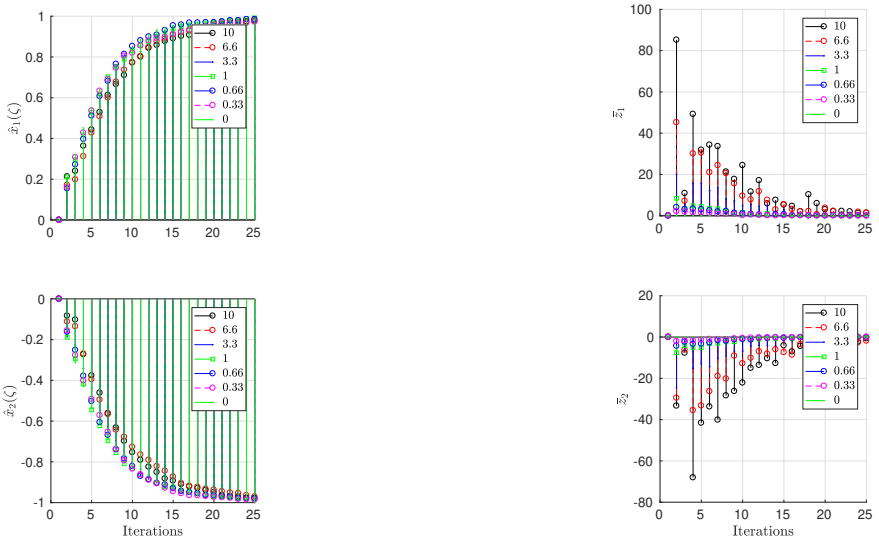

a. Asymptotic sequence of barycenter $\{\hat{x}_n\}$-points in source $\mathcal{X}$-space

b. Mean vector $\bar{z}$-sequence

Figure 15: Barycenter $\{\hat{x}_n\}$-points and mean $\{\bar{z}_n\}$-vector sequences for hyperparameter ξ-values on legend

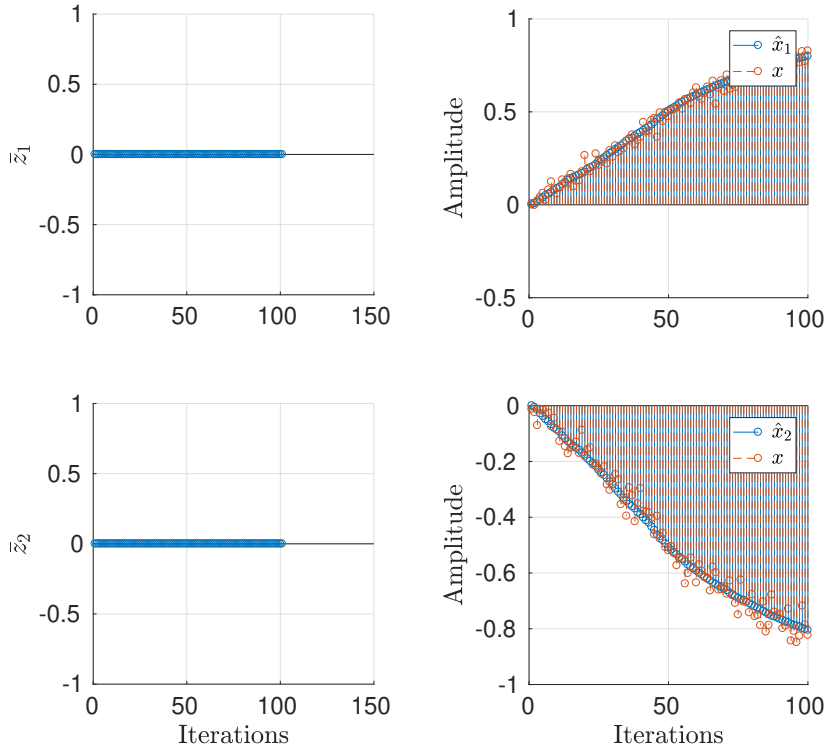

a. Zero mean $\bar{z}$-vector b. Barycenter $\{\hat{x}_n\}$-points in source $\mathcal{X}$-space

Figure 16: Non-augmented barycenter sequence

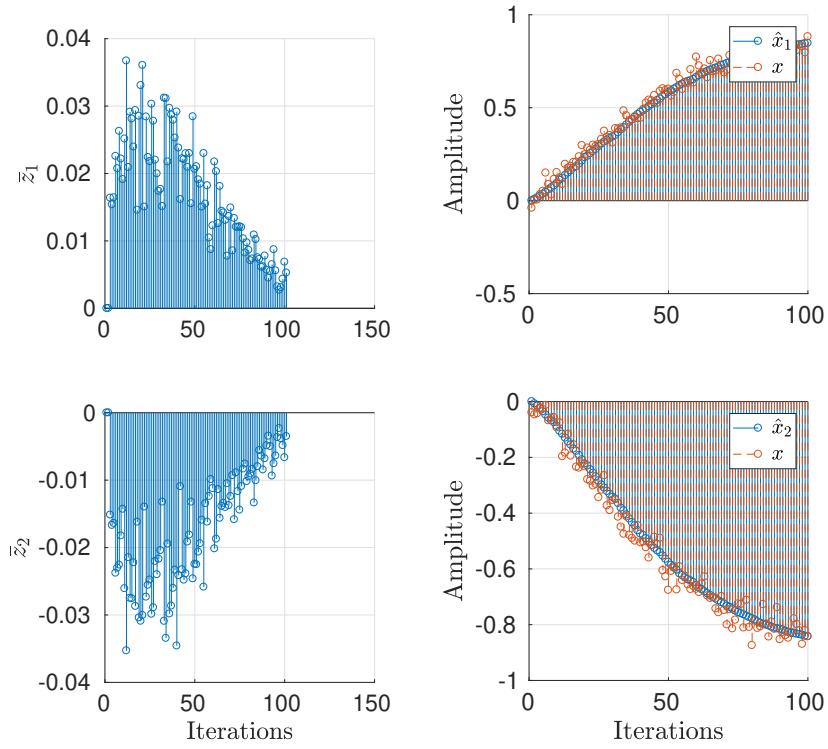

a. Mean vector $\bar{z}$ b. Barycenter $\{\hat{x}_n\}$-points in source $\mathcal{X}$-space

Figure 17: Augmented barycenter sequence as suggests [2]-work

Figure 18: Augmented barycenter sequence as suggests (2.5)-equality

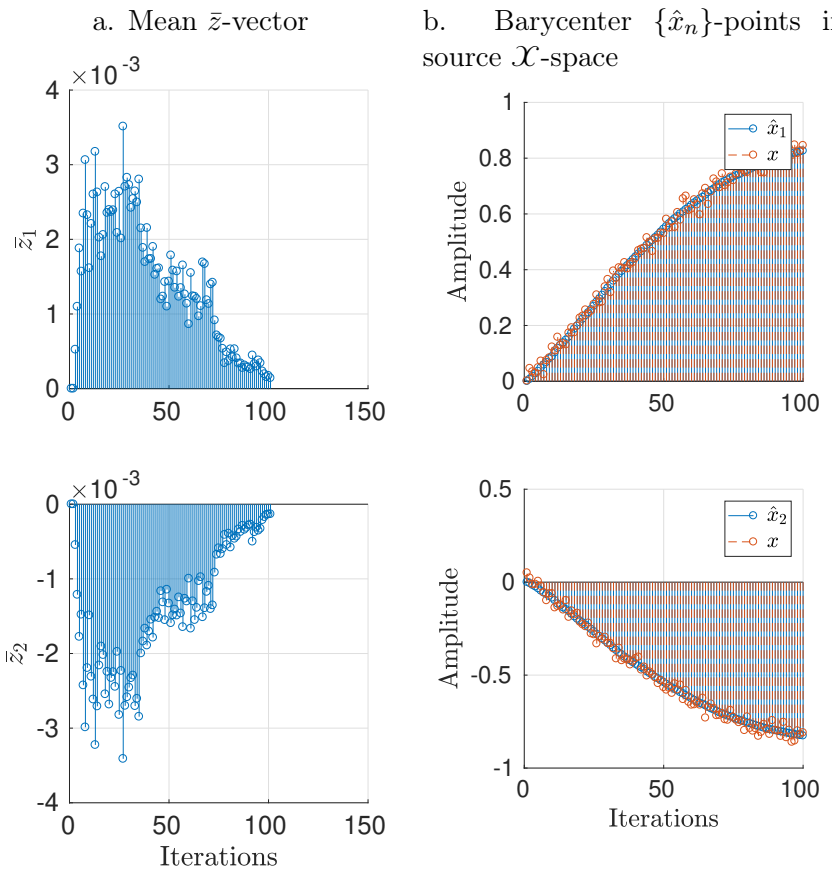

Source seeking construction

Source seeker models

This section explores the dynamical modeling of two well-known robotic agents: the unicycle and omnirobot. In the next two subsections, we present the physical description of these dynamical systems. The method systematically extends to curved spaces, motivated the following remark.

Remark 10. Although the results follow for navigation space equal to Euclidean $\mathbb{R}^2$-plane, its substitution by smooth $\mathcal{S}$-surface as well as cartesian (x, y)-tuple by some 2-dimensional $p(t)$-point on $\mathcal{S}$-surface. It means, the system modeling operates on the contact state $C\mathcal{S}$-space.

Simplified unicycle

A unicycle mobile robot, also known as *Dubin's car*, exhibits constraints on its translation in the Euclidean $\mathbb{R}^2$-plane related to wheels' non-slipping equality condition. The unicycle agent of current work constitutes the wheels assembly on a chassis.

Kinematics

The left-hand-side Pfaffian constraint term of a simplified unicycle corresponds to

$(\dot{x}\,\sin\theta - \dot{y}\,\cos\theta)$-expression. In a tensorial form, the equation turns into (6.1)-equality. The velocity $\dot{q}$-vector constitutes the right-annihilator column B-span by quasi-velocity p-vector, also with usual u-notation by authors Kane & Levinson.

$$\underbrace{\begin{bmatrix}\sin\theta & -\cos\theta & 0\end{bmatrix}}_{a}\underbrace{\begin{bmatrix}\dot{x}\\ \dot{y}\\ \dot{\theta}\end{bmatrix}}_{\dot{q}} = 0 \overset{a\,B=0}{\Longrightarrow} \begin{bmatrix}\dot{x}\\ \dot{y}\\ \dot{\theta}\end{bmatrix} = \underbrace{\begin{bmatrix}\cos\theta & 0\\ \sin\theta & 0\\ 0 & 1\end{bmatrix}}_{B}\underbrace{\begin{bmatrix}v\\ \omega\end{bmatrix}}_{p} \tag{6.1}$$

Dynamics

The dynamical description of a discrete connected mechanism requires its kinetic and potential maps, for the case, given respectively by $\left(\frac{I_3}{2}\,\dot{\theta}^2 + \frac{m}{2}\,(\dot{x}^2 + \dot{y}^2)\right)$-maps and zero[15]. The external inputs i.e. actuator efforts come from the τ_i-torque applied on each wheel and equal to $f_i\,R_i$-product, for i-index equal either to left or right notation on $\{l,\,r\}$-set.

Although possible, the input $(f_x,\,f_y,\,\tau)$-tuple does not represent feasible robot inputs from an engineering perspective. Hence, the map between $[(f_x,\,f_y,\,\tau),(\tau_r,\,\tau_l)]$-tuples is useful. The distance between the wheel and symmetric longitudinal x_m-axis is the capital L_i-letter. The distance relation satisfies $(L_r + L_l = 2L)$-equality.

$$\begin{aligned}\begin{bmatrix}m\,\mathrm{Id}_{T\mathbb{R}^2} & 0\\ 0 & I_3\end{bmatrix}\begin{bmatrix}\dot{x}\\ \dot{y}\\ \dot{\theta}\end{bmatrix} &= \begin{bmatrix}\sin\theta\\ -\cos\theta\\ 0\end{bmatrix}\lambda + \begin{bmatrix}f_x\\ f_y\\ \tau\end{bmatrix}\\ &= \begin{bmatrix}\sin\theta\\ -\cos\theta\\ 0\end{bmatrix}\lambda + \begin{bmatrix}\frac{\cos\theta}{R_r} & \frac{\cos\theta}{R_l}\\ \frac{\sin\theta}{R_r} & \frac{\sin\theta}{R_l}\\ \frac{L_r}{R_r} & -\frac{L_l}{R_l}\end{bmatrix}\begin{bmatrix}\tau_r\\ \tau_l\end{bmatrix}\\ \overset{\square}{\Longrightarrow}\begin{bmatrix}m & 0\\ 0 & I_3\end{bmatrix}\begin{bmatrix}\dot{v}\\ \dot{\omega}\end{bmatrix} &= \begin{bmatrix}\frac{1}{R_r} & \frac{1}{R_l}\\ \frac{L_r}{R_r} & -\frac{L_l}{R_l}\end{bmatrix}\begin{bmatrix}\tau_r\\ \tau_l\end{bmatrix}\end{aligned} \tag{6.2}$$

The $\square$-implication stands here for the left-multiplication of left-annihilator codistribution $B^\intercal$ and acceleration $\ddot{q}$ substitution by differential span $B\dot{p} + \dot{B}p$. The right-hand-side (6.2)-equality left-multiplication by $B^\intercal$-matrix and assembly to constrained velocity (6.1)-vector leads to the dynamical (6.3)-equality. Finally, we express the resulting velocity and acceleration $(\dot{q}, \dot{p})$-vectors in state space notation on (6.3)-equality. The *states* variables corresponds to $\begin{bmatrix}x & y & \theta & v & \omega\end{bmatrix}^\intercal$-vector.

$$\begin{bmatrix}v\,\cos\theta\\ v\,\sin\theta\\ \omega\\ 0\\ 0\end{bmatrix} + \begin{bmatrix}0 & 0\\ 0 & 0\\ 0 & 0\\ \frac{1}{m\,R_r} & \frac{1}{m\,R_l}\\ \frac{L_r}{I_3\,R_r} & -\frac{L_l}{I_3\,R_l}\end{bmatrix}\begin{bmatrix}\tau_r\\ \tau_l\end{bmatrix} \tag{6.3}$$

[15] We may consider, on a curved navigation topology, the geometry-related potential ρ-map.

Omnidirectional robot

The omnidirectional robot wheels are built on its perimeter. The wheels constructive disposal of $\frac{2}{3}\pi$ rad allows the quasi-movement on tangential $T_p\,\mathcal{S}$-space. Due to the rotation and translation superposition movements, the wheel-ground contact point has a zero velocity vector. This condition for each wheel provides robot movement constraints. The respective Pfaffian constraints and resulting velocity $\dot{q}$-vector follow on (6.4)-equation.

Kinematics

The seeking agent on 19-figure corresponds to an omnidirectional mobile robot. Despite extensive and comprehensible discussion on [68]-work about this dynamical class, this section explores the approach described in the next paragraph. For the robot at hand, it is sufficient to define $(q \in \mathcal{S} \times \mathbb{S}^3)$-states and quasi-velocity $(p \in T\,\mathcal{S} \otimes T\,\mathbb{S}^3)$-vector, both given respectively by vectors below.

Figure 19: Omnidirectional robot top view

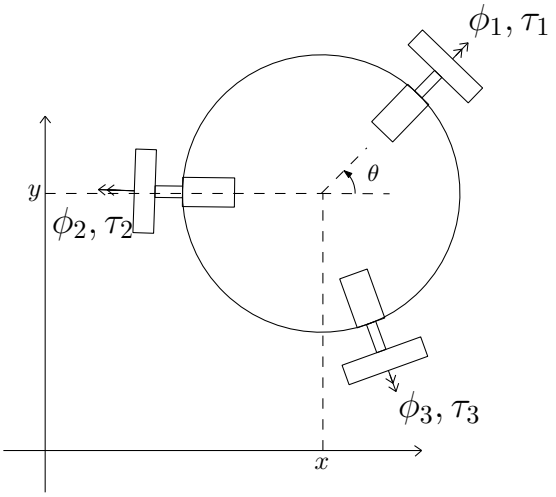

$$q = \begin{bmatrix} x & y & \theta & \phi_1 & \phi_2 & \phi_3 \end{bmatrix}^\intercal$$

$$p = \begin{bmatrix} v_x & v_y & \omega \end{bmatrix}^\intercal$$

The kinematic constraints require the Pfaffian $\left(A_k\,\dot{q}^k = 0\right)$-equality. The necessary constraint relations emerge from the non-slipping wheels' hypothesis, given by each wheel velocity vector projection along the longitudinal wheel axis. The $\langle {}^0v_i, {}^0e_2^i \rangle^{\mathcal{S}}$-projection is equal to $\dot{\phi}_i\,R$-speed along its longitudinal axis and equal to the respective translational $\dot{\phi}_i\,R$-speed, for given wheel R-radius. The θ_i-argument corresponds respectively to values 0, $\frac{2\pi}{3}$ and $\frac{4\pi}{3}$ rad, for i-index within $\{1, 2, 3\}$-set. The L-length corresponds to the distance between the geometric robot center point and the respective wheel.

The ${}^0e_2^i$-versor and velocity ${}^0v_i$-vector correspond respectively to $\mathrm{rot}\left(\theta + \theta_i, {}^0e_3^0\right) {}^0e_2^0$-versor and $\left(\begin{bmatrix} \dot{x} & \dot{y} & 0 \end{bmatrix}^\intercal + \left[{}^0e_3^0\right]_\times {}^0e_1^i\,\dot{\theta}\,L\right)$-vector. These constraints' concatenation leads to the required Pfaffian and kinematic equality definition. Matrix E^i-rows results from row-vector ${}^0e_2^{i\intercal} \begin{bmatrix} {}^0e_1^0 & {}^0e_2^0 & \left[{}^0e_3^0\right]_\times {}^0e_1^i\,\mathrm{L} \end{bmatrix}$-multiplication.[16] [17]

$$\underbrace{\begin{bmatrix} \mathrm{E} & -\mathrm{Id}_{T\mathbb{S}^3} & R \end{bmatrix}}_{A^\intercal} \dot{q} = 0 \Longrightarrow \dot{q} = \underbrace{\begin{bmatrix} \mathrm{Id}_{T\mathbb{R}^2 \times T\mathbb{S}} \\ \frac{1}{R}\,\mathrm{E} \end{bmatrix}}_{B} p \tag{6.4}$$

[16] The $[\cdot]_\times$-notation stands for the skew-symmetric matricial form for a given vectorial entry, which allows the cross product between two vectors.

$$[v]_\times = \begin{bmatrix} 0 & -v_z & v_y \\ v_z & 0 & -v_x \\ -v_y & v_x & 0 \end{bmatrix}$$

Dynamics

The acceleration $\dot{p}$-vector defines the quasi-velocity vector derivative on constrained $(\vartheta \subseteq \mathcal{Q})$-submanifold. For simplicity, it corresponds to Euclidean $\mathbb{R}^2$-plane, also known as $(x \times y)$-plane. The constrained wheels' surface contact constrains the generalized state velocity tangential $T\,\mathcal{Q}$-space by (6.4)-relation. Its expression follows on Lagrangian representation (2.17)-equality.

Both inertial (M, Θ)-tensors are diagonal and are available on [(6.5), (6.6)]-terms. We also provide the input coupling $\frac{1}{2}\,B^{\intercal}\,q_*$-tensor and non-constrained Christoffelian $\Gamma(q,\,\dot{q})$-vector both related to objects and their geometrically-distributed physical properties.

$$\begin{cases} m_{11} = m_{22} = m_R + 3\,m_r \\ m_{33} = I_R^{33} + 3\,(I_r^{33} + m_r\,L^2) \;+\; (I_r^{22} - I_R^{33})\,(\sin^2(\phi_1) + \sin^2(\phi_2) + \sin^2(\phi_3)) \\ m_{44} = I_r^{11}\;\mathrm{Id}_{T\,\mathbb{S}^3} \end{cases} \tag{6.5}$$

$$\begin{cases} \theta_{11} \;= \theta_{22} = m_R + 3\,m_r + \frac{3}{2}\,\frac{I_r^{11}}{R^2} \\ \theta_{33} \;= I_R^{33} + 3\,\left(I_r^{11}\;\left(\frac{L}{R}\right)^2 + I_r^{33} + m_r\,L^2\right) + \\ \qquad (I_r^{22} - I_r^{33})\;\left(\sin^2(\phi_3) + \sin^2(\phi_2) + +\sin^2(\phi_1)\right) \end{cases} \tag{6.6}$$

$$B^{\intercal}\,q_* = \frac{1}{R}\begin{bmatrix} -\sin(\theta) & \cos(\theta) & L \\ -\cos\left(\theta + \frac{\pi}{6}\right) & -\cos\left(\theta - \frac{\pi}{3}\right) & L \\ \sin\left(\theta + \frac{\pi}{3}\right) & -\cos\left(\theta + \frac{\pi}{3}\right) & L \end{bmatrix} \tag{6.7}$$

$$\Gamma(q,\dot{q}) = \begin{bmatrix} 0_{2\times 1} \\ \dot{\theta}\;(I_r^y - I_r^z)\;\left(\dot{\phi}_1\;\sin(2\,\phi_1) + \dot{\phi}_2\;\sin(2\,\phi_2) + \dot{\phi}_3\;\sin(2\,\phi_3)\right) \\ -\frac{I_r^y - I_r^z}{2}\,\dot{\theta}^2\;\sin(2\,\phi_1) \\ -\frac{I_r^y - I_r^z}{2}\,\dot{\theta}^2\;\sin(2\,\phi_2) \\ -\frac{I_r^y - I_r^z}{2}\,\dot{\theta}^2\;\sin(2\,\phi_3) \end{bmatrix} \tag{6.8}$$

Source seeker control synthesis

Simplified unicyle

This mobile robot exhibits similar kinematics to a rolling wheel. For its control synthesis, we require the distance convergence between desired tracking states and reference curves towards zero according to desired closed-loop behavior. On the current plant, the dynamic extension 1-algorithm, in the C-Appendix, results on the relative degree $\begin{bmatrix}2 & 2\end{bmatrix}^{\intercal}$-vector for tracking output $\begin{bmatrix}x & y\end{bmatrix}^{\intercal}$-vector. For Cartesian $x \times y$ representation, the

[17] Lee on [63]-textbook remarks the cross product $\times$-operator on canonical Euclidean $\mathbb{R}^3$-space corresponds to a Lie bracket operator.

new output states on (6.9)-equalities follow steps presented in 4-appendix for controller synthesis. We omit the state's dependency to provide a light notation.

$$\begin{cases} y^1 = x^1 = h^1 \\ \dot{y}^1 = x^4 \cos(x^3) = L_f\, h^1 \\ \ddot{y}^1 = v^1 \cos(x^3) - x^4\, x^5 \sin(x^3) = L_f^2\, h^1 + L_{g_1} L_f\, h^1\, v^1 + L_{g_2} L_f\, h^1\, v^2 \\ y^2 = x^2 = h^2 \\ \dot{y}^2 = x^4 \sin(x^3) = L_f\, h^2 \\ \ddot{y}^2 = v^1 \sin(x^3) + x^4\, x^5 \cos(x^3) = L_f^2\, h^2 + L_{g_1} L_f\, h^2\, v^1 + L_{g_2} L_f\, h^2\, v^2 \end{cases} \tag{6.9}$$

Since the decoupling $\left(\Delta \coloneqq \begin{bmatrix} L_{g_1} L_f\, h & L_{g_2} L_f\, h \end{bmatrix}\right)$-distribution on (6.10)-matrix is rank-deficient for every $(x \in \mathcal{X})$-point, thus the system requires the dynamic extension procedure. For this study case, the addition of 1 integrator variable suffices.

$$\begin{bmatrix} \cos(x^3) & 0 \\ \sin(x^3) & 0 \end{bmatrix} \tag{6.10}$$

The inverse map theorem brings us information about diffeomorphism regularity: it assures local invertibility for every $(q \in \mathcal{Q})$-point in which the differential dz is regular. With computer algebra system aid, we obtain the z-map differential determinant $\det(d\,z)$-map on (6.11)-equation. dz-One-form, also denoted by transposed pushforward $z_*^\intercal$-vector, loses rank for the case under study on $x \in \mathcal{X}$-points such that $(x_4 \neq 0)$-condition holds. The x_4-state corresponds to linear v-speed. We conjecture the following physical interpretation: the change in linear v-speed direction loses information about past traversed curves.

$$z(x) = \begin{bmatrix} h^1 \\ L_f\, h^1 \\ h^2 \\ L_f\, h^2 \\ \omega \end{bmatrix} = \begin{bmatrix} x^1 \\ x^4 \cos(x^3) \\ x^2 \\ x^4 \sin(x^3) \\ x^5 \end{bmatrix} \iff x(z) = \begin{bmatrix} z^1 \\ z^3 \\ \arctan\left(\frac{z^2}{z^4}\right) \\ \pm\sqrt{(z^2)^2 + (z^4)^2} \\ z^5 \end{bmatrix}$$

$$z_*(x) = \begin{bmatrix} 1 & 0 & 0 & 0 & 0 \\ 0 & 0 & -x^4 \sin(x^3) & \cos(x^3) & 0 \\ 0 & 1 & 0 & 0 & 0 \\ 0 & 0 & x^4 \cos(x^3) & \sin(x^3) & 0 \\ 0 & 0 & 0 & 0 & 1 \end{bmatrix} \tag{6.11}$$

Sastry suggests on [41]-textbook to isolate the full-rank columns of Δ-distribution on the left side of the matrix by right matrix-multiplication i.e. redefinition of input v-vector by linear $V\tilde{v}$-map, and definition of input derivative as a further state, which names the algorithm as *dynamic extension*.

For this study case, the V-matrix is the identity $\mathrm{Id}_{\mathbb{R}^2}$-matrix. Hence, we add the disk rolling acceleration as an additional state.

$$
\begin{aligned}
v &= \overbrace{\begin{bmatrix} 1 & 0 \\ 0 & 1 \end{bmatrix}}^{V} \begin{bmatrix} z^1 \\ w^2 \end{bmatrix} \\
\dot{z}^1 &= w^1
\end{aligned}
\tag{6.12}
$$

The equivalent system on coordinate (6.13)-map takes the linear form defined by controllable (2.26)-matrices on curly brackets.

$$
z(x) = \begin{bmatrix} x \\ \dot{x} \\ \ddot{x} \\ y \\ \dot{y} \\ \ddot{y} \end{bmatrix} = \begin{bmatrix} x^1 \\ x^4 \, \cos\left(x^3\right) \\ x^6 \, \cos(x_3) - x_4 \, x_5 \, \sin(x^3) \\ x^2 \\ x^4 \, \sin\left(x^3\right) \\ x^6 \, \sin(x^3) + x^4 \, x^5 \, \cos(x^3) \end{bmatrix} \Longleftrightarrow x(z) = \begin{bmatrix} z^1 \\ z^3 \\ \arctan\left(\frac{z^2}{z^4}\right) \\ \sqrt{(z^2)^2 + (z^4)^2} \\ \frac{z^2 \, z^6 - z^3 \, z^4}{(z^2)^2 + (z^4)^2} \\ \frac{z^2 \, z^3 + z^4 \, z^6}{\sqrt{(z^2)^2 + (z^4)^2}} \end{bmatrix}
\tag{6.13}
$$

The new steering control w-map from its original position to the planned trajectory curve also follows. The augmented relative degree κ-vector for the omnirobot is given by $\begin{bmatrix} 3 & 3 \end{bmatrix}^{\intercal}$-vector.

$$
\begin{aligned}
\underbrace{\begin{bmatrix} 1 & 0 \\ 0 & 1 \end{bmatrix}}_{B^\kappa} w &= \underbrace{\begin{bmatrix} \dddot{x} \\ \dddot{y} \end{bmatrix}}_{y^\kappa} + \underbrace{A_2 \begin{bmatrix} \ddot{x} \\ \ddot{y} \end{bmatrix} + A_1 \begin{bmatrix} \dot{x} \\ \dot{y} \end{bmatrix} + A_0 \begin{bmatrix} x \\ y \end{bmatrix}}_{\underbrace{\begin{bmatrix} a_0^0 & a_1^0 & a_2^0 & & \bigcirc & \\ & \bigcirc & & a_0^1 & a_1^1 & a_2^1 \end{bmatrix}}_{A^\kappa} z} \\
&\Longrightarrow w = \tilde{\Delta}^{-1} \left(y_*^\kappa - L_f^\kappa \, h - A^\kappa \, \tilde{z} + B^\kappa \, w \right)
\end{aligned}
\tag{6.14}
$$

The above deviation equality governs the system's behavior. The system does not exhibit zero dynamics. The polynomial a_j^i-coefficients are equal to elements on diagonal entries of the square A_i-matrix. For simplicity, we choose all linearization eigenvalues to equal 0, as on 6.15-equality. The auxiliary A^κ-matrix results in null $0_{2\times 6}$-matrix. Author Eduardo Sontag refers on his [36]-book to this matrix with null eigenvalues and control matrix with canonical vectors as *controllable canonical* or *Brunóvsky* form.

$$
\dot{\tilde{z}} = \underbrace{\begin{bmatrix} A^0 & 0 \\ 0 & A^0 \end{bmatrix}}_{A} \tilde{z} + \underbrace{\begin{bmatrix} e_3 & 0 \\ 0 & e_3 \end{bmatrix}}_{B} w, \quad \text{for matrix } A^0 \text{ equal to } \begin{bmatrix} 0 & 1 & 0 \\ 0 & 0 & 1 \\ 0 & 0 & 0 \end{bmatrix}
\tag{6.15}
$$

The coupling $\tilde{\Delta}$-distribution, deviation, and its derivatives follow on (6.17)-equation. The resulting control $(u,\, v,\, w)$-maps on curly brackets (6.16)-equalities follow as we expect on control (2.34)-structure.

$$
\begin{cases}
\dot{z}_1 &= w_1 \\
u &= \frac{R}{2} \begin{bmatrix} m & \frac{1}{L} I_3 \\ m & -\frac{1}{L} I_3 \end{bmatrix} v \\
v &= \mathrm{Id}_{\mathbb{R}^2} \begin{bmatrix} z_1 \\ w_2 \end{bmatrix} \\
a^i &= \begin{bmatrix} -\lambda_1^i \, \lambda_2^i \, \lambda_3^i & \lambda_1^i \, \lambda_2^i + \lambda_1^i \, \lambda_3^i + \lambda_2^i \, \lambda_3^i & -\lambda_1^i - \lambda_2^i - \lambda_3^i \end{bmatrix} \\
K &= a^1 \oplus a^2 \\
w &= \tilde{\Delta}^{-1} \left(y_\star^\kappa - L_f^\kappa \, h - K \, \tilde{z} \right)
\end{cases}
\tag{6.16}
$$

$$
\begin{cases}
\tilde{\Delta} = \begin{bmatrix} \cos(x_3) & -x_4 \, \sin(x_3) \\ \sin(x_3) & x_4 \, \cos(x_3) \end{bmatrix} \\
L_f^\kappa h = \begin{bmatrix} -x_4 \, \cos\left(x_3\right) \, {x_5}^2 - 2 \, x_6 \, \sin\left(x_3\right) \, x_5 \\ 2 \, x_5 \, x_6 \, \cos\left(x_3\right) - x_4 \, {x_5}^2 \, \sin\left(x_3\right) \end{bmatrix} \\
\tilde{y} = \begin{bmatrix} x_1 - x_1^\star \\ x_2 - x_2^\star \end{bmatrix} \\
\dot{\tilde{y}} = \begin{bmatrix} x_4 \, \cos(x_3) - \dot{x}_1^\star \\ x_4 \, \sin(x_3) - \dot{x}_2^\star \end{bmatrix} \\
\ddot{\tilde{y}} = \begin{bmatrix} x_6 \, \cos(x_3) - x_4 \, x_5 \, \sin(x_3) - \ddot{x}_1^\star \\ x_6 \, \sin(x_3) + x_4 \, x_5 \, \cos(x_3) - \ddot{x}_2^\star \end{bmatrix}
\end{cases}
\tag{6.17}
$$

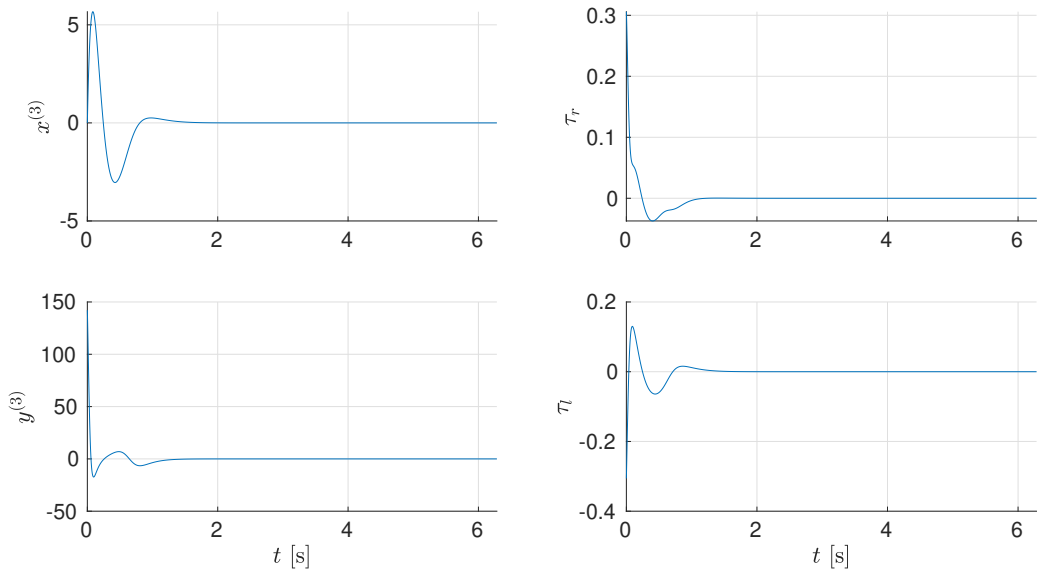

Figure 20: Derivative $\left(x^{(3)}, y^{(3)}\right)(t)$-curves and torque $(\tau_\phi, \tau_\theta)(t)$-time-series along $(t \in [0, 2\,\pi])$-time.

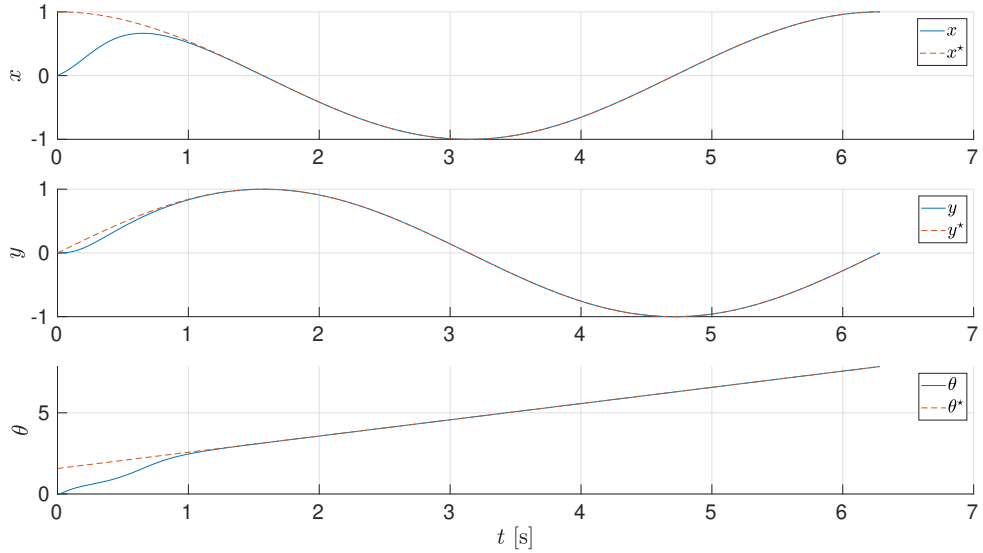

Figure 21: Unicycle states $(x, y, \theta)(t)$-time-series along $(t \in [0, 2\,\pi])$-time.

Omnidirectional robot

The omnirobot control with tracking (x, y, θ)-states does not require additional integrators. However, the procedure to obtain the control map and steer the system follows the dynamic extension 1-algorithm in the appendix. The states and diffeomorphic φ-map correspond to the relations on curly (6.19)-brackets.

The control u-map for given robot corresponds to $\left[\Delta^{-1}\left(y_{\star}^{\kappa}(t) - \tilde{A}\,\tilde{z} - L_f^{\kappa} h\right)\right]$-map, with Hurwitz $\left(\tilde{A} \coloneqq A^{\kappa} + B^{\kappa} K\right)$-matrix.

$$
\begin{cases}
a^i = \left[\lambda_{1i}^i \; \lambda_2^i \quad -\lambda_1^i - \lambda_2^i\right],\ \lambda \in \mathbb{C}^- \\
A^{\kappa} = a^1 \oplus a^2 \oplus a^3,\ B^{\kappa} = \mathrm{Id}_{T\mathbb{S}^3} \\
\Delta = \Theta^{-1}\, B^{\intercal}\, q_* \\
L_f^{\kappa}\, h = \left(B^{\intercal}\, q_*\right)^{-1} \left(I(q,\, p) + \mathrm{grad}^{\vartheta}\, \varrho\right) \\
k^i = -a^i + \left[\mu_1^i \, \mu_2^i \quad -\mu_1^i - \mu_2^i\right],\ \mu \in \mathbb{C}^- \\
v = K\, \tilde{z}
\end{cases}
\tag{6.18}
$$

Remark 11. $(\lambda_{1i}, \lambda_{1i}, \mu_{1i}, \mu_{1i})$-Eigenvalues must be, if they are complex, then conjugate due real-valued control map.

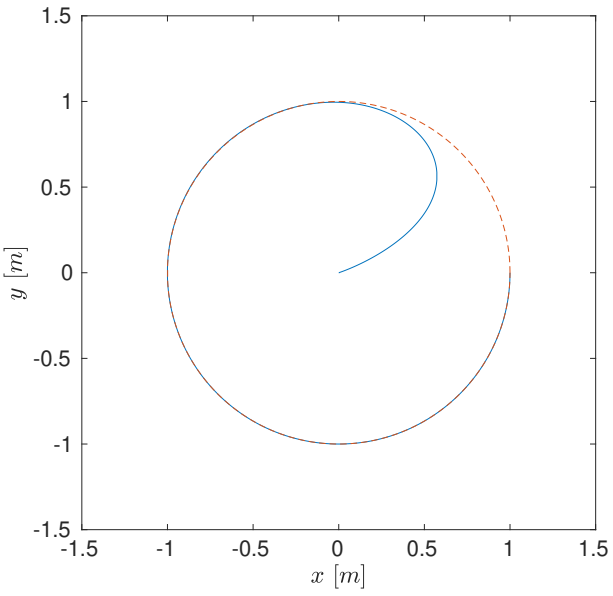

Figure 22: Trajectory tracking of a circular curve on Euclidean $\mathbb{R}^2$-plane

The necessary control map elements follow on curly (6.18)-brackets. Its synthesis corresponds to the linearization algorithm in C-Appendix. In this case, the controller K-matrix corresponds to tensorial $(k^1 \oplus k^2 \oplus k^3)$-sum. Finally, the diffeomorphic map respective to coordinate Z-chart and its inverse are available on curly (6.19)-brackets. The P_{ij}-matrix is also known as a

permutation matrix due to its rows/columns swap property by right/left multiplication, on A.1-lemma.

$$\begin{cases} x = \begin{bmatrix} q^\intercal & p^\intercal \end{bmatrix}^\intercal = \begin{bmatrix} x & y & \theta & \phi^1 & \phi^2 & \phi^3 & v_x & v_y & \omega \end{bmatrix}^\intercal \\ z = \varphi(x) = \begin{bmatrix} x & v_x & y & v_y & \theta & \omega & \phi^1 & \phi^2 & \phi^3 \end{bmatrix}^\intercal \\ \quad = \begin{bmatrix} x^1 & x^7 & x^2 & x^8 & x^3 & x^9 & x^4 & x^5 & x^6 \end{bmatrix}^\intercal \\ \quad = \underbrace{P_{27}\, P_{48}\, P_{59}\, P_{74}\, P_{58}\, P_{69}}_{P}\, x \\ x = \varphi^{-1}(z) = P^{-1}\, z = P^\intercal\, z \\ \quad = P_{69}^\intercal\, P_{58}^\intercal\, P_{74}^\intercal\, P_{59}^\intercal\, P_{48}^\intercal\, P_{27}^\intercal\, z \end{cases} \tag{6.19}$$

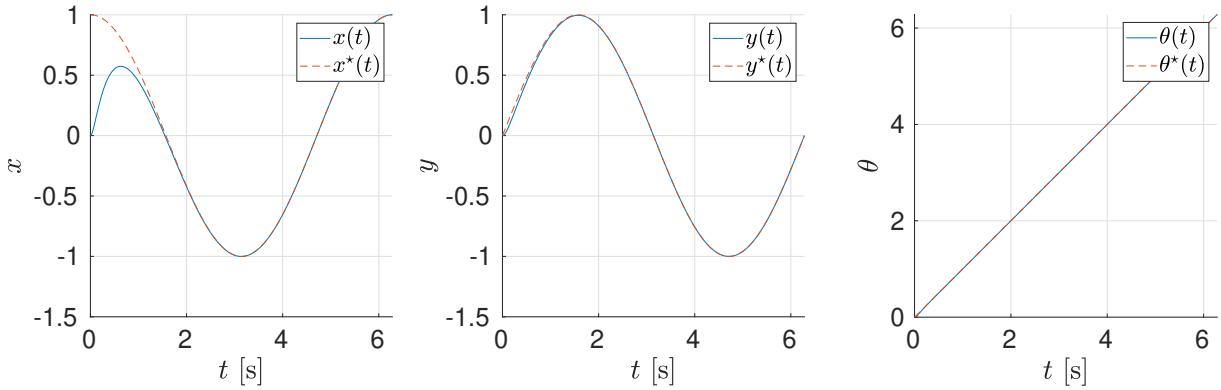

a. Position and orientation state $(x, y, \theta)(t)$-time-series

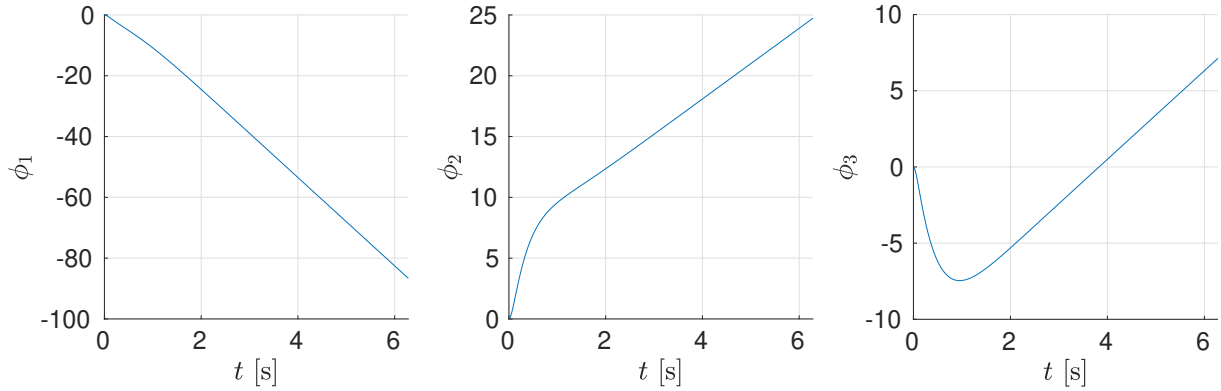

b. Wheel orientation state $\phi_i(t)$-time-series

Figure 23: States along $(t \in [0,\, 2\pi])$-time for initial null $0_{6\times1}$-point and reference $\begin{bmatrix} \cos(t) & \sin(t) & t \end{bmatrix}^\intercal$-curve.

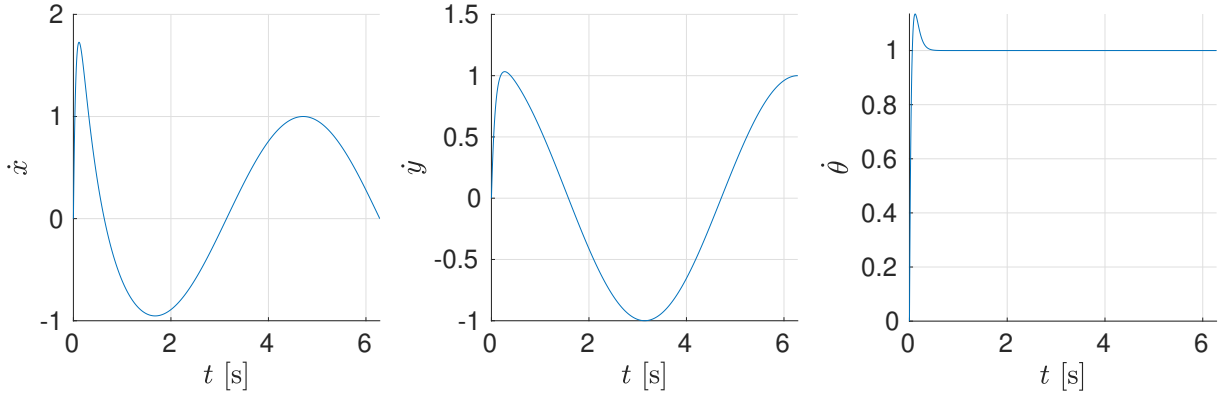

Figure 24: Speeds states $(v_x, v_y, \omega_\theta)(t)$-time-series

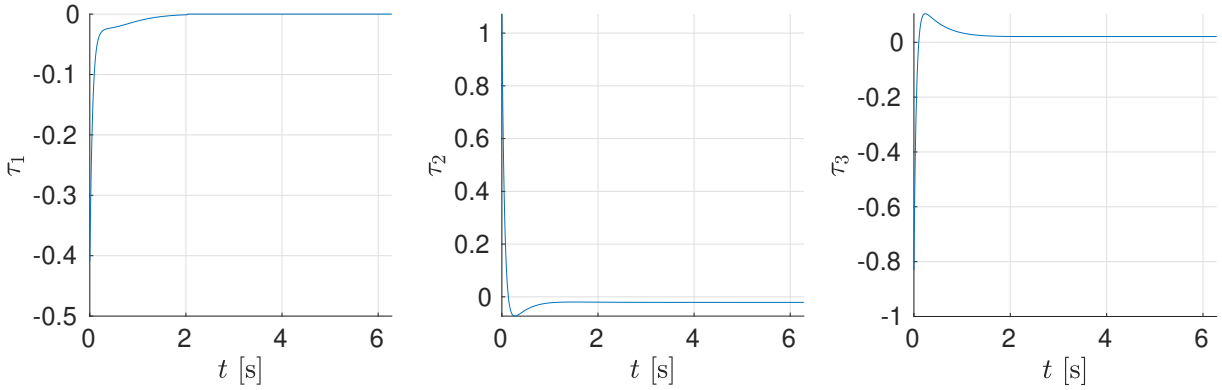

Figure 25: Motor shaft torques $\tau_i(t)$-time-series

Simulation results

This section presents simulation results respective to the flow diagram in Fig. 11. The integration step is the most relevant issue among numerical requirements for source-seeking strategy implementation. Hence, the simulation instances utilize numerical integration methods with adequate relation steps per simulation time. Typical Taylor-based integration methods like Euler and Runge-Kutta are prone to virtual total energy dissipation. Physical systems are energy-invariant except there are dissipative interactions related to, e.g., Coulomb or viscous friction. Among references on this numerical topic, one may cite [69]-work.

Noise addition to destination, trajectory curve or control map

This subsection exhibits source-seeking simulation results by adding Gaussian noise to the following map signals: control input, tracking trajectory, trajectory destination, and barycenter coordinates at the end of curiosity time intervals. These strategies affect the deterministic control signal only such that the input $u(t, x)$-map becomes noise-dependent $\tilde{u}(t, x, z)$-map.

According to driven simulations, the Gaussian stochastic contribution sole to the input control signal is not standalone sufficient to deviate the dynamical system in the direction of some source signal minimum on the neighborhood. It occurs due to noise suppression

related to dynamical system *eigen* damping properties.

In conclusion to the previous paragraph discussion, since sole noise contribution to the control map may not be sufficient in general for the source-seeking strategy, an additional source estimation, independent of dynamical system properties, plays a relevant role in the task. Among options, the environment exploration strategies as investigation points along the neighborhood of to-source-candidate trajectory and descriptive points of the dynamical system at specific instants are encouraging. The latter strategy is present in simulation instances in 26-figure.

The simulation instances require, additionally to plant model parameters, a set of algorithmic seeking parameters referred on (1, 2, 3)-tables. They relate respectively to time, controller synthesis hyperparameters, and barycenter coordinates.

Description	Symbol	Unit	Value
Simulation interval	$\Delta\tau_n$	ms	1
Curiosity interval	$\Delta\tau_s$	ms	100
Estimation interval	$\Delta\tau_e$	ms	500
Planning interval	$\Delta\tau_t$	ms	500
Simulation duration	t_f	s	20
Control map poles	λ	-	-10

Table 1: Simulation and control time parameters

Description	Symbol	Unit	Value
Speed enhancer	ν	-	5
Standard deviation	σ	m	0.5
Mean speed enhancer	ξ	-	0

Table 2: Barycenter method parameters

Description	Symbol	Unit	Value
Trajectory	σ_d	m	0.1
Interval goal point	σ_t	m	0.1
Control input	σ_u	Nm	0.5

Table 3: Zero-mean gaussian noise standard deviation

$$3\,(1-x)^2\,e^{-x^2-(y+1)^2} - 10\left(\frac{x}{5} - x^3 - y^5\right)e^{-x^2-y^2} - \frac{1}{3}\,e^{-(x+1)^2-y^2} \tag{6.20}$$

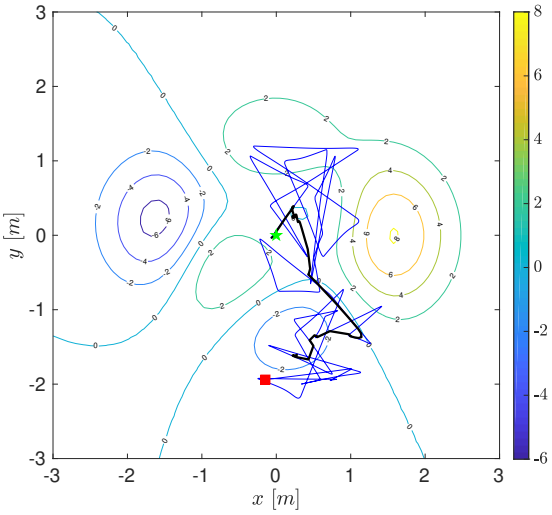

a. On estimated source $\begin{bmatrix}\hat{x} & \hat{y}\end{bmatrix}^{\intercal}$-point at estimation t_i-instants.

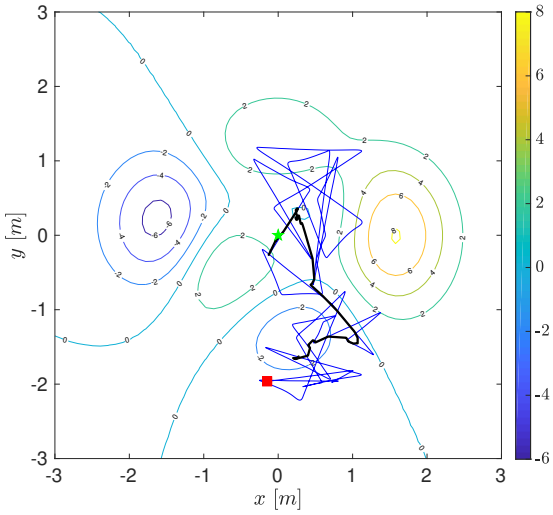

b. On estimated source $\begin{bmatrix}\hat{x} & \hat{y}\end{bmatrix}^{\intercal}$-point for every time $(t \in [t_i,\, t_{i+1}])$-instant.

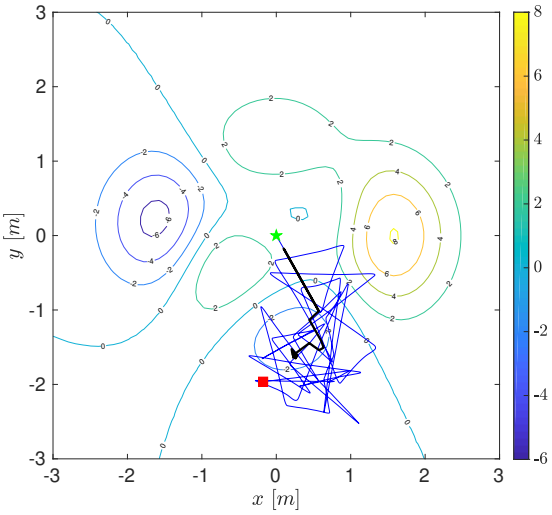

c. On reference $\begin{bmatrix}x^{\star} & y^{\star}\end{bmatrix}^{\intercal}(t)$-curve for every time instant $t \in [t_i,\, t_{i+1}]$.

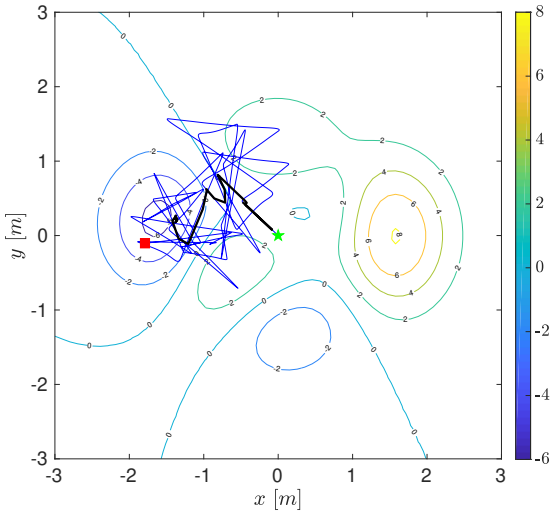

d. On control $u(t)$-time-series for every time $(t \in \mathbb{R}_{\geq \tau_0})$-instant

Figure 26: Barycenter-based source seeking on Cartesian $\mathbb{R}^2$-plane for source signal map as expression given by (6.20)-expression. Isochromatic level curves represent the geometric loci with identical map values. The ($\star$, $\blacksquare$)-markers denote respectively the curve start and endpoints. The blue and black lines denote the robot trajectory curve and the barycenter points along time.

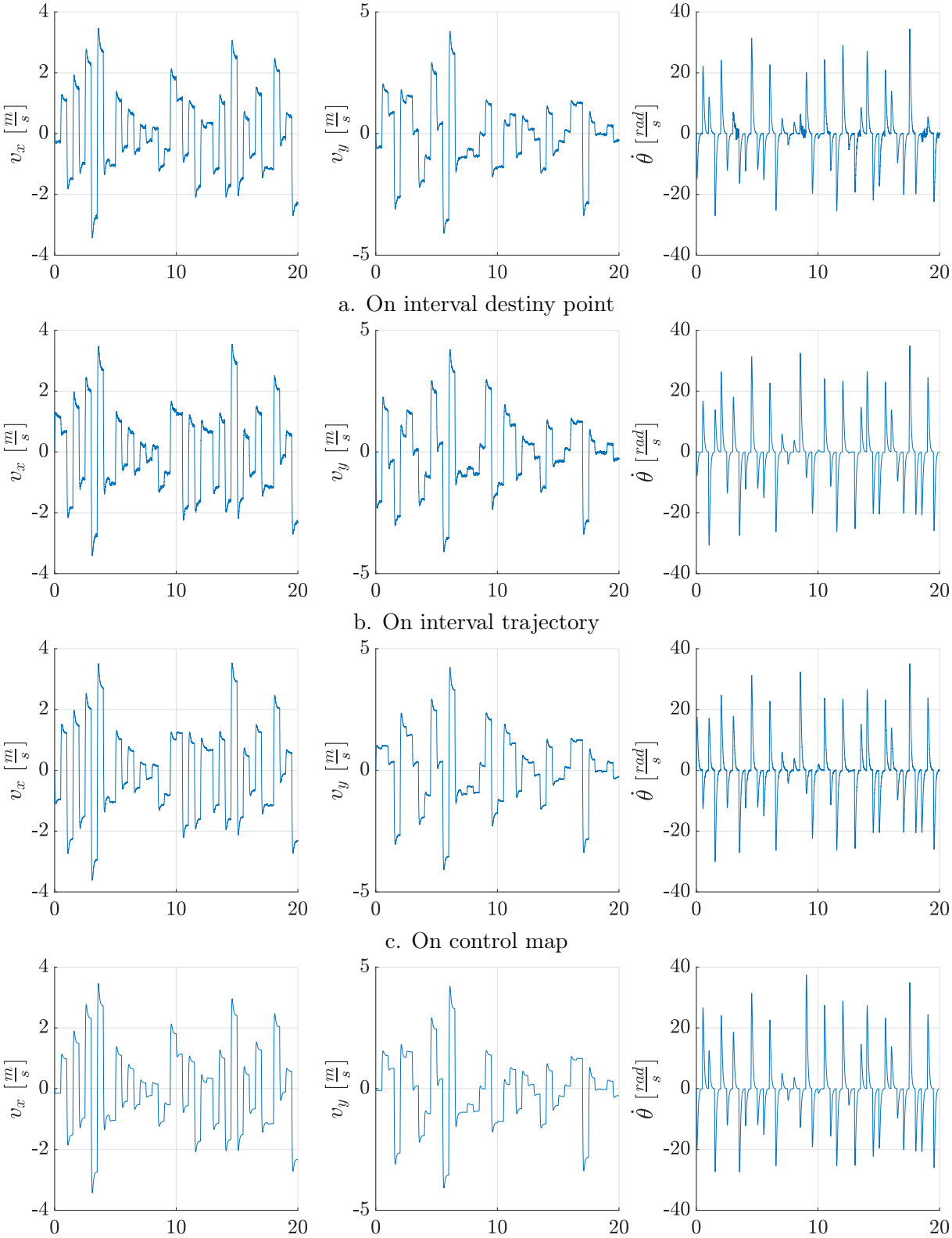

Figure 27: Mobile agent velocity vector $p(t)$-time-series under zero-mean Gaussian stochastic noise.

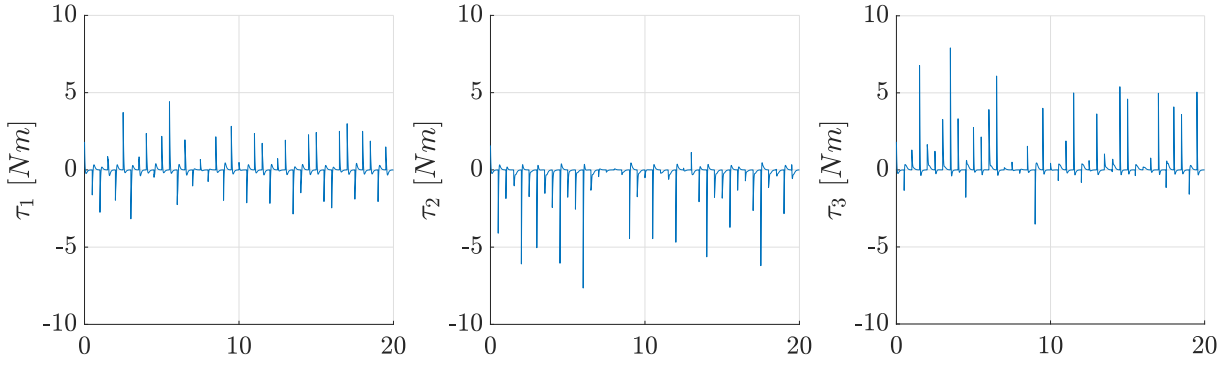

a. On goal coordinate at curiosity interval instants

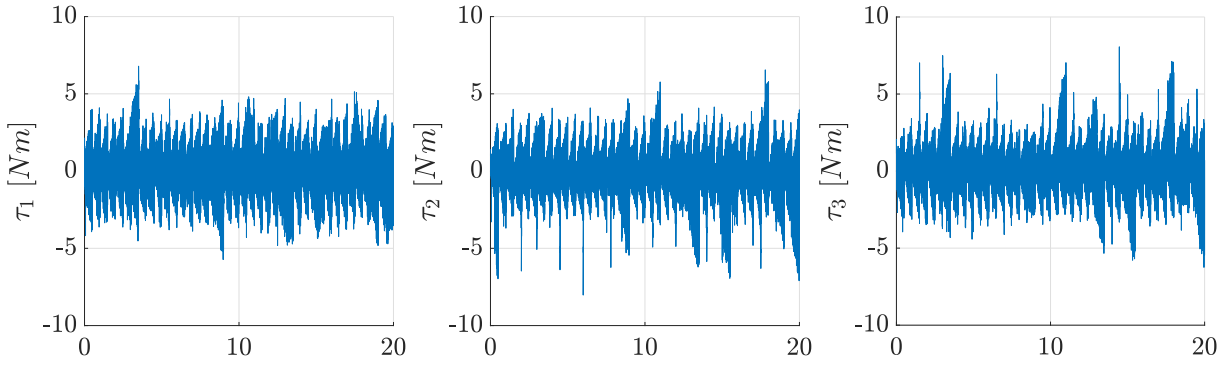

b. On interval destiny point

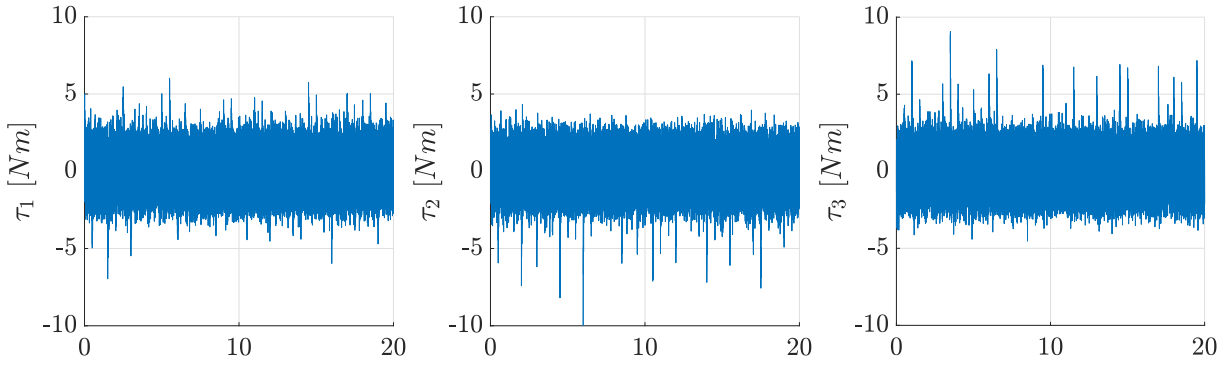

c. On interval trajectory

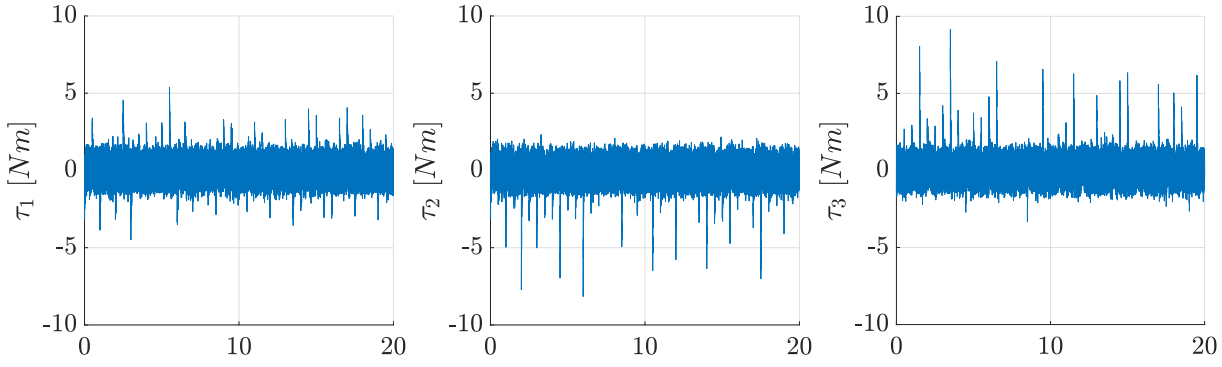

d. On control map

Figure 28: Control $u(t)$-time-series under zero-mean Gaussian stochastic noise.

Simulation instances averaging

The stochastic curiosity contribution to the source-seeking algorithm provides a random walk around the base $\mathcal{X}$-space. The simulation scenarios presented in the previous section suggest the necessity of time-series expected value due to additional stochastic behavior.

For simplicity, we assign the first interval $\bar{y}^{i,0}$-element as estimation $\hat{y}_i$-point of curiosity interval $\{\bar{y}^{i,j}\}$-sequence, equal to immediately best $\bar{y}^{i-1,n_s}$-estimation to some stochastic noise z_i-vector. Given fixed i-index, the $\{\bar{y}^{i,j}\}$-sequence within $[\tau_i,\, \tau_{i+1}]$-interval has n_s-cardinality. For brevity, maps dependency on $(\hat{y}_i, \bar{y}^{i,j})$-elements receive respectively the i-subscript and $(i,\, j)$-superscript. The source estimation formation rule within the curiosity $[\tau_i,\, \tau_{i+1}]$-interval is below to consult.

$$\begin{cases} \bar{y}^{i+1,0} & = \hat{y}_{i+1} = \bar{y}^{i,n_i} + z^i \\ \bar{y}^{i,j+1} & = (1 - F_{i,j})\, \bar{y}^{i,j} + F_{i,j}\, y^s_{i,j} \end{cases} \tag{6.21}$$

We assign for the all-first $(\hat{y}_0, \bar{y}^{0,\,0})$-points at τ_0-instant to $(y^0_s + z_0, y^0_s)$-points. By finite induction, the source estimation point recursion (6.21)-rule at $(\tau_0 + i\,\Delta\tau_e + j\,\Delta\tau_s)$-instant follows on (6.22)-expression.

$$\bar{y}^{i,j} = \hat{y}_i + \sum_{k=1}^{j} f_{i,j,k}\, (y^s_{i,k} - \hat{y}_i) \tag{6.22}$$

The scalar $f_{i,j,k}$-maps correspond to the product $\left(F_{i,k} \prod\limits_{l=k+1}^{j} (1 - F_{i,l})\right)$-terms. The corner case for equality $(j = k)$-condition i.e. $f_{i,j,j}$-term corresponds to the scalar $F_{i,j}$. The limit case corresponds to j-index equal to n_s-cardinal. In its turn, we substitute $\bar{y}_{i,n_s}$-vector by difference $(\hat{y}_{i+1} - z_{i+1})$-computation on (6.21)-equation. By algebraic manipulation, the following recursion emerges.

$$\begin{aligned} \hat{y}_{i+1} &= \hat{y}_i + \sum_{k=1}^{n_s} f_{i,n_i,k}\, (y^s_{i,k} - \hat{y}_i) + z^{i+1} \\ &= \varphi_i\, \hat{y}_i + Y^i_k\, f^k + z^{i+1} \end{aligned} \tag{6.23}$$

For briefness, row f^k-elements corresponds to row $f_{i,n_i,k}$-elements, the X_i-matrix composes column-wise by $y^s_{i,k}$-vectors. Scalar φ_i-maps corresponds to the $\left(1 - \sum\limits_{k=1}^{n_i} f_{i,n_i,k}\right)$-element. We nominate the sum $Y^i_k\, f^k$-term by input w_i-vector: the right-hand side of the recursive $(\varphi_i\, \hat{y}^i + w_i + z_{i+1})$-equation takes the form of a linear discrete dynamical system, familiar to control theorists. On iteration n-step, the iterative formula application gives the source estimation $\hat{y}_n$-point.

$$
\begin{aligned}
\hat{y}_1 &= \varphi_0\,\hat{y}_0 + w^0 + z^1 \\
\hat{y}_2 &= \varphi_1\,\hat{y}_1 + w^1 + z^2 \\
&= \varphi_1\,\varphi_0\,\hat{y}_1 + \varphi_1\,w^0 + w^1 + \varphi_1\,z^1 + z^2 \\
\hat{y}_3 &= \varphi_2\,\hat{y}_2 + w^2 + z^3 \\
&= \varphi_2\,\varphi_1\,\varphi_0\hat{y}_2 + \varphi_2\,\varphi_1\,w^0 + \varphi_2\,w^1 + w^2 + \varphi_2\,\varphi_1\,z^1 + \varphi_2\,z^2 + z^3 \\
&\vdots \\
\hat{y}_n &= \Phi_n\,y_s^0 + \psi_n + \omega_n
\end{aligned}
\tag{6.24}
$$

The anew map $(\Phi_n,\ \psi_n,\ \omega_n)$-tuple is respectively given by (6.25)-tuple. The indexed $\bar{\varphi}_k$-map corresponds to product $\left(\prod_{l=k+1}^{n-1}\varphi_l\right)$-map. Einstein's summation convention is in force.

$$
\left(\bar{\varphi}_{-1},\quad \bar{\varphi}_k\,w^k,\quad \bar{\varphi}_k\,z^k\right) \tag{6.25}
$$

The recursive (6.24)-computation requires current (indexed) barycentric $\left(y_{i,j}^s \coloneqq y_s(x(t))\right)$-points, for the barycentric seeking algorithm. For the case under subject, they are, by hypothesis, the cartesian position vector $\left(\begin{bmatrix} x & y \end{bmatrix}^\intercal(t)\right)$-time-series. By its turn, for every curiosity time $[i,\ i+1]\,\Delta\tau_e$-interval, it converges asymptotically towards source estimation position $\hat{y}_i$-point by error dynamic rule as follows: the tracking output y-points given by $y^\star(t) + e^{A\,(t-t_i)}\,\tilde{y}_i$-curve, for Hurwitz-stable A-matrix, $\tilde{y}$-point equal to the deviation between output and reference curve. The reference $y^\star$-curve represents the time development for design-chosen trajectory $\gamma(t, \hat{y}_i)$-curve and its necessary derivatives.

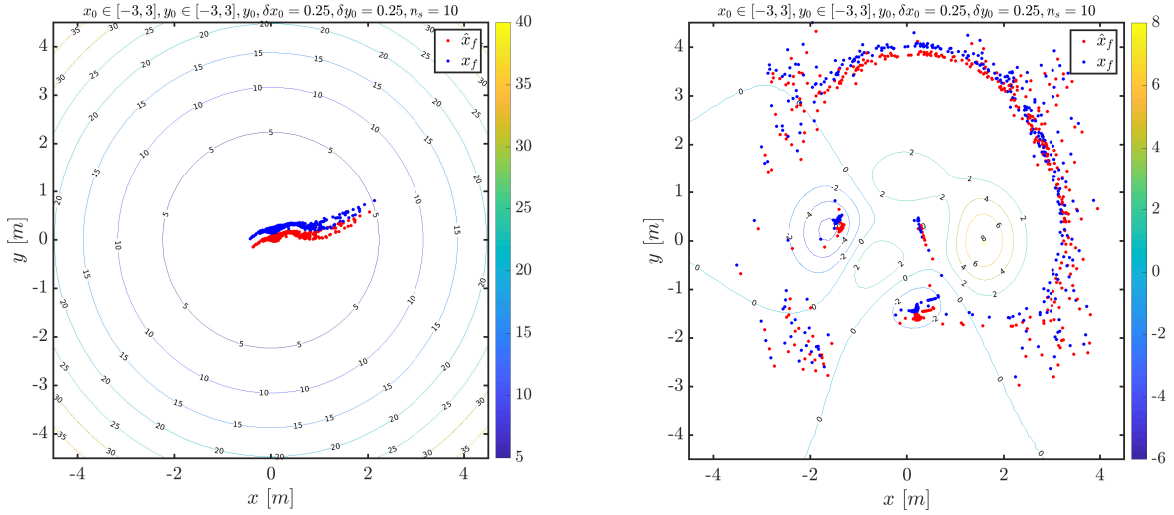

a. Parable map with center $\begin{bmatrix} 0 & 0 \end{bmatrix}^\intercal$-point

b. Peaks map

Figure 29: Cartesian representation of final points and source estimation with source signal map as a parable and *peaks* expressions for 10 simulation instances, spatial discretization $(\delta_{x_0}, \delta_{y_0})$-intervals equal to 0.25 m and final simulation time equal to 20 s. Each simulation instance $\bar{\tau}_s$-duration is (9.05 ± 0.53) s.

The duration of each source-seeking simulation is a relevant analysis metric for real-time simulation feasibility. We employ the Simulink environment of software *Matlab*

2017a for results reproduction with parameters as specified in table 1. The required real-time simulation τ_f-duration depends on spatial deviation δ-vector between 2-dimensional positional initial points, spatial hull diameter Δ-vector, simulation instances p-cardinality for each initial positional x_0-point and average actual simulation instance $\bar{\tau}_s$-time. Thus, the computational time complexity is proportional to the simulation instances cardinality, defined by Big-O $O(m\,n\,p)$-complexity.

$$\underbrace{\left(\left\lfloor\frac{\Delta_x}{\delta_{x_0}}\right\rfloor+1\right)}_{m}\underbrace{\left(\left\lfloor\frac{\Delta_y}{\delta_{y_0}}\right\rfloor+1\right)}_{n}\,p\;\bar{\tau}_s \tag{6.26}$$

7 DISCUSSIONS

"All truths are easy to understand once they are discovered; the point is to discover them."

-- Galileo Galilei

This section discusses the thesis results: it summarizes the main heuristics characteristics based on the Euclidean barycenter method. The former discussion concerns the tuning parameters and their influence on the convergence towards a source signal minimum. Then, we refer to the properties of constrained systems and asymptotic convergence towards a reference trajectory. Subsequently, the trajectory synthesis flavors are the central topic. Finally, the strategy on flow 11-diagram concerning the coupling heuristics of control, trajectory generation, and source estimation strategies is under investigation.

The main tuning parameters on the barycenter method refer to the enhancement ν-term, covariance Σ-tensor, speed enhancement ζ-term, and forgetting λ-factor. The former is responsible for system convergence towards the gradient direction. The standard deviation Σ-tensor corresponds to an exploration term around the surface gradient. The ξ-term intensifies the gradient direction given by the previous barycenter $\Delta\hat{x}_{n-1}$-step. Finally, as the name recalls, the forgetting λ-factor relies on recent barycenter steps by mitigation of past ones. Its application for values lower than 1 resembles a geometric series with a λ-ratio.

According to each 18-figure's grid first row, the greater the ν-hyperparameter, the longer the gradient trace blue line. Likewise, the greater the standard deviation, the broader the distribution on a neighborhood from the respective line, coherent with the standard deviation behavior. Although the speed ξ-enhancer impresses significant influence on probability support map mean $\bar{z}$-vector, the estimation $\hat{x}$-point does not exhibit great improvement by this parameter variation. For the least, λ-ratio lower than 1 turns the points distribution "less behaved", erratic, respective to a known gradient vector field.

Aside from dynamical system characteristics, by the hypothesis of barycentric convergence towards a local minimum, it is reasonable to consider the decrease of oracle map evaluation at barycenter points since it follows on average the gradient direction. By exploitation of the Lyapunov discrete stability criterium, we obtain a further argument for its decreasing behavior. A null mean vector choice and application of Jensen's inequality translates the intuition into a quantitative criterium regarding its convergence. A more rigorous investigation may follow up in the future, but for the current work, it suffices.

On the interpolation trajectories between barycenter (A, B)-points, the barycenter point related to a curve corresponds to the resulting point from the barycenter batch evaluation on (2.1)-equality. The barycenter point for a given curve or continuous region refers to the continuous version of the barycenter method, available on [70]-work. For simplicity and engineering perspective, we utilize its discrete version. A remark raises of curves, given as an intrinsic method property: Non-rectilinear curves within the source

signal field result in points inside its convex hull. Mainly, geodesic curves contain their barycenter on their path.

Regarding the trajectories, they are free to choose insofar as it considers the information available at the moment. For the current work, the robot disposes of its current position and the estimated source position as the reference point. Therefore, a natural path choice considers both beginning and endpoints as boundary conditions. A suitable choice considers, as already mentioned, polynomial and exponential-based paths. A famous polynomial path is the *Bézier's curve*. Due to its tangency property to the curve of either two first and last points, it is problem-suitable since we keep the system orientation on the curve tail. Alternative curves are possible, as the curve-line-based from section 6.

Finally, the current author discusses the proposed investigation of source seeking depicted on the flow 11-diagram. The heuristic relies on time interval relations, controller time constants, and barycenter tuning parameters. The influence of barycenter parameters on the convergence and the relation between algorithm time intervals are in 5-section. A further argumentation regards the control time constants and the curiosity time interval. 2.5-Lemma exposes the relation between time and precision on asymptotic stabilization. Therefore, the eigenvalues choice for the tracking controller synthesis comes out by the precision criterium of mentioned lemma.

8 CONCLUSIONS AND IMPROVEMENTS

"Has this world been so kind to you that you should leave with regret? There are better things ahead than any we leave behind."

-- Clive Staples Lewis

The current work describes an application for the barycenter method to seek the position of a scalar signal source. Although the primary objective concerns the source search, the mechatronic search agent may exhibit constraints on its own dynamical description. Due to its kinematic properties, the problem requires awareness regarding its movement in its current configuration.

The proposed approach defines a trajectory curve to move the robot toward the source estimation point and steer it somewhat to explore and acquire new source sample data. The trajectory synthesis is research-relevant due to the already-mentioned constraints. A possible requirement intends an optimal time or minimal energy, although it is not even a necessary requirement. Therefore, the current author employs reference trajectory curves with a low computational cost to allow implementation.

We employ the algorithmic procedure of the partial linearization method to develop a control map and drive the system toward the developed reference curve. Its choice is not compulsory but relies on the author's choice of a comprehensive synthesis tool for the current application.

Barycentric source-seeking research disposes of improvement aspects. Among others, it figures the multiple sensors and/or source-seeking agents extension due to method parallelization property, as presented on [2]-reference.

Finally, we present below several research suggestions for future endeavors on application possibilities.

A possible control synthesis strategy consists of the sliding mode control, first investigated by the author Utkin in [71]-work and further developed for particular dynamic classes by Anthony Bloch and Roger Brockett. Among works of mentioned methods, the current author cites his mentor's [72]-work about hybrid control and nonholonomic systems and author Utkin's kinematic and dynamic-oriented ([71] [73])-works.

Parametric uncertainties on the nominal plant parameter partition generate a system flow trajectory deviation. A common deviation mitigation/suppression strategy employs the sliding mode control by Lyapunov stability and boundedness properties. However, due to the partial linearization method as control synthesis, we rely on the diffeomorphic map between nonlinear and linear system versions, which also experience parametric deviation. Formally, the statement refers to the robustness property of composition $x \circ z$-map i.e. $z \circ x$, which is akin to identity map $\mathrm{Id}_{\mathcal{X}}$ i.e. $\mathrm{Id}_{\mathcal{Z}}$ except for some to-define bounded deviation δ_x-map i.e. δ_z. Since this robust approach deserves further development, the

current author motivates his readers to further investigate this approach as a forthcoming research topic.

Discretized control strategies are also available to control maps by a plant's discrete dynamical description. For instance, the dynamical Σ-system on 6-subsection allows obtaining its time-invariant discrete representation: the reader might refer to the integral solution form of velocity $\dot{x}$-vector equal to evaluation $f(x, u_k)$-map, for constant control u_k-vector within discretization $[\tau_k,\, \tau_k + \Delta\tau_d]$-interval. Alternatively, we also evaluate the region of convergence (ROC for short) for the discrete control u_k-map as the continuous control u-map applied at a sufficiently small discretization $\Delta\tau_d$-interval.

BIBLIOGRAPHY

1. Sagan, C. *The demon-haunted world: Science as a candle in the dark* (Ballantine Books, 2011).
2. Pait, F. M. The Barycenter Method for Direct Optimization. *arXiv:1801.10533* (2018).
3. Åström, K. J. & Wittenmark, B. *Adaptive control* (Courier Corporation, 2013).
4. Ariyur, K. B. & Krstic, M. *Real Time Optimization by Extremum Seeking Control* ISBN: 0471468592 (John Wiley & Sons, Inc., New York, NY, USA, 2003).
5. Angélico, B. A., Chamon, L. F., Paternain, S., Ribeiro, A. & Pappas, G. J. *Source seeking in unknown environments with convex obstacles* in *2021 American Control Conference (ACC)* (2021), 5055–5061.
6. Peixoto, B., Pait, F. & Angélico, B. *The barycenter-based source seeking* in *Simpósio Brasileiro de Automação Inteligente-SBAI* **1** (2021).
7. Zhang, C., Arnold, D., Ghods, N., Siranosian, A. & Krstic, M. Source seeking with non-holonomic unicycle without position measurement and with tuning of forward velocity. *Systems & Control Letters* **56,** 245–252. ISSN: 0167-6911 (2007).
8. Cochran, J. & Krstic, M. Nonholonomic Source Seeking With Tuning of Angular Velocity. *IEEE Transactions on Automatic Control* **54,** 717–731. ISSN: 0018-9286 (Apr. 2009).
9. Liu, S.-J. & Krstic, M. Stochastic source seeking for nonholonomic unicycle. *Automatica* **46,** 1443–1453. ISSN: 0005-1098 (2010).
10. Cochran, J., Siranosian, A., Ghods, N. & Krstic, M. 3-D Source Seeking for Underactuated Vehicles Without Position Measurement. *IEEE Transactions on Robotics* **25,** 117–129. ISSN: 1552-3098 (Feb. 2009).
11. Lin, J., Song, S., You, K. & Krstic, M. Stochastic source seeking with forward and angular velocity regulation. *Automatica* **83,** 378–386. ISSN: 0005-1098 (2017).
12. Raisch, A. & Krstic, M. Overshoot-Free Steering-Based Source Seeking. *IEEE Transactions on Control Systems Technology* **25,** 818–827. ISSN: 1063-6536 (May 2017).
13. Jinbiao, L., Shiji, S., Keyou, Y. & Miroslav, K. Overshoot-free nonholonomic source seeking in 3-D. *International Journal of Adaptive Control and Signal Processing* **31,** 1285–1295.
14. Zou, R., Kalivarapu, V., Winer, E., Oliver, J. & Bhattacharya, S. Particle Swarm Optimization-Based Source Seeking. *IEEE Transactions on Automation Science and Engineering* **12,** 865–875. ISSN: 1545-5955 (July 2015).
15. Zhu, S., Wang, D. & Low, C. B. Cooperative Control of Multiple UAVs for Moving Source Seeking. *Journal of Intelligent & Robotic Systems* **74,** 333–346. ISSN: 1573-0409 (Apr. 2014).

16. Azuma, S. I., Sakar, M. S. & Pappas, G. J. Stochastic Source Seeking by Mobile Robots. *IEEE Transactions on Automatic Control* **57,** 2308–2321. ISSN: 0018-9286 (Sept. 2012).

17. Atanasov, N. A., Ny, J. L. & Pappas, G. J. Distributed Algorithms for Stochastic Source Seeking With Mobile Robot Networks. *ASME Journal of Dynamic Systems, Measurement, and Control* **137,** 031004-1 - 031004–9 (Mar. 2014).

18. Feynman, R. P. *QED: The strange theory of light and matter* (Princeton University Press, 2006).

19. Wright, M. H. Direct search methods: Once scorned, now respectable. *Pitman Research Notes in Mathematics Series,* 191–208 (1996).

20. Pellicer, L. F. A. O. & Pait, F. M. *BarySearch: Algoritmo de tuning de Modelos de Machine Learning com o Método do Baricentro* in *Anais do XIV Brazilian e-Science Workshop* (2020), 1–8.

21. Jensen, J. L. W. V. *et al.* Sur les fonctions convexes et les inégalités entre les valeurs moyennes. *Acta mathematica* **30,** 175–193 (1906).

22. Lyapunov, A. M. The general problem of the stability of motion. *International journal of control* **55,** 531–534 (1992).

23. Papoulis, A. Random Variables and Stochastic Processes. *McGraw Hill* (1976).

24. Udwadia, F. E. & Kalaba, R. E. *Analytical dynamics: a new approach* (Cambridge University Press, 2007).

25. Frobenius, G. Über das Pfaffsche Problem. *Journal für die reine und angewandte Mathematik* **82,** 230–315 (1877).

26. Bloch, A. M., Marsden, J. E. & Zenkov, D. V. Nonholonomic dynamics. *Notices of the AMS* **52,** 320–329 (2005).

27. Bloch, A. M., Krishnaprasad, P., Marsden, J. E. & Murray, R. M. Nonholonomic mechanical systems with symmetry. *Archive for Rational Mechanics and Analysis* **136,** 21–99 (1996).

28. Gauss, C. F. in *Werke* 23–28 (Springer, 1877).

29. Goldstein, H., Poole, C. & Safko, J. *Classical mechanics* 2002.

30. Meyer, C. D. *Matrix analysis and applied linear algebra* (Siam, 2000).

31. Laub, A. J. *Matrix analysis for scientists and engineers* (Siam, 2005).

32. Burke, W. L. *Applied differential geometry* (Cambridge University Press, 1985).

33. Baruh, H. *Analytical dynamics* (WCB/McGraw-Hill Boston, 1999).

34. Tsai, L.-W. *Robot Analysis and Design: The Mechanics of Serial and Parallel Manipulators* 1st. ISBN: 0471325937 (John Wiley & Sons, Inc., New York, NY, USA, 1999).

35. Stewart, J. *Calculus* (Cengage Learning, 2015).

36. Sontag, E. D. *Mathematical control theory: deterministic finite dimensional systems* (Springer Science & Business Media, 2013).

37. Di Benedetto, M. & Grizzle, J. in *Analysis and Optimization of Systes* 843–850 (Springer, 1990).

38. Di Benedetto, M. & Grizzle, J. Intrinsic notions of regularity for local inversion, output nulling, and dynamic extension of nonsquare systems. *C-TAT* **6,** 357–381 (1990).

39. Isidori, A. Feedback control of nonlinear systems. *International Journal of Robust and Nonlinear Control* **2,** 291–311 (1992).

40. Khalil, H. K. Nonlinear systems. *Upper Saddle River* (2002).

41. Sastry, S. *Nonlinear systems: analysis, stability, and control* (Springer Science & Business Media, 2013).

42. Tzafestas, S. G. *Introduction to mobile robot control* (Elsevier, 2013).

43. Liu, X. *Further Results on the Differential Geometric Approach to Nonlinear Systems Affine in Control* PhD thesis (University of Virginia, 2010).

44. D'Souza, R. Algorithmic Transverse Feedback Linearization (2022).

45. Fliess, M., Lévine, J., Martin, P. & Rouchon, P. Flatness and defect of non-linear systems: introductory theory and examples. *International journal of control* **61,** 1327–1361 (1995).

46. Isidori, A. The zero dynamics of a nonlinear system: From the origin to the latest progresses of a long successful story. *European Journal of Control* **19.** The Path of Control, 369–378. ISSN: 0947-3580. `http://www.sciencedirect.com/science/article/pii/S0947358013000836` (2013).

47. Hermann, R. & Krener, A. Nonlinear controllability and observability. *IEEE Transactions on automatic control* **22,** 728–740 (1977).

48. Wonham, W. M. in *Optimal control theory and its applications* 392–424 (Springer, 1974).

49. Da Cruz, J. J. *Controle Robusto Multivariável: O Método LGQ/LTR Vol. 05* (Edusp, 1996).

50. Marquez, H. J. *Nonlinear control systems: analysis and design* (John Wiley Hoboken^ eN. JNJ, 2003).

51. Ishikawa, M. & Sampei, M. *State estimation of non-holonomic mobile robots using nonlinear observers* in *Proceedings of 1995 IEEE International Conference on Robotics and Automation* **2** (May 1995), 1379–1384 vol.2.

52. Tertychnyi, V. Y. Integral estimation and adaptive stabilization of non-holonomic controlled systems. *Journal of Applied Mathematics and Mechanics* **56,** 881–888 (1992).

53. Hespanha, J. P., Liberzon, D. & Morse, A. S. *Towards the supervisory control of uncertain nonholonomic systems* in *Proceedings of the 1999 American Control Conference (Cat. No. 99CH36251)* **5** (June 1999), 3520–3524 vol.5.

54. Di Benedetto, M. D., Grizzle, J. & Moog, C. Rank invariants of nonlinear systems. *SIAM journal on control and optimization* **27,** 658–672 (1989).

55. Do Carmo, M. P. *Geometria Riemanniana* (Instituto de Matemática Pura e Aplicada, 2008).

56. Callioli, C. A., Domingues, H. H. & Costa, R. C. F. *Álgebra linear e aplicações* (Atual, 2007).

57. Choi, J.-w., Curry, R. & Elkaim, G. *Path planning based on Bézier curve for autonomous ground vehicles* in *Advances in Electrical and Electronics Engineering-IAENG Special Edition of the World Congress on Engineering and Computer Science 2008* (2008), 158–166.

58. Farin, G. & Hansford, D. *The essentials of CAGD* (CRC Press, 2000).

59. Dubins, L. E. On curves of minimal length with a constraint on average curvature, and with prescribed initial and terminal positions and tangents. *American Journal of mathematics* **79,** 497–516 (1957).

60. Reeds, J. & Shepp, L. Optimal paths for a car that goes both forwards and backwards. *Pacific Journal of Mathematics* **145,** 367–393 (1990).

61. Paternain, S., Koditschek, D. E. & Ribeiro, A. Navigation functions for convex potentials in a space with convex obstacles. *IEEE Transactions on Automatic Control* **63,** 2944–2959 (2017).

62. Do Carmo, M. P. *Differential Geometry of Curves and Surfaces: Revised and Updated Second Edition* (Courier Dover Publications, 2016).

63. Lee, J. M. in *Introduction to Smooth Manifolds* 1–31 (Springer, 2013).

64. Dombrowski, P. Krümmungsgrößen gleichungsdefinierter Untermannigfaltigkeiten Riemanniescher Mannigfaltigkeiten. *Mathematische Nachrichten* **38,** 133–180. eprint: `https://onlinelibrary.wiley.com/doi/pdf/10.1002/mana.19680380302`. `https://onlinelibrary.wiley.com/doi/abs/10.1002/mana.19680380302` (1968).

65. Penrose, R. *A generalized inverse for matrices* in *Mathematical proceedings of the Cambridge philosophical society* **51** (1955), 406–413.

66. Gielis, J. A generic geometric transformation that unifies a wide range of natural and abstract shapes. *American journal of botany* **90,** 333–338 (2003).

67. Kane, T. R. & Levinson, D. The use of Kane's dynamical equations in robotics. *The International Journal of Robotics Research* **2,** 3–21 (1983).

68. Campion, G., Bastin, G. & Dandrea-Novel, B. Structural properties and classification of kinematic and dynamic models of wheeled mobile robots. *IEEE transactions on robotics and automation* **12,** 47–62 (1996).

69. Newman, M. *Computational physics* (CreateSpace Independent Publ., 2013).

70. Pait, F. *Reading Wiener in Rio* in *2014 IEEE Conference on Norbert Wiener in the 21st Century (21CW)* (2014), 1–4.

71. Utkin, V. Variable structure systems with sliding modes. *IEEE Transactions on Automatic control* **22,** 212–222 (1977).

72. Piccoli, B., Pait, F. M. & Bittar, A. A hybrid controller for a nonholonomic system. *SBA Cont. Aut* **9,** 85–89 (1998).

73. Aguiar, A. P. & Pascoal, A. Stabilization of the extended nonholonomic double integrator via logic-based hybrid control. *IFAC Proceedings Volumes* **33,** 351–356 (2000).

74. Lee, J. M. *Riemannian manifolds: an introduction to curvature* (Springer Science & Business Media, 2006).

75. Spivak, M. *Calculus on manifolds: a modern approach to classical theorems of advanced calculus* (CRC press, 2018).

76. Lee, J. *Introduction to topological manifolds* (Springer Science & Business Media, 2010).

77. Sontag, E. D. A universal construction of Artstein's theorem on nonlinear stabilization. *Systems & control letters* **13,** 117–123 (1989).

78. Nijmeijer, H. & Van der Schaft, A. *Nonlinear dynamical control systems* (Springer, 1990).

79. Pait, F. & Colón, D. *On the Lyapunov partial differential equation* in *Proceedings of the 45th IEEE Conference on Decision and Control* (2006), 5102–5107.

80. Pait, F. & Colón, D. *Some properties of the Riemannian distance function and the position vector X, with applications to the construction of Lyapunov functions* in *49th IEEE Conference on Decision and Control (CDC)* (2010), 6277–6280.

APPENDIX A – GEOMETRIC CONTROL TOPICS

The main concepts presented in this chapter comprehend several topics of the vast branches *differential geometry* and *Lie Algebra*. The current author attempts to hold on to essentials for brevity and continence despite the extensive definition amount.

Topics on Analysis

Definition A.1 (**Class K, KR maps** [41])**.** A α-map on $(\mathbb{R}_+ \mapsto \mathbb{R}_+)$-relation belongs to K-class if it is continuous, strictly increasing and the $(\alpha(t_0) = 0)$-equality holds. The same previous α-map belongs to KR-class if it is K-class and $(p \to \infty)$-condition implies on $(\alpha(p) \to \infty)$-condition.

Definition A.2 (**Locally positive definite maps** [41])**.** A v-map on $(\mathbb{R}^n \times \mathbb{R}_+ \mapsto \mathbb{R}_+)$-relation is locally positive definite (l.p.d. for short) if, for some $(h \in \mathbb{R}_{>0})$-constant and K-class α-map, we hold $(v(0,\, t) = 0, v(x,\, t) \geq \alpha(|x|))$-conditions, for every $(x \in B_h)$-point and $(t > t_0)$-instant.

Definition A.3 (**Positive definite maps** [41])**.** A v-map on $(\mathbb{R}^n \times \mathbb{R}_+ \mapsto \mathbb{R}_+)$-relation is positive definite (p.d.f. for short) if, for some KR-class α-map, we hold $v(0,\, t) = 0$ and $v(x,\, t) \geq \alpha(|x|)$, for every $(x \in \mathbb{R}^n)$-point and $(t > t_0)$-instant.

Definition A.4 (**Decrescent maps** [41])**.** A continuous v-map on $(\mathbb{R}^n \times \mathbb{R}_+ \mapsto \mathbb{R}_+)$-relation is decrescent if there is a K-class β-map, such that $(v(x,t) \leq \beta(|x|))$-condition holds for every $(x \in B_h)$-point and $(t > t_0)$-instant.

Definition A.5 (**Isomorphism** [63])**.** An φ-isomorphism is a structure-preserving morphism from object X to Y with an inverse morphism:

1. $\varphi^{-1} \circ \varphi = \mathrm{Id}_X$;
2. $\varphi \circ \varphi^{-1} = \mathrm{Id}_Y$.

Theorem A.1 (**Global Existence and Uniqueness Theorem** ([41], page 88))**.** *Consider the dynamical system given by velocity $\dot{x}(t)$-vector as vectorial $f(t,\, x)$-map, piecewise continuous respective to initial $(t \geq t_0)$-instant and initial x_0-point such that, for each time $(T \in \mathbb{R}_{>0})$-constant, there are finite $(k_T,\, h_T)$-constants for every $(t \in [0,\, T])$-instant and $(x, y \in \mathbb{R}^n)$-point. Therefore, the below conditions hold.*

1. $|f(x, t+\delta) - f(y, t+\delta)| \leq k_T\,|x-y|$;

2. $|f(x_0,\, t)| \leq h_T$.

We call 1-hypothesis on A.1-theorem as *Lipschitz continuity condition.*

Definition A.6 (**Lipschitz continuity condition** [41])**.** A f-map is locally Lipschitz continuous in x-point if there is a finite $(l \geq 0)$-constant for some scalar $(h > 0)$-constant such that the $(|f(t,\, x_1) - f(t,\, x_2)| \leq l\,|x_1 - x_2|)$-condition hold, for every $(x_1,\, x_2 \in B_h)$-point and $(t \geq t_0)$-instant.

Theorem A.2 (**Flow vector field continuous dependency on initial point** x_0 ([41], page 88))**.** *We consider a dynamical Σ-system whose velocity $\dot{x}$-vector corresponds to smooth vector field $f(x,\, u)$-map. Additionally, let f-map satisfy A.1-theorem hypotheses. Let x and y be system solutions starting respectively from points x_0 and y_0. Then, for given $(\varepsilon > 0)$-constant, there is scalar $\delta(\varepsilon, T)$-map such that implication condition $|x_0 - y_0| \leq \delta \Longrightarrow |x - y| \leq \varepsilon$ hold.*

We extend globally the concept by substitution of open B_h-set for $\mathbb{R}^n$-set and $(t \geq 0)$-instant. The semi-global extension holds for some scalar $l(h)$-map. By assumption, the Lipschitz property is uniform over t-instant, we call time-invariant systems (T.I.S. for short).

Useful abstract algebra operations and elements concern matricial actions: to permute, concatenate, and inverse, among others. Despite the $\mathbb{C}^{2\times 2}$-family matrices calculation does not exhibit an intricate toolset, its explicit formula also follows.

Lemma A.1 ([30])**.** *The permutation $(P_{ij} \in \mathbb{R}^{n\times n})$-matrix maps the interchange of $(i,\, j)$-index rows/columns by left/right multiplication of resulting expression* $\mathrm{Id}_{\mathbb{R}^n} + E_{ij} + E_{ji} - E_{ii} - E_{jj}$.[18]

Lemma A.2. *The inverse A^{-1}-matrix of a 2-dimensional $(A \in \mathbb{C}^{2\times 2})$-matrix is given on* (A.1)*-expression, for determinant $det(A)$-map equal to expression $a_{11}\,a_{22} - a_{12}\,a_{21}$.*

$$\frac{1}{det(A)} \begin{bmatrix} a_{22} & -a_{12} \\ -a_{21} & a_{11} \end{bmatrix} \tag{A.1}$$

Topics on Differential Geometry

Geometry is a prolific topic. The early masters in Ancient Greece are famous worldwide for their statements. However, geometric developments arise in many other civilizations over time. The modern approach utilizes the formal concepts of points, curves, surfaces, and their further generalizations to operate geometric objects. The list of concerned authors and textbooks is extensive. The current author utilizes the work from authors do Carmo, Lee, Burke, Spivak and Dombrowski.

[18] E_{ab}-Matrix corresponds to a dimension-compatible matrix with 0-entries except at index $(a,\, b)$-tuple, which entry is real 1.

Author Dombrowski promotes on [64]-work a comprehensive explanation of curvature-related measures defined on Riemannian submanifolds. In a *variational calculus* notation, a $\mathcal{M}$-manifold corresponds to a surface with homeomorphic Euclidean $\mathbb{R}^n$-space attached to every $(p \in \mathcal{M})$-point.

We present the main concepts necessary in this work for a Riemannian manifold construction. They are not sufficient conditions for a novice reader since it requires prior knowledge of basic topology concepts. Interested readers may refer to Lee's [76]-textbook to familiarize themselves and cover necessary ideas. We utilize in this work the Levi-Civita ∇-connection. Its main properties refer to symmetry[19] and compatibility[20] with Riemannian $\langle \cdot, \cdot \rangle$-metric. We begin with definition statements in a manner to cover the algebraic-defined surfaces.

Definition A.7 (Coordinate chart [63])**.** Let us define a C^∞-class coordinate chart (U, η)-tuple by linear vector U-space and an $C^\infty(U)$-class cover η-map such that it assigns a $(u \in \mathbb{I}\mathrm{m}_\eta)$-point for every $(p \in \mathbb{D}_\eta)$-point.

Definition A.8 (Riemmanian $\mathcal{M}$-manifold [55])**.** We define a differentiable $\mathcal{M}$-manifold endowed with Riemannian g-metric by countable cover chart $\{U_\alpha\}$-family and respective cover η_α-maps, such that, for each U_α-chart, we have $(i,\, j)$-entries of 2-form metric g_{ij}-tensor given by inner $\langle \partial_i, \partial_j \rangle$-product.

Definition A.9. The covariant derivative $(\nabla \in \mathrm{Hom}\,(T\,\mathcal{M} \otimes T\,\mathcal{M}))$-operator of j-entry of vector field ∂_j-operator respective to vector field ∂_i-operator, for every $(p \in \mathbb{D}_u)$-point satisfies, for Einstein's summation convention, the equality below.

$$\nabla_{\partial_i} \partial_j = -\Gamma_{ij}^k\, \partial_k$$

Definition A.10 (Christoffel's Γ_{ij}^k-maps of a Levi-Civitta ∇-connection)**.** Let us define the so-called *Christoffel*'s Γ_{ij}^k-maps as the coefficients of unique Levi-Civitta ∇-connection within defined C^∞-chart $(U,\, \eta)$-tuple by covariant derivative A.9-definition.

$$\frac{1}{2} g^{kl}\ (g_{jl;i} + g_{li;j} - g_{ij;l}) \tag{A.2}$$

Several Riemannian metric examples arise as submanifolds, products, and quotients of Riemannian manifolds. Lee on [74]-textbook begins with Riemannian manifold definition $(\tilde{\mathcal{M}}, \tilde{g})$-tuple, and manifold f-map on $(\mathcal{M} \to \mathcal{N})$-relation. Since the push-forward f_*-operator constrains the tangent vectors on manifold $\mathcal{M}$, the induced pullback metric on tangent $T\mathcal{M}$-bundle defines a Riemannian g-metric on $\mathcal{M}$-manifold. For instance, the standard metric on the $(\mathbb{S}^n \subset \mathbb{R}^{n+1})$-sphere employs this calculation.

Corollary A.1 (The induced pullback metric [74] [55])**.** *Let $(\mathcal{M}, g)$-tuple be a Riemannian embedding i.e. submanifold on Riemannian $\mathcal{N}$-manifold. The induced $\tilde{g}$-metric on $\mathcal{M}$-manifold is the 2-form tensor by pullback f^*g-map on smooth $\mathcal{E}(f^*\,\mathrm{Hom}\,(T\mathcal{M},\, T\mathcal{M}))$-section, whose expression is on* (A.3)*-equality.*

[19] An affine ∇-connection on $\mathcal{M}$-manifold is symmetric if $(\nabla_X Y - \nabla_Y X = [X,\, Y])$-equality hold, for every vector $(X,\, Y \in \mathbb{V}(\mathcal{M}))$-fields

[20] A connection is symmetric only if $X\langle Y, Z\rangle$-map is equal to inner product $(\langle \nabla_X\, Y, Z\rangle + \langle Y, \nabla_X\, Z\rangle)$-sum, for vector $(X,\, Y,\, Z \in \mathbb{V}(\mathcal{M}))$-fields

$$\tilde{g}_{ab} = \operatorname{tr}\left(f_{;\,a}\, f_{;\,b}^{\intercal}\, g\right) \tag{A.3}$$

Proof. The induced $\tilde{g}$-metric by pullback operation on differentiable f-map and injective differential df-operator on $(T_p\mathcal{N} \to T_{f(p)}\mathcal{M})$-relation for every $(p \in \mathcal{M})$-point by inner $\langle \partial_i, \partial_j \rangle_p$-product equal to $\langle f_*(\partial_i), f_*(\partial_j) \rangle_p$-product, for $(i,\, j)$-indexes on $\mathbb{N}^*_{\leq n}$-family. ■

The following operators on $\mathcal{C}^\infty(\mathcal{M})$-class φ-maps and vector $(Z \in \mathcal{E}(T\mathcal{M}))$-fields are well-known to undergraduates but require further treatment on manifolds. Among others, we present the divergence $\operatorname{div}^\nabla$-operator of the Z-vector field respective to ∇-connection.

Definition A.11 (The divergent $\operatorname{div}^\nabla$-operator of a Z-vector field)**.** For every p-point of open $\mathbb{D}_Z$-set on $\mathcal{M}$-manifold, the $\nabla_v Z$-map, is, for every vector $v \in T_p\mathcal{M}$, according to covariant derivative properties on [64]-work, an endomorphism $(\nabla Z)_p \coloneqq \nabla Z_p$ of vector $T_p\mathcal{M}$-space, and ∇Z-map on $(p \to (\nabla Z)_p)$-relation is a $\mathcal{C}^\infty$-class $\mathcal{E}(\operatorname{Hom}(T\mathcal{M}, T\mathcal{M}))$-section. Therefore, the divergence $\operatorname{div}^\nabla Z$-map on $(p \to \operatorname{tr}(\nabla Z_p))$-relation operates on ∇-connection for every $(p \in \mathbb{D}_Z)$-point.

Remark 12. Riemannian manifolds defined by map equalities require recurrently partial derivative expressions $\partial_i\, \partial_j \varphi \coloneqq \varphi_{;ij}$. We denote the $(i,\, j)$-entry of Ξ-tensor by uppercase greek indexed notation $\Xi^i_j \coloneqq \varphi_{;ij} - \sum_k \Gamma^k_{ij}\, \varphi_{,k}$. The respective tensorial representation in Einstein's sum convention is expression $\partial\partial^\intercal\varphi - \Gamma^h\, \varphi_{;h}$.

Based on the above definition and remark, we expose curvature-related forms mentioned in this section introduction. We omit the point dependency of a base manifold $\mathcal{M}$ to mitigate over-notation.

Definition A.12 (Gradient and Hesse's bilinear forms [64])**.** Let us define a $\mathcal{C}^\infty(\mathcal{M})$-class φ-map for every point $p \in \mathbb{D}_\varphi$ and vector $(v, w \in T_p\,\mathcal{M})$-pair, respectively given by local coordinate $[(v^i\, \partial_i)_p, (w^i \partial_i)_p]$-vectors. Then:

1. The *gradient* vector grad-field on $\mathcal{E}(T\mathcal{M})$-section respective to Riemannian $\langle \cdot, \cdot \rangle$-metric: the $\operatorname{grad}_p \varphi$-vector on tangent $T_p\mathcal{M}$-bundle satisfies the $(\langle \operatorname{grad}^{\mathcal{M}}_p \varphi, v \rangle = \varphi_*(v))$-equality. In local coordinates, it exhibits the conventional vectorial $g^{-1}\, \varphi_u$-notation. In Einstein's notation, the i-entry corresponds to $g^{ij}\, \varphi_{;\,i}\, \partial_j$-expression.

2. The Hesse Hess-tensor on $\mathcal{E}(\operatorname{Hom}(T\mathcal{M}, T\mathcal{M}))$-section respective to $\mathcal{C}^\infty$-class Riemannian $\langle \cdot, \cdot \rangle$-metric: It corresponds to the $\nabla_p(\operatorname{grad}^{\mathcal{M}}_p \varphi)$-endomorphism i.e. the covariant ∇-derivative of $\operatorname{grad}^{\mathcal{M}} \varphi$-vector. In local coordinates and conventional vectorial notation, it exhibits the $g^{-1}\, \Xi\, v$-format. On Einstein's notation, it is equal to the $g^{ij}\, \Xi^i_j\, v^j\, \partial_j$-expression.

3. The Laplacian Δ-operator on $(\mathcal{C}^\infty(\mathcal{M}) \to \mathcal{C}^\infty(\mathcal{M}))$-relation: it corresponds to the trace of Hesse tensor $\operatorname{Hess}^{\mathcal{M}}_p \varphi$ i.e. the divergence $\operatorname{div}^\nabla$-operation on gradient vector field $\operatorname{grad}^{\mathcal{M}}$ condition at point $p \in \mathbb{D}_\varphi$. In conventional vectorial form, it exhibits either format $\operatorname{tr}(g^{-1}\, \Xi)$ or $g^{-1} : \Xi$.

4. The Hesse 2-form $\left(\operatorname{hess}^{\mathcal{M}} \varphi \in \mathcal{E}(T^*\mathcal{M} \otimes T^*\mathcal{M})\right)$-tensor respective to $\mathcal{C}^\infty$-class Riemannian $\langle \cdot, \cdot \rangle$-metric: It assigns the $\langle (\operatorname{Hess}^{\mathcal{M}}_p \varphi)(v), w \rangle$-form, also given by inner

$\langle \overset{m}{\nabla}_v \operatorname{grad}_p^m \varphi, w\rangle$-product. In conventional vectorial form, it exhibits the $v^\intercal\, g^{-1}\, \Xi\, w$-format. Alternative formats correspond to either $\operatorname{tr}(g^{-1}\, \Xi\, w\, v^\intercal)$-computation or $\sum_{ij} g^{ij}\, \Xi_{ji}\, v^i\, w^j$-summation.

Definition A.13 (**Relation between gradient vector** $\operatorname{grad}\varphi$**-field and differential covector** $d\varphi$**-field**)**.** Let $d\varphi$ be the differential covector field of a C^∞-class φ-map a 1-form and gradient vector $\operatorname{grad}^m \varphi$-field. We define the gradient vector (grad φ)-map as the musical vector field $(g^\sharp \circ d\varphi)$-composition. The $g^\sharp$-map on $(T^*\mathcal{M} \to T\mathcal{M})$-relation is the musical vector bundle *sharp*-isomorphism induced by g-metric. Since, we have in local coordinates the differential $d\varphi$-covector given in Einstein's $\varphi_{;\,i}\, \partial^i$-notation, then we obtain the gradient $g^{ij}\, \varphi_{;\,i}\, \partial_j$-description.

For the case of $\mathcal{M}$-manifold equivalent to canonical $\mathbb{R}^n$-Euclidean manifold and its inner $(\langle a, b\rangle \coloneqq a_i\, b^i)$-product, i.e., the $\left(g_{ij} = g^{ij} = \delta^i_j\right)$-equalities hold ($g$ is the identity tensor as well as $g^\sharp$), and $(e_i = \partial_i)$-vector is the standard basis, Then the gradient grad φ-vector on $\mathbb{V}(\mathcal{M})$-class corresponds to $\varphi_{;\,i}\, e_i$-expression.

Definition A.14 (**Lie derivative** L_X**-operator of a** $\mathcal{C}^\infty$**-class** φ**-map defined on** $\mathcal{M}$**-manifold** [41])**.** Given a vector X-field on $(\mathcal{M} \mapsto T\mathcal{M})$-relation and a smooth φ-map on $(\mathcal{M} \mapsto \mathbb{R})$-relation the Lie derivative L_X-operator of φ-map respective to the vector X-field is a new vector $L_X\varphi$-map on $(\mathcal{M} \mapsto \mathbb{R})$-relation for every p-point. We denote by either $X(\varphi)(p)$ or $\varphi_*(X_p)$-notation. In local coordinates and Einstein's notation in force, for vector field $(X \coloneqq X^i\, \partial_i)$-representation, we have the Lie derivative $X^i\, \varphi_{;\,i}$-representation.

Informally, the Lie L_X-derivative of a $\mathcal{C}^\infty$-class h-map concerning a vector X-field is the h-map directional derivative operation in X-direction. Due to $\mathcal{M}$-manifold differentiability, we state the following lemma.

Lemma A.3 ([77])**.** *Vector* $(f, g \in \mathbb{V}(\mathcal{M}))$*-fields on* $(p \in \mathcal{M})$*-point are equal only if* $(L_f = L_g)$*-equality holds.*

The Lie L_f-derivative is a first-order operator, while the $(L_f \circ L_g)$-composition i.e. $L_f\, L_g\, \varphi \coloneqq g^\intercal\, H_\varphi\, f + \varphi_*\, g_*\, f$ is a second-order operator on a $\mathcal{C}^{\geq 2}$-class φ-map. Since the H_φ-tensor, given by $\partial\partial^\intercal\varphi$-tensor, is symmetric for $\mathcal{C}^{>2}(\mathcal{M})$-class maps, the difference $L_f\, L_g - L_g\, L_f$ reduces to the Lie derivative $L_{g_*\, f - f_*\, g}$. It suggests the Lie bracket definition as follows.

Definition A.15 (**Lie** $[\cdot, \cdot]$**-bracket of vector fields on** $\mathcal{M}$**-manifold** [36])**.** The *Lie* $[f, g]$*-bracket* defined on $\mathbb{V}(\mathcal{M})$-class by vector $(f, g \in \mathbb{V}(\mathcal{M}))$-fields on $(p \in \mathcal{M})$-point is equal to vector $(g_*\, f - f_*\, g)$-field.

Alternatively, we denote $[f,\, g]$-operator as $\operatorname{ad}_f g$-notation and call it adjoint ad_f-operator on $(\mathbb{V}(\mathcal{M}) \to \mathbb{V}(\mathcal{M}))$-relation. This is an first order operator concerning the Lie bracket, which holds the following identity:

$$\operatorname{ad}_f[g, h] = [\operatorname{ad}_f g, h] + [g, \operatorname{ad}_f h]$$

Definition A.16 (**Lie $\mathcal{L}$-algebra of vector $\mathbb{V}(\mathcal{M})$-fields on $\mathcal{M}$-manifold**)**.** The *Lie algebra* on $(p \in \mathcal{M})$-point is a linear $(S \in \mathbb{V}(\mathcal{M}))$-subspace such that it is closed under Lie bracket operation, i.e., given vector (f, g)-fields in S-space, then $[f, g] \in T\,S$.

Corollary A.2 ([39])**.** *The Lie $W_{\mathcal{L}}$-algebra generated by vector fields W-set on $\mathcal{M}$-manifold is the smallest linear subspace of all Lie algebras*[21] *of vector fields that contain W.*

Lemma A.4. *Let us define a finite $(W \in \mathbb{V}(\mathcal{M}))$-set of vector fields and assign W_0-set as W. Hence, the Lie $W_{\mathcal{L}}$-algebra corresponds to linear* $\operatorname{span}(W_\infty)$*-space, defined by the* $\left(\bigcup_{k\geq 0} W_k\right)$*-union. The recursive formation W_{k+1}-rule corresponds to the set below:*

$$\{\operatorname{ad}_f g \,|\, f \in W_k,\, g \in W\} \tag{A.4}$$

Remark 13. In this work, we write the iterated adjoint operator of ℓ-length by linear $\operatorname{ad}_g^{I_\ell}$-operator, such that I_ℓ corresponds to an ordered set of the permutation index $\mathbb{I}_\ell(A)$-family with $(\ell \leq |A|)$-cardinality.

Additional concepts relate to the spanned linear space by vector fields on $(p \in \mathcal{M})$-point: a vector space of vector fields, namely a *vector field space*, is a *distribution*, and its dual, i.e. row-wise, space of covector fields is a *co-distribution*. In linear algebra, it refers to the vector space duality, given by transposed vector spaces, as we may refer to on [31]-textbook. A ω-covector, and consequently a *covector Ω_x-field*, constitutes a row-wise spanned space and plays an important role in geometric control theory.

Definition A.17 (**Distribution** [41])**.** Given a smooth vector field $\{X_{n_\Delta}\}$-set, we define a Δ_x-distribution on open $(\mathcal{D} \subseteq \mathcal{X})$-set to be its spanned vector subspace on $(x \in \mathcal{D})$-point.

Hence, a $(X \in \mathbb{V}(\mathcal{D}))$-(vector field) on $(p \in \mathcal{D})$-point is *pointwise* in distribution Δ_p-space. We denote it as the pointwise $(X \in_p \Delta)$-relation. Moreover, the familiar invariance concept to linear control theorists also holds for distributions.

Definition A.18 (Distribution invariance)**.** An **invariant** distribution is *pointwise closed under Lie brackets*, for every vector $(X \in_p \Delta)$-field.

$$X,\, Y \in_p \Delta \Longrightarrow [X,\, Y] \in_p \Delta$$

We define naturally $\operatorname{rank}(\Delta_p)$-cardinal to every $(p \in \mathbb{D}_\Delta)$-point generated by vector field $\{X_{n_\Delta}\}$-set.

Definition A.19. A Δ-distribution has $(\dim(\Delta_p) \coloneqq r \leq n_\Delta)$-rank on every p-point on its domain $(\mathbb{D}_\Delta \subseteq \mathcal{M})$-set.

Definition A.20 (**Codistribution** [41])**.** Given a smooth covector field $\{\omega_{n_\Omega}\}$-set, we define a Ω_x-distribution on open $\mathbb{D}_\Omega$-set to be the spanned dual vector subspace for every $(p \in \mathbb{D}_\Omega)$-point.

[21] This algebra set is non-empty since it includes vector field $\mathbb{V}(\mathcal{M})$-class

Definition A.21 (**Annihilator** [41])**.** A Ω-codistribution is said to *annihilate* a Δ-distribution if the following identity holds for every $(\omega \in \Omega_x)$-covector and $(\varsigma \in \Delta_x)$-vector.

$$\omega_k \, \varsigma^k = 0$$

Remark 14. Let us define x_0-point as a regular point of a smooth Δ_x-distribution. Then, x_0-point is also a regular point of also smooth Ω-annihilator $\mathrm{Ann}_{\mathcal{X}}\,(\Delta)$.

Geometric analysis on smooth affine velocity vector fields

The control strategy applied in this work, the *partial linearization method*, requires fundamental concepts related to smooth affine dynamical systems. We present in this section a compilation of required definitions and statements.

Definition A.22 (Smooth affine dynamical system [36])**.** Let us define an affine real-valued continuous dynamical Σ-system given by $(\mathbb{R}_+,\, \mathcal{X},\, \mathcal{U},\, \phi,\, \mathcal{Y}, h)$-tuple as a velocity vector $(\dot{x} \in T_x\,\mathcal{X})$-field at $(x \in \mathcal{X})$-point equal to affine $(f + G\,u)$-map, for vector field $(f,\, g_i \in \mathbb{V}(\mathcal{X}))$-maps. We aim to design a measurable control $(u \in \mathcal{U})$-map to track an $(y \in \mathcal{Y})$-output defined by a tracking h-map on $(\mathcal{X} \to \mathcal{Y})$-relation, for every $(x \in \mathbb{D}_{\dot{x}})$-point.

We define the lowest natural δ_i-constant for affine dynamical Σ-systems by output h^i-map of the affine dynamical Σ-system. In set-theoretical terms, we define this set as below:

Definition A.23 (Input-output relative δ_i-degrees of the affine dynamical Σ-system)**.** We define the relative degree as natural δ_i-constant respective to the output h^i-map of affine dynamical Σ-system by the set below.

$$\left\{\delta_i \in \mathbb{N}_{>0} \,|\, L_G L_f^{\delta_i - 1} h^i \neq 0\right\}$$

The above statement suggests the definition of relative degree κ-vector with $\{\delta_{n_y}\}$-elements and a total δ-sum of relative degrees for the Σ-system. From a computational perspective, the accumulated relative ζ_i-degree emerges on partial linearization formulation. Its definition follows below.

Definition A.24. We define the accumulated relative ζ_i-degree, for $(i \in \mathbb{N}^*_{\leq p})$-index, by recursion formation $(\zeta_{i-1} + \delta_i)$-rule.

The partial linearization method requires the (co-)distribution concept as on definition A.20. Then, its definition follows.

Definition A.25. The relative degree $(\Delta \subseteq T\mathcal{X})$-distribution of the affine dynamical Σ-system from definition A.22 follows below.

$$\mathrm{span}\left(\left\{L_{g_1} L_f^{\delta_1 - 1} h,\, \cdots,\, L_{g_p} L_f^{\delta_p - 1} h\right\}\right) \tag{A.5}$$

We interest also in necessary and sufficient conditions to design a control u-map on some state-space $\mathcal{V}$-set. For linear systems, if a dynamical system given by matrix $(A,\, B)$-tuple is controllable, we steer the system trajectories in finite time T-constant from a state x_0-point to some other x_1-point only if the system is controllable by means of B-vector field and invariant $A^k\, B$-spaces, for $(k \in \mathbb{N}_{[1,\, n-1]})$-indexes. An equivalent condition degenerates into the linear case for nonlinear affine dynamical systems under the assumption of linear time-invariant (co-)vector fields. We present the necessary aspects for readers to inform themselves about the subject.

A Lie $W_{\mathcal{L}}$-algebra of vector fields is the *accessibility Lie Algebra* associated with Σ-system. From its meaning, we define the accessibility rank condition below.

Definition A.26. The **accessibility rank condition** at some $(x \in \mathcal{X})$-point holds if the $(\dim(W_{\mathcal{L}}) = n)$-equality also hold for some open $(\mathcal{V} \subseteq \mathcal{X})$-set.

Lemma A.5 ([36])**.** *It is sufficient for control-affine systems to generate the Lie $\mathcal{W}_{\mathcal{L}}$-algebra from vector field $\{f,\, g_1,\, \cdots,\, g_m\}$-set.*

Lemma A.5 characterizes the accessibility rank condition as the existence of n vector X-fields by means of iterated brackets formed by vector field $\{f,\, g_1,\, \cdots,\, g_m\}$-set which is linearly independent when evaluated at some $(x \in \mathcal{X})$-point.

The above definition allows further investigation on the system mobility degree, which we call *nonholonomy degree*. The authors Campion *et al.* classify affine smooth systems into five types according to their nonholonomy degree. It motivates the development and presentation of controllability concepts for nonlinear smooth systems.

Definition A.27 (Reachable $\mathcal{R}$-set [36])**.** For each $(\mathcal{V} \subseteq \mathcal{X})$-subset, initial $(x_0 \in \mathcal{V})$-state and $(t > t_0)$-instant, we define the $\mathcal{R}^t_{\mathcal{V}}(x_0)$-set of *reachable* states from x_0-point, in exact time t-instant, without leaving $\mathcal{V}$-set.

$$\{z_0 \,|\, \exists\, \omega \in \mathcal{C}^{\infty}_{[t_0,\, t]}(\mathcal{U}) \text{ s.t. } \phi(s,\, t_0,\, x_0,\, \omega) \in \mathcal{V},\, \forall\, s \in [t_0, t] \text{ and } \phi(t,\, t_0,\, x_0,\, \omega) = z_0\}^1$$

For each time $(T \geq 0)$-constant, we consider the $\mathcal{R}^{\leq T}_{\mathcal{V}}(x_0)$-set of reachable states at time at most T-instant and given by the disjoint $\left(\bigcup\limits_{t\, \in\, [0,\, T]} \mathcal{R}^t_{\mathcal{V}}(x_0)\right)$-union. In case we adopt the equivalence $(\mathcal{V} \equiv \mathcal{X})$-condition, then we drop the subscript. The total reachable $\mathcal{R}(x_0)$-set from initial x_0-point is the disjoint $\left(\bigcup\limits_{t\, \geq\, 0} \mathcal{R}^t(x_0)\right)$-union.

Likewise, for each open $\mathcal{V}$-set, z_0-point and $(t > t_0)$-instant, we consider the states set *controllable to* z_0 in exact t-time without leaving $\mathcal{V}$-set, namely given by set-definition below. The notation is similar to the reachable set by substitution of $\mathcal{R}$-notation by $\mathcal{C}$.

$$\{x_0 \,|\, \exists\, \omega \in \mathcal{C}^{\infty}_{[t_0,\, t]}(\mathcal{U}) \text{ s.t. } \phi(s,\, t_0,\, x_0,\, \omega) \in \mathcal{V},\, \forall\, s \in [t_0, t] \text{ and } \phi(t,\, t_0,\, x_0,\, \omega) = z_0\}$$

[1] The abbreviation *s.t.* stands for implicative conjunction "*such that*".

Hence, we define the following result about the relation between the accessibility rank condition and the above-defined sets.

Theorem A.3. *Given* $(x_0 \in \mathcal{X})$*-point such that the accessibility rank condition holds. Then, the* $\left(\mathcal{R}_{\mathcal{V}}^{\leq T}(x_0), \mathcal{C}_{\mathcal{V}}^{\leq T}(x_0)\right)$*-sets have non-empty interiors, for each neighborhood* $\mathcal{V}$*-set of* x_0*-point, and each time* $(T > 0)$*-constant. Finally, the* $(\mathcal{R}(x_0), \mathcal{C}(x_0))$*-sets also have non-empty interiors.*

$$\begin{aligned} int\left(\mathcal{R}_{\mathcal{V}}^{\leq T}(x_0)\right) &\neq \emptyset \\ int\left(\mathcal{C}_{\mathcal{V}}^{\leq T}(x_0)\right) &\neq \emptyset \end{aligned} \tag{A.6}$$

Sontag states that the accessibility rank condition is not sufficient for controllability implication. Thus, we require a further concept to accomplish controllability in terms of concepts defined so far.

Definition A.28 (Reversibility [36])**.** A system is **weakly reversible** if the implicative $(x_0 \rightsquigarrow z_0 \Longleftrightarrow z_0 \rightsquigarrow x_0)$[22]-relation hold, and **strongly reversible** if, for each x_0-point and each admissible control $\left(\omega \in \mathcal{C}^{\infty}_{[0,\,T]}(\mathcal{U})\right)$-measure for admissible x_0-point, there is some admissible input $(\nu \in \mathcal{C}^{\infty}_{[0,\,T]}(\mathcal{U}))$-map such that z_0-point given by $\phi(T,\, 0,\, x_0,\, \omega)$-evaluation as well as the reverse $(\phi(t,\, 0,\, x_0,\, \omega) = \phi(T - t,\, 0,\, z_0,\, \nu))$-equality hold, for every $(t \in [0,\, T])$-instant.

The above ideas allow reachable/controllable set definition by means reversibility hypothesis. That is, *weakly reversible* means that $(z_0 \in \mathcal{R}(x_0),\, x_0 \in \mathcal{R}(z_0))$-conditions hold together, and *strongly reversible* means that the same curve from point x_0 to z_0 also travels backward.

Proposition A.1 ([36])**.** *Let* x_0 *be a point on* $\mathcal{X}$*-manifold such that the accessibility rank condition holds. If the* Σ*-system is weakly reversible, then the* $int\,(\mathcal{R}(x_0) \cap \mathcal{C}(x_0))$*-set is not empty, for some* $(x_0 \in \mathcal{X})$*-point. Moreover, if it is strongly reversible, then for every neighborhood* $\mathcal{V}$*-set of* x_0*-point and time* $(T > 0)$*-constant, the* $\text{int}\left(\mathcal{R}_{\mathcal{V}}^{\leq T}(x_0) \cap \mathcal{C}_{\mathcal{V}}^{\leq T}(x_0)\right)$*-set is also non-empty.*

Corollary A.3 ([36])**.** *For a weakly reversible system, if the accessibility rank condition holds at every state* $(x \in \tilde{\mathcal{X}} \subseteq \mathcal{X})$*-point and* $\tilde{\mathcal{X}}$*-space is connected, then the system is completely controllable within* $\tilde{\mathcal{X}}$*-space.*

We develop the observability concept and reconstruction of system states. It will prove itself dual to the above-presented topic. The concept regards the physical application of sensor readings to acquire information about the system states either for monitoring or subsequent control. Intuitively, there must be enough information to reconstruct the system description.

The duality between reachability and controllability regards the action of covector fields spanned by output derivatives. It means, we utilize analogous concepts of spanned codistribution and distinguishability-observability sets as we construct for reachability-controllability. Likewise, we obtain an equivalent rank condition statement for observability, as presented in [78]-textbook.

[22]The squiggle arrow $\rightsquigarrow$-symbol denotes reachability among former to latter points.

Definition A.29. ([78]) States $(x_1,\, x_2 \in \mathcal{M})$-points are indistinguishable for every admissible u-input, we call $x_1 \mathcal{I} x_2$, if, the output $((h \circ \phi)(t,\, t_0,\, x_1,\, u) = (h \circ \phi)(t,\, t_0,\, x_2,\, u))$-equality hold, for initial state $(x_1,\, x_2)$-points. We call the system *observable* if $x_1 \mathcal{I} x_2$-condition implies the $(x_1 = x_2)$-equality.

In other words, a system is locally observable if, for every state $(x \in \mathcal{X})$-point, it is distinguishable from its neighbors by nearby close trajectories to x-point.

Before we explain the observability property of affine dynamical systems, the combinatorics definition of the below family is helpful in further statements. The notation allows the construction of Lie derivative chains.

Definition A.30. Given a permutation $\mathbb{P}_k$-family of an J-element-set belonging to index set $\mathbb{I}_n$-family, we define a $(I_k \in \mathbb{P}_k(J))$-set-element as every ordered permutation of J-set with k-cardinality.

For affine dynamical systems under analysis, on definition A.22, the *observable* $\mathcal{O}$-*space* associated to the Σ-system from Lie algebra-equivalent covector differential fields of output $\{h^j\}_{n_y}$-maps.

Theorem A.4 (*Observable* $\mathcal{O}$*-space* [78])**.** *The* observable $\mathcal{O}$-space associated to the Σ-system *is co-vector space spanned by the set of all Lie derivative chain maps on* (A.7)*-equality over possible index permutations of* $(k > 0)$*-cardinality from* $\mathbb{N}_{\leq m}$*-set and* $(j \in \mathbb{N}^*_{\leq p})$*-index.*

$$L_{g_{i_1}} \cdots L_{g_{i_k}} h^j \coloneqq L^{I_k}_{\{g_i\}} h^j \tag{A.7}$$

Proof. We prove, for a sufficiently close neighborhood $\mathcal{V}$-set of $(x_1 \in \mathcal{X})$-point that, if state $(x_1,\, x_2 \in \mathcal{V})$-points are indistinguishable i.e. $x_1 \, \mathcal{I}^{\mathcal{V}} \, x_2$, then they are equal. Thus, consider a piecewise constant control u^k on the $([t_{k-1}, t_k] + t_1 + \cdots + t_{k-2})$-interval. For small enough instants i.e. limit values, control u^k is admissible for both x_1 and x_2. By indistinguishability, the resulting output at instant t is equal to $(t_1 + \cdots + t_k)$-sum. It follows that the output t_i-derivatives are also equal for state (x_1, x_2)-points and every such piecewise constant control u^i. Let us denote the j-entry of output h-map, for initial state x-point, by notation $h^j(t_1, \cdots, t_k, u^1, \cdots,\, u^k,\, x)$. Firstly, we construct an instant time set $\{t_i\}_k$. By induction, the following time chain derivative holds:

$$\begin{aligned} \partial_{\{t_k\}} h^j(t_1, \cdots, t_k, u^1, \cdots,\, u^k,\, x)\big|_{t_1 = t_2 = \cdots = 0} &= (L_{X_1} \cdots L_{X_k} h^j)(x) \\ &= (L^{I_k}_{\{X_l\}} h^j)(x) \end{aligned} \tag{A.8}$$

Vector X_l-fields correspond to instant vector fields $f + g_i \, u^i_l$. By the above expression awareness as linear respective to input u^i_l-entries and inverse function theorem application, a further d-differentiation with respect to these control value coordinates shows that (x_1, x_2)-points coincide on the definition domain only if there is n-rank around (A.7)-generators. ■

In the analytic case, separability, the opposite of indistinguishability, by $\mathcal{O}$-set is necessary as well sufficient because we express the output h^j-map by input u_k-sequence as a power series in terms of the (A.7)-generators.

Definition A.31 ([78])**.** We exchange vector X_i-fields on A.4-theorem, (A.7)-equality, to belong to the accessibility Lie algebra $\{f, g_1, \cdots, g_m\}_{\mathcal{L}}$.

Finally, we call (A.5)-theorem the observability rank condition. The system satisfies the observability rank condition if (A.5)-condition holds for any $(x \in \mathcal{M})$-point.

Theorem A.5 (Observability rank condition [78])**.** *Consider the affine system on A.22-definition with* $\dim(\mathcal{X})$*-dimension as natural* n_x*-constant. We define the smallest observation codistribution denoted by* $d\mathcal{O}$[23] *below:*

$$\left\{ d\, L^{I_k}_{\{g_i\}} h^j \,|\, \forall I_k \in \mathbb{P}_k(\mathbb{N}_{\leq m}) \wedge k > 0 \wedge j \in \mathbb{N}^*_{\leq m} \right\} \tag{A.9}$$

Thus, the system is locally distinguishable *on a neighborhood-set to* $(x_0 \in \mathcal{I} \subseteq \mathcal{X})$*-point if* $(\text{rank}\,(d\,\mathcal{O}(x_0)) = n)$*-equality holds.*

A.5-Theorem suggests that, even if an affine system is locally observable, the $d\mathcal{O}$-codistribution may have singular $(q \in \mathbb{D}_{\mathcal{O}})$-points with $(n_{\mathcal{O}} \coloneqq \text{rank}(d\mathcal{O}(q)) < n)$-dimension. On the other hand, Isidori shows that in a locally accessible and analytic system, the $d\mathcal{O}$-codistribution local constant dimension is due to Taylor's polynomial series representation.

Proposition A.2 ([78])**.** *Let affine dynamical* Σ*-system be a locally accessible and analytic system and* $\mathcal{M}$*-manifold connected such that the* $d\mathcal{O}$*-codistribution is dimensionally constant. Then, an affine system is locally observable if it satisfies the observability rank condition on* (A.5)*-definition.*

Finally, we build a Venn diagram to summarize the relation between $\mathcal{R}/\mathcal{I}/\mathcal{C}/\mathcal{O}$-sets on a neighborhood-set to $(x_0 \in \mathcal{X})$-point. In a smooth general case, there may exist an intersection between $(\mathcal{R}, \mathcal{I})$-sets. $(\mathcal{C}, \mathcal{O})$-Sets require a further implication condition, which constrains each $(\mathcal{I}, \mathcal{R})$-subsets. Likewise, they may exhibit an intersection set. Its pictorial representation follows in 30-figure.

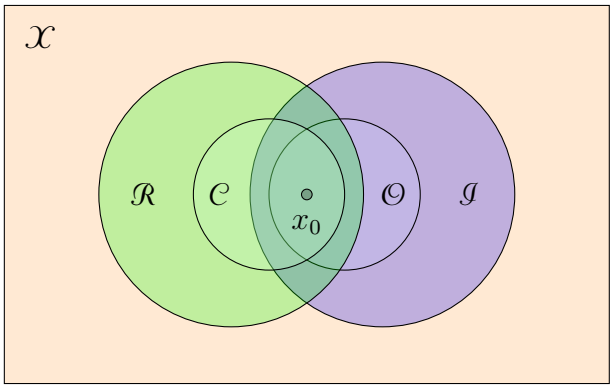

Figure 30: Relation between $\mathcal{R}$-reachable, $\mathcal{C}$-controllable, $\mathcal{I}$-indistinguishable and $\mathcal{O}$-observable sets from initial x_0-point.

[23]For convenience, we here-refer to vector f-field as g_0-notation.

Lyapunov stability analysis

Lyapunov brings a geometric perspective to the dynamical systems stability theory. His criterium comprehends the effort to analyze dynamical systems, oftentimes described in $(\mathcal{T},\, \mathcal{X},\, \mathcal{U},\, \phi)$-tuple form on geometrical objects. Authors Pait & Colón present the theory in terms of a $\mathcal{C}^{\infty}$-class Riemannian manifold and provide useful comprehensive insights for further construction of a Lyapunov scalar v-map defined from some state $\mathcal{X}$-manifold to $\mathbb{R}_{\geq 0}$-space. These map properties follow below. The current author enlights the notation by x-dependency omission.

Definition A.32 (**Resting x_e-point** [80])**.** Let $\mathcal{X}$ define a manifold and the velocity vector $(\dot{x} \in T_x\,\mathcal{X})$-field given by velocity vector $a(x)$-field , a x_e-point within $\mathcal{X}$-manifold is a *resting point* if it satisfies $(a(x_e) = 0)$-equality. The disjoint union of resting $(x_e \in \mathcal{X}_e)$-points, is a subset of $\mathcal{X}$-manifold, we call it *resting* $(\mathcal{X}_e \subseteq \mathcal{X})$*-set*.

Definition A.33 (**Lyapunov map** [80])**.** Let us choose a $\mathcal{C}^{\infty}$-class positive v-map and a $\mathcal{C}^{\infty}$-class dynamical system whose velocity $(\dot{x} \in T_x\mathcal{M})$-vector is given by vector field $a(x)$-map for every $(x \in \mathbb{D}_a)$-point. Then, v-map calls a Lyapunov map to stability analysis around a resting $(x_e \in \mathcal{X}_e)$-point if it satisfies the properties below within an open neighborhood B_{x_e}-set, for every $(x \in B_{x_e})$-point.

1. $v \geq 0$;
2. $\nabla_D\, v \leq 0$.

Definition A.34 (**Lyapunov stability** [79])**.** Let ℓ be a positive definite map with level $(\ell = 0)$-sets only at resting $(x_e \in \mathcal{X}_e)$-points. We assume that the Lyapunov partial differential (A.10)-equality (L.P.D.E. for short) has a v-map solution such that $(v(x_e) = 0)$-equality hold. Then, the equilibrium point x_e of the dynamical Σ-system is asymptotically stable only if v-map is positive definite.

$$L_a v + \ell = 0 \tag{A.10}$$

Henceforth, a linear system, as Pait & Colón define on [79]-work, satisfies stability (A.10)-condition only if there is a so-defined linear Lyapunov $P_{ij}\, x^i\, x^j$-map, for K-class tensor P and position $(X \coloneqq x^i\, \partial_i)$-vector respective to original o-point such that linear dynamical linear system trajectories are given by (Killing) velocity linear vector $A_k\, X^k$-field satisfies (A.10)-condition for some K-class Q-tensor. We represent (A.11)-equality in the compact $(\Lambda + A^{\intercal}\, P + P\, A = -Q)$-format, for the $(i,\, j)$-entry Λ-element equal to $\big(L_{A_k\, x^k}\, P_{ij}\big)$-map.

$$\big(L_{A_k\, x^k} P_{ij}\big)\; x^i\, x^j + P_{ij}\, A^i_k\, x^k\, x^j + P_{ij}\, A^j_k\, x^i\, x^k \coloneqq -Q_{ij}\, x^i\, x^j \tag{A.11}$$

APPENDIX B – INSTRUCTIONS FOR RESULTS REPRODUCTION

These work results require the below software tools. They allow library setup proceeding.

- A git-based source management software (`https://git-scm.com/`) e.g. TortoiseGit, Github Desktop, or Git for Windows;
- Matlab version 2017a or above;

In sequence with the above installation, the below instructions allow the installation and usage of the required libraries:

1. Run the command chain below to clone the necessary repositories.

```
» mkdir ~/github
» cd ~/github
» export ASMOVE_REPO="https://github.com/asmove"
» for repo in "$ASMOVE_REPO/"{quindim,matils,baryopt,sseek}; do
      git clone $repo;
  done
```

2. Open MatLab;
3. The command to reproduce the source-seeking results follows below

```
» cd ~/github/sseek
» loadlibs
» cd ~/github/sseek/code
» main
```

APPENDIX C – PARTIAL INPUT-OUTPUT LINEARIZATION ALGORITHM

Algorithm 1 The dynamic extension pseudocode algorithm

$\left(\tilde{x},\, \tilde{f},\, \tilde{G},\, \tilde{h}\right) \leftarrow (x,\, f,\, G,\, h)$
$\tilde{n},\, \tilde{m} \leftarrow \dim(\tilde{G})$
$p \leftarrow dim(\tilde{h})$
$S \leftarrow \mathrm{Id}_{\mathbb{R}^m}$
$i \leftarrow 0$
do
  $i \leftarrow i + 1$
  $\left(y^{\delta},\, \Delta,\, \delta,\, L^{\delta}_{\tilde{f}}h\right) \leftarrow \emptyset$
  for each $j \leftarrow 1$ to n_y **do**
    $k \leftarrow 1$
    { Calculates relative degree κ-vector }
    do
      $L^k_f h^j = \frac{\partial}{\partial x} h^j \cdot L^{k-1}_f h^j$
      $L_{\tilde{G}} L^{k-1}_f h^j = \frac{\partial}{\partial x} L^{k-1}_f h^j \cdot \tilde{G}$
      $\Delta \leftarrow \begin{bmatrix} \Delta \\ L_{\tilde{G}} L^{k-1}_{\tilde{f}} \tilde{h}^j \end{bmatrix}$
      $y^{\delta} \leftarrow \begin{bmatrix} y^{\delta} \\ L^k_{\tilde{f}} \tilde{h}^j \end{bmatrix}$
      $L^{\delta}_{\tilde{f}} \tilde{h} \leftarrow \begin{bmatrix} L^{\delta}_{\tilde{f}} \tilde{h} \\ L^k_{\tilde{f}} \tilde{h}^j \end{bmatrix}$
      $k \leftarrow k + 1$
    while $L_{\tilde{G}} L^k_f \tilde{h}^i \neq 0, \forall\, x \in \mathcal{X}$
  end for

Algorithm 1 The dynamic extension pseudocode algorithm

if $\operatorname{rank}(\Delta_x) < n_y,\ \forall\, x \in \mathcal{X}$ **then**
$\delta_j \leftarrow k$
S_i-distribution such that $\left(\Delta\, S_i = \begin{bmatrix}\Delta_{1i} & 0\end{bmatrix}\right)$-equality and $(u \coloneqq S_i\, w_i)$-map hold
$S \leftarrow S\, S_i$
$\tilde{x} \leftarrow \begin{bmatrix}\tilde{x} \\ w_{1i}\end{bmatrix}$
$\tilde{f} \leftarrow \begin{bmatrix}\tilde{f} + \tilde{G}\, S_{1i} \\ 0\end{bmatrix}$
$\tilde{G} \leftarrow \begin{bmatrix}0 & \tilde{G}\, S_{2i} \\ \mathrm{Id}_{TW_{1i}} & 0\end{bmatrix}$
$\tilde{h} \leftarrow h$ continue
end if
while $\operatorname{rank}(\Delta_{\tilde{x}}) \neq n_y$, for some $\left(\tilde{x} \in \tilde{\mathcal{X}}\right)$-space
$v = \{y_\star^{\delta_a} - \sum_{b=0}^{\delta_a - 1} k_{ba}\,(y^{(b)} - y_\star^{(b)})\}_{a \in \mathbb{N}^*_{\leq p}}$ for the $\left(\{k_{ba}\}_{a \in \mathbb{N}^*_{\leq n_y}}\right)$-monomials of characteristic polynomial with $\{\lambda_{\delta_i}\}$-roots on the left complex $\mathbb{C}^-$-plane
$w = \Delta^{-1}\left(-L_f^\kappa\, h + v\right)$
$u = S_i \begin{bmatrix}z_{1i} \\ w_{2i}\end{bmatrix}$

APPENDIX D – SEEKING ALGORITHM

Algorithm 2 Flow diagram pseudocode implementation from 11-figure

Require:

Initial τ_0-instant;
Trajectory reference $\hat{\gamma}$-curve;
Input u-map;
Signal sampling and estimation $(\Delta\tau_s, \Delta\tau_e)$-intervals;
Assign index map $(i,j)(s)$-tuple respectively to map $\left(\left\lfloor \frac{s-\tau_0}{\Delta\tau_e} \right\rfloor, \left\lfloor \frac{s-\tau_0}{\Delta\tau_s} - i(s)\,\frac{\Delta\tau_e}{\Delta\tau_s} \right\rfloor\right)$-tuple;
Update:
  Indexes (i,j)-tuple to natural $(i,j)(\tau_0)$-tuple;
  Source signal sample instant τ_s-variable to τ_0-instant;
  Extremum estimation point $\hat{y}^{i\,j}(\tau_0)$-variable to $(y_s(\tau_0)+z)$-point;

while $\tau \in \mathbb{R}_{\geq\tau_0}$ **do**
  Get current τ-instant
  Update indexes (i,j)-tuple to natural $(i,j)(\tau)$-tuple;
  Update (at least 1 option):
    Trajectory curve $\hat{\gamma}^{ij}$-endpoint to $(\hat{y}_s^{i\,j}+z_\gamma)$-vector;
    Control u-map to $(u(x(\tau),\hat{\gamma})+z_u)$-vector;
  Apply input u-map to dynamical Σ-system;
  if $\tau \in [\tau_i,\, \tau_{i+1}]$ **then**
    if $\tau \in \tau_s + [0,\, \Delta\tau_s]$ **then**
      Continue;
    else
      Update:
        Point $\hat{y}^{i\,j}(\tau_0)$-variable to $(\hat{y}^{i\,j-1} + F_j(y(\tau))(y_s(\tau) - \hat{y}_s^{i\,j-1}) + z_{\hat{y}})$-point;
        Instant τ_s-variable to τ-instant;
        Index j-variable value by increment 1;
    end if
  else
    Update:
      Index i-variable value by increment 1;
      Estimation point $\hat{y}^{i\,0}$-variable to $\hat{y}^{i-1\,j}$-point;
  end if
end while